

Table A1. 1-Å resolution spectra: I_{sol} and $I_{\text{enh}} - I_{\text{sol}}$ for $[Z/Z_{\odot}] = -2.0$

T_{eff}	4000								5250							
$\log g$	1.5		2.5		3.5		4.5		1.5		2.5		3.5		4.5	
	I_{sol}	(δI)														
CN1	0.043	0.024	0.057	0.041	0.050	0.044	0.047	0.043	-0.025	0.002	-0.029	0.003	-0.035	0.005	-0.041	0.009
CN2	0.092	0.039	0.129	0.056	0.126	0.062	0.143	0.055	-0.001	0.002	-0.009	0.004	-0.022	0.007	-0.034	0.014
Ca4227	0.328	1.228	1.272	1.460	2.213	1.564	3.872	1.296	0.095	0.081	0.042	0.121	0.033	0.209	0.135	0.358
G4300	8.302	-0.881	8.620	-1.429	7.356	-1.431	6.386	-1.885	3.053	0.216	4.441	0.045	5.746	-0.203	6.863	-0.616
Fe4383	5.127	-1.010	5.742	-1.282	5.221	-1.029	5.448	-1.329	1.079	0.086	1.067	0.020	1.270	-0.100	1.700	-0.253
Ca4455	1.208	0.102	1.253	0.105	1.082	0.122	1.141	0.019	0.341	0.055	0.302	0.062	0.278	0.055	0.276	0.053
Fe4531	3.218	0.044	3.025	0.035	2.611	0.098	2.678	0.018	1.276	0.260	1.131	0.253	1.002	0.224	0.888	0.197
C ₂ 4668	0.705	0.192	0.335	0.144	-0.029	0.174	-0.359	0.165	-0.096	0.116	-0.072	0.091	-0.039	0.075	-0.006	0.079
H β	0.129	0.065	-0.085	0.026	-0.212	-0.009	-0.296	-0.077	1.666	0.061	1.389	0.042	1.167	0.033	1.046	0.014
Fe5015	3.714	-0.101	2.826	-0.226	2.068	-0.200	1.432	-0.250	1.435	0.267	1.372	0.249	1.285	0.237	1.136	0.231
Mg1	0.076	0.044	0.162	0.062	0.188	0.082	0.272	0.081	-0.004	0.000	-0.003	0.000	-0.004	0.001	-0.004	0.004
Mg2	0.165	0.068	0.303	0.095	0.353	0.124	0.459	0.099	0.022	0.005	0.026	0.009	0.036	0.017	0.057	0.031
MgB	1.966	0.902	3.586	1.133	4.091	1.336	4.374	0.762	0.372	0.151	0.528	0.285	0.959	0.547	1.723	0.955
Fe5270	2.168	0.103	2.555	0.001	2.516	-0.005	2.695	-0.207	0.526	0.158	0.550	0.149	0.606	0.138	0.704	0.126
Fe5335	2.085	0.053	2.294	-0.038	2.201	-0.078	2.437	-0.338	0.762	0.087	0.741	0.090	0.735	0.085	0.769	0.070
Fe5406	1.215	0.010	1.538	-0.074	1.594	-0.086	1.844	-0.287	0.274	-0.022	0.316	-0.015	0.358	-0.001	0.417	0.006
Fe5709	0.652	0.040	0.559	0.028	0.365	0.018	0.227	-0.012	0.085	0.016	0.091	0.016	0.090	0.017	0.077	0.017
Fe5782	0.254	-0.013	0.240	-0.026	0.153	-0.024	0.107	-0.030	0.020	0.000	0.022	0.000	0.022	0.001	0.019	0.001
NaD	1.030	-0.126	1.860	-0.237	2.550	-0.214	4.313	-0.724	0.286	-0.011	0.307	-0.013	0.394	-0.021	0.606	-0.030
TiO1	0.002	0.003	0.002	0.004	0.000	0.005	-0.001	0.003	0.000	0.000	0.000	0.000	0.000	0.000	-0.001	0.000
TiO2	0.015	0.000	0.014	0.002	0.010	0.005	0.006	0.002	0.001	0.000	0.001	0.000	0.001	0.000	0.000	0.000
H δ A	-3.633	1.244	-3.861	1.420	-3.422	1.295	-3.158	1.614	0.759	0.008	0.349	0.040	-0.278	0.119	-1.028	0.212
H γ A	-7.774	0.086	-9.516	0.809	-8.939	0.900	-9.083	1.805	-1.041	-0.133	-2.589	0.036	-4.228	0.289	-5.810	0.686
H δ F	-1.682	0.282	-1.887	0.409	-1.685	0.455	-1.473	0.689	1.075	0.049	0.750	0.070	0.344	0.113	-0.046	0.150
H γ F	-3.023	0.287	-3.953	0.688	-3.831	0.761	-3.823	1.129	0.667	0.038	-0.263	0.118	-1.319	0.263	-2.316	0.487
D4000	2.422	-0.130	2.335	-0.184	2.276	-0.152	2.312	-0.200	1.407	0.032	1.380	0.028	1.397	0.028	1.450	0.030

T_{eff}	7250								10000			13000				
$\log g$	1.5		2.5		3.5		4.5		2.5		3.5	4.5	2.5		3.5	4.5
	I_{sol}	(δI)														
CN1	-0.129	0.000	-0.235	0.000	-0.344	0.000	-0.077	0.000	-0.149	0.000	-0.235	0.000	-0.185	0.003	-0.197	0.002
CN2	-0.042	0.000	-0.137	0.000	-0.258	0.000	-0.016	0.000	-0.069	0.000	-0.152	0.000	-0.093	0.003	-0.113	0.002
Ca4227	0.018	0.000	0.010	0.002	0.003	0.006	0.007	0.000	0.006	0.000	0.002	0.000	0.032	0.027	0.044	0.022
G4300	-0.851	0.018	-2.462	0.020	-3.990	0.017	-0.416	0.000	-1.309	0.001	-2.598	-0.005	-1.320	0.192	-1.669	0.207
Fe4383	-0.175	0.005	-1.023	0.004	-3.234	0.004	0.075	0.003	-0.300	0.004	-1.318	-0.001	-0.166	0.043	-0.658	0.009
Ca4455	0.030	-0.020	0.014	-0.021	-0.002	-0.023	0.257	-0.023	0.236	-0.024	0.210	-0.021	-0.006	-0.007	0.017	-0.012
Fe4531	0.056	0.004	0.036	0.003	0.026	0.002	0.024	0.002	0.023	0.001	0.017	0.001	0.371	0.058	0.299	0.040
C ₂ 4668	0.052	0.000	0.047	0.000	-0.024	0.001	0.146	0.001	0.123	-0.001	0.099	-0.002	-0.170	0.031	-0.120	0.025
H β	6.063	-0.002	8.825	-0.003	9.741	-0.001	3.894	-0.001	6.203	-0.001	8.037	0.005	7.151	0.021	7.134	0.018
Fe5015	0.059	-0.044	0.043	-0.028	-0.034	-0.017	0.133	-0.059	0.087	-0.053	0.046	-0.039	0.200	0.022	0.164	0.023
Mg1	0.007	0.000	0.004	0.000	-0.007	0.000	0.008	0.000	0.007	0.000	0.003	0.000	0.001	0.000	-0.003	0.000
Mg2	0.009	0.000	0.008	0.001	-0.001	0.001	0.009	0.000	0.009	0.000	0.006	0.000	0.014	0.003	0.011	0.002
MgB	0.066	0.010	0.070	0.021	0.079	0.037	0.034	-0.002	0.035	0.000	0.028	0.001	0.383	0.111	0.384	0.101
Fe5270	-0.002	0.001	0.002	0.001	0.003	0.001	0.006	0.001	0.007	0.001	0.007	0.001	0.024	0.033	0.052	0.035
Fe5335	0.020	0.002	0.014	0.002	0.012	0.002	0.012	0.004	0.010	0.002	0.007	0.001	0.170	0.030	0.164	0.029
Fe5406	0.003	0.001	0.002	0.001	0.002	0.000	0.003	0.001	0.003	0.001	0.003	0.001	0.021	-0.016	0.036	-0.007
Fe5709	0.002	0.000	0.002	0.000	0.002	0.000	0.002	0.000	0.002	0.000	0.002	0.000	0.003	0.002	0.004	0.003
Fe5782	0.001	0.000	0.001	0.001	0.001	0.000	0.001	0.000	0.002	0.000	0.001	0.000	0.002	0.000	0.002	0.000
NaD	-0.031	0.000	-0.013	0.000	0.000	0.000	-0.136	-0.001	-0.102	-0.001	-0.075	-0.001	0.145	-0.001	0.155	-0.001
TiO1	0.003	0.000	0.003	0.000	0.003	0.000	0.003	0.000	0.003	0.000	0.003	0.000	0.002	0.000	0.001	0.000
TiO2	0.003	0.000	0.003	0.000	0.003	0.000	0.004	0.000	0.004	0.000	0.004	0.000	0.003	0.000	0.002	0.000
H δ A	6.543	-0.014	11.170	-0.013	15.360	-0.009	4.197	-0.016	7.510	-0.012	11.130	0.012	8.941	-0.026	9.384	-0.003
H γ A	6.628	-0.018	11.270	-0.019	15.520	-0.015	4.152	-0.003	7.445	-0.003	11.140	0.015	8.708	-0.108	9.262	-0.102
H δ F	5.935	-0.014	9.009	-0.010	10.460	-0.005	3.837	-0.016	6.380	-0.012	8.434	0.002	7.587	-0.008	7.484	0.004
H γ F	5.969	-0.005	8.880	-0.006	10.300	-0.004	3.885	-0.001	6.304	-0.001	8.291	0.008	7.366	-0.005	7.354	-0.005
D4000	1.080	0.001	1.199	0.001	1.377	0.001	1.017	0.000	1.084	0.000	1.187	0.001	1.217	0.008	1.276	0.007

Absorption line indices from high resolution spectra. I. New Response Functions

Table A2. 1-Å resolution spectra: I_{sol} and $I_{\text{enh}} - I_{\text{sol}}$ for $[Z/Z_{\odot}] = -1.5$

T_{eff}	4000								5250							
	1.5		2.5		3.5		4.5		1.5		2.5		3.5		4.5	
	I_{sol}	(δI)														
CN1	0.082	0.007	0.088	0.022	0.072	0.031	0.051	0.030	-0.032	0.001	-0.039	0.003	-0.043	0.006	-0.046	0.013
CN2	0.150	0.018	0.178	0.030	0.171	0.043	0.158	0.037	-0.006	0.002	-0.018	0.005	-0.029	0.011	-0.038	0.021
Ca4227	1.041	1.791	2.400	1.764	3.824	1.872	5.133	1.518	0.160	0.143	0.055	0.218	0.050	0.347	0.250	0.556
G4300	8.389	-0.879	8.376	-1.330	7.356	-1.067	5.699	-1.084	5.157	0.054	6.424	-0.181	7.216	-0.444	8.064	-0.922
Fe4383	6.349	-1.099	7.111	-1.565	6.858	-1.241	6.265	-1.374	1.685	0.033	1.888	-0.069	2.329	-0.317	2.985	-0.609
Ca4455	1.751	0.075	1.843	0.046	1.691	0.151	1.538	0.069	0.580	0.015	0.515	0.031	0.465	0.054	0.459	0.067
Fe4531	4.012	0.037	3.818	-0.004	3.482	0.149	3.317	0.095	2.032	0.268	1.877	0.279	1.713	0.264	1.584	0.236
C ₂ 4668	1.390	0.063	0.795	0.141	0.246	0.379	-0.242	0.422	-0.018	0.156	-0.011	0.126	0.014	0.099	0.041	0.096
H β	0.093	0.058	-0.200	0.028	-0.395	0.024	-0.476	-0.022	1.787	0.098	1.464	0.090	1.213	0.071	1.056	0.044
Fe5015	4.747	-0.274	3.736	-0.264	2.934	-0.057	2.134	-0.042	2.497	0.384	2.376	0.362	2.256	0.331	2.119	0.295
Mg1	0.131	0.048	0.230	0.052	0.279	0.085	0.331	0.087	0.001	0.000	0.001	0.001	0.000	0.002	0.001	0.007
Mg2	0.241	0.079	0.397	0.090	0.482	0.147	0.531	0.130	0.030	0.007	0.038	0.013	0.057	0.024	0.093	0.045
Mgb	2.632	1.099	4.334	1.271	5.007	1.750	4.601	1.267	0.308	0.223	0.626	0.419	1.360	0.755	2.590	1.293
Fe5270	2.849	0.041	3.231	-0.100	3.331	-0.053	3.278	-0.159	0.872	0.241	0.890	0.238	0.983	0.223	1.180	0.200
Fe5335	2.840	0.008	3.056	-0.154	3.011	-0.139	2.944	-0.331	1.110	0.129	1.115	0.138	1.150	0.138	1.258	0.124
Fe5406	1.687	-0.022	2.042	-0.166	2.174	-0.134	2.204	-0.259	0.403	0.023	0.457	0.014	0.541	0.011	0.672	0.008
Fe5709	0.952	0.074	0.830	0.055	0.613	0.061	0.378	0.015	0.210	0.037	0.220	0.038	0.220	0.037	0.203	0.036
Fe5782	0.491	-0.033	0.468	-0.066	0.339	-0.066	0.220	-0.072	0.055	0.003	0.061	0.003	0.062	0.003	0.058	0.003
NaD	1.563	-0.180	2.744	-0.398	3.994	-0.308	5.614	-0.695	0.332	-0.027	0.379	-0.036	0.542	-0.062	0.910	-0.095
TiO1	0.006	0.004	0.005	0.007	0.005	0.015	0.002	0.014	0.000	0.000	0.000	0.000	0.000	0.000	0.000	0.000
TiO2	0.025	0.001	0.024	0.007	0.022	0.021	0.014	0.018	0.004	0.001	0.003	0.001	0.003	0.001	0.002	0.001
H δ A	-5.011	1.471	-5.262	1.690	-4.782	1.360	-3.510	1.324	0.258	0.065	-0.193	0.158	-0.932	0.312	-1.945	0.496
H γ A	-9.139	0.177	-10.690	0.988	-10.540	0.684	-9.443	1.217	-2.950	-0.006	-4.475	0.236	-5.746	0.523	-7.302	1.026
H δ F	-2.400	0.217	-2.641	0.426	-2.425	0.418	-1.727	0.553	0.774	0.089	0.489	0.136	0.094	0.208	-0.382	0.291
H γ F	-3.279	0.293	-4.072	0.648	-4.115	0.552	-3.576	0.699	-0.039	0.117	-1.045	0.272	-1.959	0.446	-2.947	0.726
D4000	2.633	-0.131	2.571	-0.223	2.548	-0.197	2.448	-0.193	1.487	0.052	1.456	0.040	1.484	0.031	1.565	0.025

T_{eff}	7250				10000			13000												
	1.5		2.5		3.5		4.5		2.5		3.5		4.5							
	I_{sol}	(δI)																		
CN1	-0.181	0.003	-0.195	0.002	-0.188	0.002	-0.171	0.001	-0.127	0.000	-0.232	0.000	-0.343	0.001	-0.075	0.000	-0.146	0.000	-0.233	0.000
CN2	-0.088	0.003	-0.110	0.002	-0.110	0.002	-0.099	0.001	-0.041	0.000	-0.134	0.000	-0.256	0.001	-0.015	0.000	-0.067	0.000	-0.150	0.000
Ca4227	0.061	0.035	0.070	0.030	0.080	0.026	0.094	0.030	0.033	0.001	0.022	0.004	0.016	0.014	0.016	0.001	0.015	0.000	0.008	0.000
G4300	-1.061	0.215	-1.396	0.233	-1.435	0.245	-1.296	0.240	-0.799	0.042	-2.396	0.047	-3.966	0.045	-0.415	-0.006	-1.284	-0.007	-2.571	-0.004
Fe4383	0.124	0.090	-0.457	0.041	-0.740	0.008	-0.769	-0.024	-0.139	0.013	-0.970	0.009	-3.164	0.007	0.087	0.011	-0.279	0.009	-1.288	0.004
Ca4455	0.016	0.038	0.031	0.018	0.061	0.000	0.090	-0.003	0.001	-0.010	-0.013	-0.014	-0.030	-0.019	0.228	-0.016	0.207	-0.017	0.184	-0.021
Fe4531	0.661	0.119	0.558	0.099	0.457	0.074	0.374	0.055	0.113	0.009	0.081	0.008	0.062	0.006	0.046	0.007	0.046	0.004	0.032	0.003
C ₂ 4668	-0.277	0.077	-0.210	0.056	-0.144	0.038	-0.080	0.030	-0.007	-0.001	0.011	0.001	-0.043	0.004	0.096	0.003	0.094	-0.001	0.083	-0.001
H β	7.225	0.044	7.213	0.036	6.761	0.029	6.170	0.026	6.015	0.008	8.781	-0.001	9.752	0.000	3.833	0.023	6.134	0.019	7.986	0.009
Fe5015	0.402	0.061	0.377	0.062	0.345	0.061	0.319	0.059	0.038	-0.067	0.041	-0.051	-0.022	-0.038	0.091	-0.074	0.049	-0.078	0.019	-0.069
Mg1	-0.001	0.000	-0.005	0.000	-0.007	0.000	-0.007	0.000	0.007	0.000	0.004	0.000	-0.007	0.000	0.007	0.000	0.007	0.000	0.003	0.000
Mg2	0.018	0.003	0.015	0.003	0.013	0.003	0.013	0.004	0.010	0.001	0.008	0.001	0.001	0.002	0.009	0.000	0.009	0.000	0.006	0.000
Mgb	0.473	0.104	0.460	0.108	0.448	0.116	0.484	0.161	0.081	0.025	0.108	0.046	0.143	0.064	0.043	-0.005	0.050	0.000	0.047	0.004
Fe5270	0.110	0.085	0.140	0.089	0.168	0.090	0.193	0.089	-0.012	0.004	-0.005	0.004	0.000	0.005	0.006	0.002	0.006	0.003	0.007	0.002
Fe5335	0.318	0.059	0.325	0.065	0.318	0.067	0.304	0.068	0.042	0.006	0.032	0.006	0.027	0.006	0.025	0.012	0.020	0.006	0.014	0.004
Fe5406	0.046	-0.027	0.078	-0.013	0.100	0.000	0.114	0.009	0.007	0.002	0.005	0.002	0.004	0.002	0.006	0.002	0.006	0.003	0.005	0.002
Fe5709	0.006	0.007	0.011	0.009	0.014	0.009	0.015	0.009	0.002	0.000	0.002	0.000	0.002	0.000	0.002	0.000	0.002	0.000	0.002	0.000
Fe5782	0.005	0.000	0.005	0.001	0.005	0.001	0.005	0.001	0.003	-0.001	0.002	0.000	0.002	0.000	0.002	-0.001	0.002	-0.001	0.002	0.000
NaD	0.204	-0.002	0.208	-0.003	0.207	-0.003	0.211	-0.004	-0.027	-0.001	-0.005	-0.001	0.015	0.000	-0.136	-0.003	-0.102	-0.002	-0.075	-0.001
TiO1	0.002	0.000	0.002	0.000	0.001	0.000	0.001	0.000	0.003	0.000	0.003	0.000	0.003	0.000	0.003	0.001	0.003	0.000	0.003	0.000
TiO2	0.003	0.000	0.002	0.000	0.002	0.000	0.001	0.000	0.003	0.000	0.003	0.000	0.003	0.000	0.004	0.000	0.004	0.000	0.004	0.000
H δ A	8.793	-0.041	9.333	-0.008	8.945	0.007	8.122	0.026	6.439	-0.003	11.040	-0.010	15.300	-0.014	4.092	0.010	7.384	0.020	11.030	0.013
H γ A	8.480	-0.123	9.105	-0.107	8.839	-0.106	8.074	-0.092	6.535	-0.025	11.160	-0.032	15.470	-0.032	4.072	0.023	7.340	0.025	11.050	0.016
H δ F	7.516	-0.010	7.457	0.007	6.984	0.017	6.336	0.027	5.851	-0.005	8.936	-0.009	10.450	-0.009	3.742	0.007	6.279	0.010	8.366	0.001
H γ F	7.326	0.005	7.349	0.005	6.935	0.002	6.320	0.004	5.915	0.002	8.826	-0.007	10.300	-0.007	3.819	0.025	6.229	0.022	8.238	0.010
D4000	1.234	0.013	1.293	0.012	1.311	0.011	1.311	0.012	1.079	0.001	1.197	0.001	1.376	0.002	1.017	0.000	1.082	0.000	1.185	0.001

Table A3. 1-Å resolution spectra: I_{sol} and $I_{\text{enh}} - I_{\text{sol}}$ for $[Z/Z_{\odot}]=-1.0$

T_{eff}	4000								5250							
log g	1.5		2.5		3.5		4.5		1.5		2.5		3.5		4.5	
	I_{sol}	(δI)														
CN1	0.135	-0.028	0.120	-0.007	0.090	0.007	0.045	0.017	-0.042	-0.001	-0.043	-0.001	-0.041	0.001	-0.040	0.005
CN2	0.222	-0.021	0.226	-0.005	0.212	0.008	0.164	0.017	-0.017	0.003	-0.022	0.004	-0.024	0.008	-0.025	0.016
Ca4227	2.303	2.289	3.863	1.913	5.836	1.509	6.731	1.204	0.209	0.293	0.037	0.424	0.053	0.588	0.441	0.803
G4300	8.401	-0.765	8.144	-1.090	7.652	-0.936	5.594	-0.399	7.032	-0.231	7.585	-0.317	7.819	-0.466	8.264	-0.862
Fe4383	7.784	-1.286	8.451	-1.812	8.915	-1.924	7.486	-1.569	2.710	-0.224	3.193	-0.448	3.800	-0.788	4.728	-1.297
Ca4455	2.336	0.044	2.440	0.018	2.460	0.081	2.109	0.093	0.849	0.043	0.782	0.047	0.731	0.070	0.747	0.095
Fe4531	4.905	0.123	4.668	0.047	4.577	0.116	4.168	0.160	3.000	0.126	2.874	0.111	2.712	0.093	2.604	0.047
C ₂ 4668	2.269	-0.120	1.376	0.305	0.722	0.933	0.103	1.189	0.512	0.007	0.478	-0.020	0.436	-0.029	0.377	0.006
H β	0.031	0.056	-0.326	0.087	-0.593	0.167	-0.669	0.157	1.870	0.188	1.539	0.184	1.247	0.177	1.027	0.147
Fe5015	5.780	-0.174	4.799	-0.036	4.258	0.297	3.256	0.380	4.109	0.297	3.888	0.266	3.713	0.191	3.618	0.047
Mg1	0.195	0.042	0.286	0.039	0.370	0.053	0.399	0.078	0.010	0.000	0.009	0.001	0.008	0.003	0.009	0.013
Mg2	0.331	0.085	0.482	0.091	0.624	0.123	0.630	0.149	0.045	0.009	0.056	0.017	0.085	0.031	0.142	0.060
MgB	3.380	1.399	4.998	1.537	6.022	1.785	5.153	1.706	0.306	0.337	0.795	0.593	1.852	1.010	3.595	1.640
Fe5270	3.586	-0.068	3.870	-0.218	4.204	-0.254	4.004	-0.186	1.485	0.211	1.521	0.181	1.690	0.121	2.041	0.039
Fe5335	3.744	-0.094	3.899	-0.308	4.054	-0.433	3.670	-0.451	1.650	0.090	1.738	0.076	1.873	0.030	2.138	-0.045
Fe5406	2.272	-0.113	2.584	-0.267	2.894	-0.320	2.728	-0.293	0.706	-0.011	0.772	-0.025	0.918	-0.073	1.188	-0.145
Fe5709	1.324	0.100	1.161	0.077	0.950	0.074	0.607	0.061	0.488	0.017	0.499	0.012	0.500	0.004	0.479	-0.005
Fe5782	0.833	-0.065	0.775	-0.123	0.626	-0.170	0.401	-0.167	0.136	0.014	0.150	0.013	0.155	0.010	0.153	0.008
NaD	2.448	-0.294	3.908	-0.596	6.147	-0.879	7.656	-0.994	0.423	-0.051	0.513	-0.076	0.765	-0.119	1.309	-0.172
TiO1	0.011	0.007	0.011	0.017	0.016	0.034	0.012	0.040	0.002	0.001	0.002	0.001	0.002	0.001	0.001	0.001
TiO2	0.039	0.006	0.038	0.022	0.045	0.049	0.035	0.060	0.009	0.000	0.008	0.000	0.007	0.000	0.006	0.000
H δ A	-7.093	2.026	-6.977	2.119	-6.823	1.896	-4.447	1.107	-0.614	0.281	-1.117	0.517	-1.995	0.849	-3.473	1.364
H γ A	-10.740	0.212	-11.950	1.021	-12.810	1.101	-10.640	0.785	-4.985	0.303	-5.887	0.434	-6.744	0.681	-8.246	1.295
H δ F	-3.441	0.244	-3.515	0.465	-3.443	0.555	-2.226	0.431	0.342	0.170	0.139	0.249	-0.224	0.374	-0.844	0.585
H γ F	-3.662	0.297	-4.236	0.569	-4.582	0.554	-3.715	0.360	-0.751	0.283	-1.488	0.387	-2.161	0.524	-3.076	0.824
D4000	2.938	-0.121	2.847	-0.243	2.905	-0.284	2.655	-0.201	1.649	0.056	1.617	0.022	1.662	-0.008	1.790	-0.047

T_{eff}	7250								10000						13000					
log g	1.5		2.5		3.5		4.5		2.5		3.5		4.5		2.5		3.5		4.5	
	I_{sol}	(δI)																		
CN1	-0.173	0.002	-0.191	0.002	-0.184	0.002	-0.169	0.001	-0.125	0.002	-0.229	0.001	-0.342	0.003	-0.073	0.002	-0.144	0.002	-0.231	0.002
CN2	-0.080	0.003	-0.106	0.002	-0.106	0.002	-0.097	0.001	-0.039	0.002	-0.131	0.002	-0.255	0.003	-0.013	0.001	-0.065	0.002	-0.148	0.002
Ca4227	0.122	0.022	0.121	0.026	0.123	0.028	0.141	0.038	0.049	-0.007	0.044	-0.002	0.051	0.008	0.041	-0.007	0.040	-0.008	0.029	-0.007
G4300	-0.758	0.296	-1.086	0.295	-1.093	0.278	-0.933	0.261	-0.729	0.115	-2.310	0.125	-3.928	0.123	-0.431	0.006	-1.281	0.025	-2.554	0.035
Fe4383	0.328	0.207	-0.313	0.150	-0.620	0.082	-0.694	0.006	-0.057	0.020	-0.861	0.017	-3.055	0.039	0.137	0.000	-0.228	0.012	-1.241	0.030
Ca4455	0.155	0.054	0.133	0.047	0.125	0.031	0.140	0.010	-0.025	-0.002	-0.037	-0.008	-0.055	-0.017	0.221	-0.026	0.204	-0.030	0.178	-0.036
Fe4531	1.166	0.103	1.040	0.110	0.896	0.093	0.772	0.065	0.229	-0.004	0.183	-0.006	0.155	-0.011	0.104	0.003	0.105	-0.004	0.081	-0.006
C ₂ 4668	-0.301	0.114	-0.262	0.089	-0.208	0.064	-0.127	0.045	-0.155	0.025	-0.096	0.028	-0.118	0.035	-0.019	0.024	0.007	0.011	0.031	0.006
H β	7.340	0.093	7.346	0.069	6.903	0.050	6.320	0.036	5.968	0.018	8.721	0.041	9.760	0.012	3.830	-0.057	6.103	-0.046	7.948	-0.037
Fe5015	1.061	-0.005	1.057	-0.002	1.006	-0.005	0.952	-0.008	0.026	-0.108	0.036	-0.091	-0.015	-0.080	0.069	-0.103	0.019	-0.122	-0.009	-0.123
Mg1	-0.002	0.000	-0.005	0.000	-0.007	-0.001	-0.008	-0.001	0.006	0.000	0.003	0.000	-0.008	0.001	0.007	0.000	0.007	0.000	0.003	0.000
Mg2	0.024	0.001	0.021	0.002	0.018	0.002	0.020	0.005	0.010	0.001	0.010	0.002	0.003	0.002	0.009	0.000	0.009	0.000	0.007	0.000
MgB	0.463	0.122	0.443	0.141	0.446	0.178	0.548	0.287	0.085	0.066	0.149	0.085	0.221	0.083	0.026	-0.005	0.043	0.005	0.057	0.011
Fe5270	0.387	0.101	0.405	0.123	0.410	0.135	0.419	0.144	-0.010	0.005	-0.011	0.011	-0.003	0.014	0.008	0.004	0.009	0.006	0.009	0.007
Fe5335	0.593	0.029	0.628	0.048	0.635	0.065	0.630	0.081	0.088	0.007	0.078	0.004	0.078	0.003	0.061	0.020	0.051	0.009	0.037	0.004
Fe5406	0.129	-0.046	0.181	-0.043	0.223	-0.032	0.251	-0.016	0.023	0.001	0.015	0.002	0.012	0.003	0.019	0.002	0.020	0.003	0.016	0.004
Fe5709	0.023	0.014	0.040	0.015	0.051	0.013	0.056	0.010	0.000	0.001	0.001	0.001	0.002	0.001	0.001	0.002	0.001	0.002	0.002	0.001
Fe5782	0.014	0.001	0.014	0.002	0.013	0.003	0.013	0.004	0.008	-0.004	0.005	-0.002	0.003	-0.001	0.007	-0.005	0.007	-0.005	0.005	-0.003
NaD	0.244	0.003	0.241	0.001	0.237	-0.001	0.247	-0.004	-0.017	-0.002	0.012	0.000	0.047	-0.002	-0.138	-0.002	-0.106	-0.001	-0.078	0.000
TiO1	0.003	0.000	0.002	0.000	0.002	0.000	0.001	0.000	0.003	0.000	0.003	0.000	0.003	0.000	0.004	0.001	0.004	0.001	0.004	0.000
TiO2	0.004	0.000	0.004	0.000	0.003	0.000	0.002	0.000	0.004	0.000	0.004	0.000	0.003	0.000	0.004	0.000	0.004	0.000	0.004	0.000
H δ A	8.520	-0.004	9.237	0.009	8.883	0.026	8.110	0.067	6.347	-0.058	10.910	-0.040	15.250	-0.073	4.058	-0.110	7.329	-0.109	10.970	-0.102
H γ A	8.217	-0.166	8.955	-0.141	8.707	-0.114	7.983	-0.082	6.427	-0.101	11.020	-0.084	15.420	-0.120	4.061	-0.082	7.297	-0.091	10.990	-0.095
H δ F	7.345	0.051	7.368	0.055	6.920	0.064	6.304	0.080	5.775	-0.038	8.850	-0.009	10.420	-0.017	3.703	-0.085	6.221	-0.075	8.304	-0.059
H γ F	7.294	0.010	7.374	0.001	6.977	-0.001	6.384	0.003	5.864	-0.026	8.764	-0.002	10.290	-0.021	3.825	-0.068	6.206	-0.060	8.201	-0.047
D4000	1.264	0.019	1.323	0.017	1.340	0.016	1.341	0.017	1.079	0.000	1.196	0.000	1.378	-0.001	1.016	0.000	1.081	-0.001	1.183	-0.002

Absorption line indices from high resolution spectra. I. New Response Functions

Table A4. 1-Å resolution spectra: I_{sol} and $I_{\text{enh}} - I_{\text{sol}}$ for $[Z/Z_{\odot}] = -0.5$

T_{eff}	4000								5250							
	1.5		2.5		3.5		4.5		1.5		2.5		3.5		4.5	
	I_{sol}	(δI)														
CN1	0.185	-0.062	0.151	-0.040	0.099	-0.020	0.030	0.002	-0.027	-0.016	-0.021	-0.018	-0.019	-0.016	-0.022	-0.009
CN2	0.284	-0.060	0.267	-0.044	0.235	-0.030	0.164	-0.003	0.000	-0.011	0.004	-0.013	0.005	-0.009	0.003	0.001
Ca4227	4.300	2.245	5.563	1.656	7.370	0.864	8.053	0.623	0.104	0.641	-0.081	0.814	-0.010	0.979	0.605	1.178
G4300	8.423	-0.536	8.049	-0.799	7.884	-0.819	6.068	0.276	7.898	-0.220	8.050	-0.286	8.039	-0.439	8.219	-0.822
Fe4383	9.299	-1.504	9.703	-2.117	10.640	-2.708	9.187	-1.864	3.774	-0.423	4.371	-0.668	5.023	-0.998	6.104	-1.582
Ca4455	2.945	0.047	3.024	0.022	3.204	-0.004	2.847	0.119	1.178	0.100	1.133	0.085	1.118	0.081	1.176	0.094
Fe4531	6.042	0.243	5.709	0.060	5.819	-0.113	5.348	0.158	3.951	0.018	3.826	-0.016	3.683	-0.055	3.597	-0.102
C ₂ 4668	3.171	-0.148	2.070	0.981	1.529	2.371	0.943	3.152	1.527	-0.153	1.490	-0.230	1.304	-0.214	1.047	-0.102
H β	-0.097	0.136	-0.429	0.322	-0.680	0.635	-0.797	0.724	2.064	0.222	1.755	0.207	1.436	0.202	1.149	0.182
Fe5015	7.168	0.229	6.287	0.431	6.154	0.771	5.004	1.307	5.867	0.286	5.495	0.248	5.216	0.139	5.107	-0.089
Mg ₁	0.258	0.024	0.330	0.014	0.419	0.001	0.465	0.050	0.027	-0.002	0.027	-0.003	0.024	0.002	0.026	0.018
Mg ₂	0.432	0.088	0.568	0.082	0.728	0.067	0.751	0.135	0.070	0.010	0.085	0.019	0.124	0.039	0.203	0.075
Mg _b	4.242	1.854	5.729	1.794	6.816	1.582	5.959	1.768	0.489	0.436	1.105	0.748	2.487	1.248	4.763	1.902
Fe5270	4.333	-0.207	4.473	-0.376	4.927	-0.545	4.839	-0.270	2.241	0.215	2.280	0.153	2.482	0.078	2.927	-0.015
Fe5335	4.798	-0.261	4.829	-0.563	5.076	-0.921	4.618	-0.749	2.292	0.110	2.472	0.069	2.701	-0.007	3.097	-0.121
Fe5406	2.952	-0.220	3.187	-0.371	3.595	-0.536	3.421	-0.340	1.024	-0.030	1.121	-0.042	1.304	-0.097	1.673	-0.196
Fe5709	1.768	0.096	1.545	0.059	1.320	0.037	0.925	0.104	0.854	0.046	0.847	0.030	0.834	0.014	0.801	-0.002
Fe5782	1.224	-0.112	1.103	-0.225	0.912	-0.363	0.627	-0.378	0.300	0.035	0.326	0.029	0.335	0.021	0.337	0.012
NaD	3.782	-0.483	5.376	-0.959	8.272	-1.803	10.170	-1.708	0.604	-0.072	0.738	-0.115	1.093	-0.174	1.855	-0.252
TiO ₁	0.019	0.021	0.025	0.044	0.043	0.077	0.042	0.100	0.002	0.001	0.002	0.001	0.002	0.001	0.002	0.001
TiO ₂	0.059	0.026	0.066	0.062	0.091	0.107	0.086	0.143	0.015	0.000	0.013	0.000	0.012	0.000	0.011	-0.001
H δ A	-9.627	2.690	-8.909	2.708	-8.914	2.685	-6.115	1.030	-1.726	0.568	-2.217	0.897	-3.101	1.323	-4.768	1.974
H γ A	-12.710	0.151	-13.440	1.035	-14.850	1.661	-12.740	0.235	-6.216	0.275	-6.763	0.399	-7.451	0.696	-8.910	1.427
H δ F	-4.793	0.438	-4.506	0.653	-4.404	0.845	-3.000	0.400	-0.016	0.165	-0.109	0.254	-0.402	0.408	-1.066	0.681
H γ F	-4.253	0.269	-4.545	0.467	-4.960	0.525	-4.198	-0.050	-1.043	0.347	-1.582	0.399	-2.147	0.536	-2.979	0.850
D4000	3.370	-0.128	3.158	-0.263	3.235	-0.375	2.936	-0.218	1.894	0.070	1.821	0.030	1.857	-0.013	2.017	-0.077

T_{eff}	7250								10000						13000					
	1.5		2.5		3.5		4.5		2.5		3.5		4.5		2.5		3.5		4.5	
	I_{sol}	(δI)																		
CN1	-0.164	0.001	-0.188	0.001	-0.183	0.001	-0.171	0.001	-0.123	0.004	-0.228	0.004	-0.341	0.006	-0.070	0.003	-0.141	0.003	-0.227	0.003
CN2	-0.071	0.002	-0.102	0.001	-0.103	0.002	-0.098	0.001	-0.037	0.003	-0.129	0.005	-0.253	0.006	-0.011	0.002	-0.062	0.003	-0.144	0.003
Ca4227	0.179	0.017	0.165	0.033	0.159	0.049	0.185	0.077	0.043	-0.004	0.046	0.006	0.070	0.006	0.057	-0.006	0.056	-0.006	0.047	-0.008
G4300	-0.385	0.353	-0.707	0.337	-0.679	0.311	-0.466	0.274	-0.622	0.173	-2.186	0.206	-3.831	0.213	-0.442	-0.007	-1.256	0.028	-2.502	0.050
Fe4383	0.474	0.223	-0.194	0.189	-0.488	0.126	-0.549	0.010	0.027	0.057	-0.723	0.054	-2.892	0.099	0.200	0.010	-0.154	0.028	-1.142	0.048
Ca4455	0.345	0.062	0.305	0.044	0.260	0.034	0.229	0.026	-0.048	-0.008	-0.062	-0.018	-0.081	-0.033	0.199	-0.012	0.187	-0.018	0.160	-0.031
Fe4531	1.769	0.113	1.655	0.149	1.476	0.164	1.302	0.152	0.373	0.009	0.320	0.000	0.286	-0.015	0.179	0.015	0.183	0.007	0.149	0.001
C ₂ 4668	-0.189	0.112	-0.174	0.084	-0.173	0.063	-0.131	0.050	-0.363	0.027	-0.252	0.038	-0.225	0.058	-0.195	0.039	-0.147	0.014	-0.080	0.007
H β	7.475	0.137	7.506	0.118	7.085	0.099	6.512	0.083	6.012	-0.004	8.802	-0.022	9.835	-0.041	3.760	-0.066	6.024	-0.058	7.885	-0.059
Fe5015	2.144	0.010	2.125	0.029	2.005	0.031	1.876	0.027	0.028	-0.124	0.031	-0.116	-0.010	-0.117	0.059	-0.101	-0.019	-0.135	-0.068	-0.159
Mg ₁	0.001	-0.001	-0.003	-0.001	-0.006	-0.002	-0.007	-0.002	0.007	-0.001	0.003	0.000	-0.009	0.001	0.008	-0.001	0.007	-0.001	0.003	0.000
Mg ₂	0.030	0.000	0.026	0.001	0.025	0.003	0.029	0.008	0.012	0.002	0.012	0.002	0.005	0.002	0.009	-0.001	0.009	0.000	0.007	0.001
Mg _b	0.361	0.145	0.340	0.174	0.403	0.242	0.666	0.434	0.113	0.106	0.214	0.108	0.297	0.093	-0.031	0.000	0.005	0.017	0.045	0.033
Fe5270	0.753	0.184	0.776	0.211	0.772	0.229	0.773	0.253	0.037	0.005	0.019	0.016	0.028	0.025	0.026	0.004	0.029	0.010	0.024	0.016
Fe5335	0.856	0.058	0.941	0.080	0.994	0.111	1.036	0.158	0.134	0.035	0.139	0.029	0.157	0.026	0.114	0.043	0.092	0.032	0.073	0.022
Fe5406	0.269	-0.023	0.326	-0.029	0.378	-0.032	0.426	-0.015	0.064	-0.003	0.043	0.003	0.034	0.008	0.049	0.003	0.054	0.006	0.043	0.010
Fe5709	0.063	0.033	0.106	0.033	0.131	0.029	0.142	0.021	-0.004	0.004	-0.001	0.003	0.002	0.004	-0.002	0.005	-0.001	0.005	0.000	0.003
Fe5782	0.038	0.003	0.038	0.006	0.037	0.008	0.037	0.009	0.022	-0.010	0.013	-0.005	0.008	-0.002	0.017	-0.014	0.018	-0.013	0.013	-0.009
NaD	0.284	-0.003	0.278	-0.011	0.276	-0.017	0.303	-0.023	0.016	-0.010	0.055	-0.006	0.100	-0.008	-0.126	-0.012	-0.097	-0.011	-0.071	-0.007
TiO ₁	0.003	0.000	0.003	0.000	0.002	0.000	0.002	0.000	0.005	0.001	0.004	0.000	0.003	0.000	0.005	0.001	0.005	0.001	0.005	0.001
TiO ₂	0.006	0.000	0.005	0.000	0.004	0.000	0.003	0.000	0.005	0.000	0.004	0.000	0.004	0.000	0.004	0.000	0.004	0.000	0.004	0.000
H δ A	8.149	0.015	9.134	0.052	8.816	0.056	8.145	0.102	6.211	-0.095	10.810	-0.118	15.170	-0.162	3.907	-0.133	7.156	-0.137	10.790	-0.135
H γ A	7.962	-0.228	8.821	-0.173	8.567	-0.133	7.856	-0.059	6.290	-0.167	10.910	-0.196	15.340	-0.245	3.948	-0.093	7.146	-0.119	10.830	-0.136
H δ F	7.113	0.097	7.253	0.109	6.843	0.109	6.284	0.126	5.693	-0.066	8.820	-0.066	10.420	-0.063	3.578	-0.098	6.089	-0.094	8.191	-0.086
H γ F	7.270	-0.009	7.414	-0.004	7.030	0.000	6.447	0.020	5.817	-0.050	8.768	-0.062	10.310	-0.078	3.750	-0.072	6.115	-0.075	8.122	-0.073
D4000	1.307	0.035	1.368	0.033	1.383	0.029	1.386	0.030	1.081	0.000	1.198	-0.001	1.381	-0.004	1.014	-0.001	1.078	-0.002	1.178	-0.002

Table A5. Spectra degraded to the Lick resolution: I_{sol} and $I_{\text{enh}} - I_{\text{sol}}$ for $[Z/Z_{\odot}] = -2.0$

T_{eff}	4000								5250							
	1.5		2.5		3.5		4.5		1.5		2.5		3.5		4.5	
$\log g$	I_{sol}	(δI)														
CN1	0.013	0.022	0.022	0.039	0.018	0.043	0.018	0.044	-0.032	0.001	-0.037	0.002	-0.044	0.004	-0.051	0.009
CN2	0.057	0.034	0.086	0.051	0.086	0.057	0.103	0.054	-0.013	0.002	-0.022	0.003	-0.034	0.006	-0.046	0.012
Ca4227	0.233	0.870	0.870	1.043	1.559	1.120	2.759	0.958	0.101	0.060	0.095	0.087	0.123	0.146	0.228	0.246
G4300	7.895	-0.882	8.195	-1.407	6.921	-1.399	5.957	-1.831	2.689	0.180	4.085	0.013	5.413	-0.235	6.552	-0.646
Fe4383	4.497	-0.817	5.123	-1.060	4.775	-0.874	5.085	-1.207	1.016	0.089	1.025	0.021	1.242	-0.092	1.671	-0.228
Ca4455	0.765	0.065	0.803	0.050	0.668	0.048	0.671	-0.040	0.222	0.012	0.196	0.021	0.178	0.018	0.173	0.014
Fe4531	2.854	0.109	2.748	0.108	2.433	0.160	2.545	0.078	1.019	0.239	0.926	0.239	0.845	0.217	0.771	0.193
C ₂ 4668	0.701	0.114	0.331	0.079	0.034	0.120	-0.217	0.114	0.032	0.105	0.036	0.088	0.040	0.077	0.042	0.082
H β	0.237	0.027	0.049	-0.008	-0.097	-0.025	-0.198	-0.077	1.671	0.051	1.424	0.039	1.221	0.035	1.108	0.020
Fe5015	3.121	-0.103	2.263	-0.209	1.659	-0.158	1.170	-0.140	1.217	0.276	1.154	0.261	1.069	0.251	0.924	0.247
Mg1	0.075	0.043	0.162	0.062	0.188	0.082	0.271	0.080	-0.004	0.000	-0.003	0.000	-0.004	0.001	-0.004	0.004
Mg2	0.165	0.068	0.303	0.095	0.353	0.124	0.459	0.100	0.022	0.005	0.026	0.009	0.036	0.017	0.056	0.031
Mgb	1.996	0.877	3.599	1.119	4.096	1.315	4.431	0.743	0.361	0.139	0.515	0.269	0.937	0.523	1.681	0.916
Fe5270	1.895	0.075	2.244	-0.023	2.209	-0.023	2.382	-0.193	0.484	0.154	0.500	0.145	0.541	0.133	0.621	0.121
Fe5335	1.756	0.039	1.986	-0.051	1.954	-0.093	2.197	-0.325	0.615	0.085	0.606	0.087	0.616	0.082	0.672	0.067
Fe5406	1.099	-0.022	1.362	-0.097	1.394	-0.104	1.595	-0.269	0.276	-0.013	0.311	-0.010	0.345	-0.001	0.394	0.005
Fe5709	0.561	0.035	0.478	0.023	0.310	0.018	0.189	-0.006	0.077	0.016	0.084	0.016	0.083	0.016	0.072	0.016
Fe5782	0.200	-0.008	0.191	-0.022	0.120	-0.023	0.083	-0.029	0.014	0.001	0.015	0.001	0.015	0.001	0.013	0.001
NaD	0.991	-0.139	1.818	-0.253	2.510	-0.231	4.250	-0.731	0.278	-0.017	0.299	-0.020	0.387	-0.028	0.601	-0.038
TiO1	0.002	0.002	0.002	0.003	0.000	0.005	-0.001	0.003	0.000	0.000	0.000	0.000	0.000	0.000	0.000	0.000
TiO2	0.014	0.000	0.013	0.002	0.009	0.005	0.005	0.002	0.001	0.000	0.001	0.000	0.000	0.000	0.000	0.000
H δ A	-3.253	1.220	-3.441	1.377	-3.017	1.265	-2.701	1.541	0.851	0.009	0.413	0.042	-0.226	0.124	-0.962	0.222
H γ A	-8.226	0.234	-9.946	0.981	-9.170	1.027	-9.156	1.923	-1.062	-0.106	-2.646	0.065	-4.342	0.331	-5.971	0.753
H δ F	-1.607	0.268	-1.777	0.373	-1.616	0.412	-1.463	0.632	0.979	0.035	0.697	0.054	0.329	0.094	-0.033	0.130
H γ F	-2.862	0.264	-3.692	0.641	-3.563	0.718	-3.549	1.072	0.608	0.041	-0.280	0.119	-1.272	0.256	-2.189	0.464
D4000	2.428	-0.131	2.336	-0.184	2.275	-0.153	2.305	-0.198	1.408	0.032	1.382	0.027	1.399	0.027	1.453	0.030

T_{eff}	7250								10000						13000					
	1.5		2.5		3.5		4.5		2.5		3.5		4.5		2.5		3.5		4.5	
$\log g$	I_{sol}	(δI)																		
CN1	-0.183	0.002	-0.194	0.001	-0.186	0.001	-0.169	0.000	-0.128	0.000	-0.230	0.000	-0.335	0.000	-0.077	0.000	-0.147	0.000	-0.230	0.000
CN2	-0.121	0.002	-0.136	0.001	-0.133	0.001	-0.120	0.000	-0.073	0.000	-0.162	0.000	-0.269	0.000	-0.039	0.000	-0.094	0.000	-0.170	0.000
Ca4227	0.033	0.021	0.043	0.017	0.049	0.015	0.057	0.016	0.011	0.000	0.006	0.001	0.001	0.005	0.005	0.000	0.004	0.000	0.001	0.000
G4300	-1.751	0.169	-2.028	0.180	-2.019	0.170	-1.828	0.143	-1.284	0.016	-2.806	0.018	-4.113	0.015	-0.729	0.001	-1.655	0.001	-2.841	-0.005
Fe4383	-0.278	0.061	-0.768	0.027	-0.955	0.003	-0.897	-0.014	-0.224	0.009	-1.179	0.008	-3.441	0.008	0.047	0.003	-0.383	0.004	-1.480	-0.001
Ca4455	-0.019	-0.014	-0.002	-0.018	0.015	-0.015	0.025	-0.007	0.020	-0.017	0.008	-0.017	-0.004	-0.019	0.191	-0.018	0.177	-0.019	0.158	-0.017
Fe4531	0.235	0.049	0.201	0.033	0.167	0.022	0.135	0.017	0.042	0.002	0.027	0.001	0.020	0.001	0.021	0.002	0.020	0.001	0.015	0.001
C ₂ 4668	-0.097	0.035	-0.067	0.028	-0.046	0.023	-0.025	0.020	0.062	-0.001	0.053	0.000	-0.021	0.001	0.151	0.000	0.126	-0.001	0.100	-0.002
H β	6.907	0.017	6.887	0.016	6.453	0.015	5.891	0.014	5.909	-0.002	8.482	-0.003	9.361	-0.001	3.818	-0.001	5.999	-0.001	7.712	0.005
Fe5015	0.189	0.029	0.147	0.027	0.110	0.025	0.086	0.023	0.080	-0.024	0.053	-0.015	-0.030	-0.009	0.156	-0.030	0.107	-0.029	0.059	-0.022
Mg1	0.000	0.000	-0.003	0.000	-0.005	0.000	-0.006	0.000	0.007	0.000	0.004	0.000	-0.008	0.000	0.008	0.000	0.007	0.000	0.003	0.000
Mg2	0.015	0.003	0.012	0.002	0.009	0.002	0.009	0.003	0.009	0.000	0.007	0.001	-0.001	0.001	0.009	0.000	0.009	0.000	0.006	0.000
Mgb	0.365	0.096	0.367	0.088	0.364	0.083	0.375	0.099	0.066	0.009	0.069	0.020	0.077	0.036	0.034	-0.002	0.035	0.000	0.027	0.001
Fe5270	0.056	0.031	0.073	0.033	0.087	0.035	0.096	0.035	0.006	0.001	0.006	0.001	0.006	0.001	0.008	0.001	0.009	0.001	0.009	0.001
Fe5335	0.103	0.030	0.108	0.029	0.109	0.028	0.110	0.026	0.007	0.002	0.006	0.002	0.006	0.002	0.007	0.004	0.006	0.002	0.005	0.001
Fe5406	0.023	-0.011	0.037	-0.005	0.048	0.000	0.054	0.003	0.003	0.001	0.002	0.001	0.003	0.000	0.003	0.000	0.003	0.001	0.003	0.001
Fe5709	0.002	0.002	0.004	0.003	0.005	0.003	0.005	0.003	0.002	0.000	0.002	0.000	0.002	0.000	0.002	0.000	0.002	0.000	0.002	0.000
Fe5782	0.001	0.000	0.001	0.000	0.001	0.000	0.001	0.000	0.001	0.000	0.001	0.000	0.001	0.000	0.001	0.000	0.001	0.000	0.001	0.000
NaD	0.145	-0.002	0.155	-0.003	0.158	-0.003	0.161	-0.004	-0.010	0.000	0.000	0.000	0.008	0.000	-0.061	-0.001	-0.045	0.000	-0.032	-0.001
TiO1	0.002	0.000	0.001	0.000	0.001	0.000	0.001	0.000	0.003	0.000	0.003	0.000	0.003	0.000	0.003	0.000	0.003	0.000	0.003	0.000
TiO2	0.002	0.000	0.002	0.000	0.001	0.000	0.001	0.000	0.003	0.000	0.003	0.000	0.003	0.000	0.004	0.000	0.004	0.000	0.004	0.000
H δ A	8.835	-0.026	9.232	-0.004	8.813	0.006	7.981	0.013	6.479	-0.011	10.950	-0.011	14.940	-0.008	4.138	-0.012	7.383	-0.009	10.870	0.013
H γ A	8.611	-0.097	9.141	-0.090	8.837	-0.080	8.035	-0.063	6.592	-0.017	11.140	-0.018	15.250	-0.014	4.136	-0.003	7.380	-0.003	10.980	0.015
H δ F	6.919	-0.011	6.849	0.002	6.414	0.007	5.819	0.011	5.481	-0.013	8.200	-0.010	9.638	-0.005	5.834	-0.012	7.693	0.002	7.693	0.002
H γ F	6.912	-0.005	6.924	-0.006	6.532	-0.007	5.946	-0.005	5.633	-0.005	8.329	-0.006	9.775	-0.004	3.685	-0.001	5.917	-0.001	7.794	0.008
D4000	1.218	0.008	1.276	0.007	1.296	0.007	1.295	0.007	1.080	0.001	1.200	0.001	1.379	0.001	1.017	0.000	1.084	0.000	1.188	0.001

Absorption line indices from high resolution spectra. I. New Response Functions

Table A6. Spectra degraded to the Lick resolution: I_{sol} and $I_{\text{enh}} - I_{\text{sol}}$ for $[Z/Z_{\odot}] = -1.5$

T_{eff}	4000								5250							
	1.5		2.5		3.5		4.5		1.5		2.5		3.5		4.5	
	I_{sol}	(δI)														
CN1	0.044	0.005	0.045	0.022	0.032	0.030	0.018	0.031	-0.043	0.001	-0.050	0.003	-0.056	0.006	-0.062	0.012
CN2	0.103	0.014	0.124	0.028	0.119	0.040	0.110	0.036	-0.023	0.001	-0.035	0.004	-0.046	0.009	-0.055	0.018
Ca4227	0.712	1.317	1.647	1.330	2.696	1.441	3.685	1.228	0.167	0.103	0.132	0.153	0.160	0.242	0.333	0.382
G4300	7.975	-0.869	7.981	-1.307	6.930	-1.034	5.296	-1.077	4.722	0.009	6.014	-0.224	6.843	-0.488	7.698	-0.953
Fe4383	5.618	-0.899	6.364	-1.329	6.253	-1.075	5.807	-1.251	1.560	0.043	1.746	-0.056	2.175	-0.283	2.819	-0.545
Ca4455	1.145	0.037	1.220	-0.005	1.083	0.049	0.919	-0.017	0.375	-0.017	0.331	-0.003	0.295	0.015	0.286	0.019
Fe4531	3.592	0.096	3.490	0.069	3.271	0.221	3.178	0.171	1.644	0.257	1.543	0.272	1.436	0.266	1.364	0.245
C ₂ 4668	1.260	-0.036	0.669	0.046	0.205	0.269	-0.154	0.323	0.139	0.123	0.131	0.103	0.131	0.086	0.129	0.090
H β	0.191	0.018	-0.055	-0.013	-0.244	-0.008	-0.346	-0.035	1.784	0.083	1.508	0.079	1.295	0.066	1.163	0.044
Fe5015	3.827	-0.260	2.839	-0.212	2.212	0.004	1.681	0.069	2.157	0.386	2.042	0.367	1.923	0.342	1.780	0.316
Mg1	0.130	0.048	0.228	0.051	0.278	0.085	0.330	0.087	0.001	0.000	0.000	0.001	0.000	0.002	0.001	0.007
Mg2	0.240	0.079	0.396	0.091	0.481	0.147	0.531	0.131	0.030	0.007	0.037	0.013	0.056	0.024	0.092	0.045
Mgb	2.700	1.079	4.411	1.238	5.070	1.709	4.700	1.229	0.304	0.211	0.613	0.401	1.323	0.724	2.510	1.235
Fe5270	2.506	0.026	2.848	-0.107	2.925	-0.060	2.886	-0.152	0.797	0.230	0.813	0.227	0.892	0.212	1.056	0.193
Fe5335	2.358	-0.007	2.600	-0.158	2.621	-0.154	2.602	-0.323	0.889	0.122	0.904	0.130	0.951	0.131	1.073	0.119
Fe5406	1.501	-0.050	1.787	-0.173	1.882	-0.147	1.897	-0.253	0.398	0.023	0.444	0.013	0.515	0.007	0.630	0.002
Fe5709	0.795	0.060	0.691	0.046	0.507	0.057	0.306	0.021	0.189	0.035	0.201	0.036	0.203	0.036	0.187	0.034
Fe5782	0.410	-0.016	0.396	-0.048	0.283	-0.054	0.179	-0.065	0.042	0.004	0.046	0.004	0.046	0.004	0.043	0.004
NaD	1.476	-0.193	2.658	-0.413	3.910	-0.329	5.509	-0.704	0.315	-0.032	0.363	-0.042	0.528	-0.068	0.896	-0.104
TiO1	0.006	0.004	0.005	0.007	0.005	0.015	0.002	0.013	0.000	0.000	0.000	0.000	0.000	0.000	0.000	0.000
TiO2	0.024	0.001	0.022	0.007	0.020	0.020	0.013	0.018	0.003	0.001	0.003	0.001	0.002	0.001	0.001	0.001
H δ A	-4.426	1.418	-4.614	1.595	-4.138	1.298	-2.917	1.241	0.448	0.069	-0.055	0.166	-0.816	0.324	-1.801	0.512
H γ A	-9.712	0.342	-11.250	1.193	-10.870	0.823	-9.519	1.325	-2.999	0.024	-4.609	0.285	-5.964	0.600	-7.568	1.134
H δ F	-2.268	0.216	-2.465	0.390	-2.297	0.375	-1.709	0.499	0.663	0.066	0.422	0.110	0.071	0.175	-0.367	0.252
H γ F	-3.104	0.283	-3.798	0.619	-3.817	0.542	-3.313	0.683	-0.097	0.120	-1.043	0.268	-1.883	0.431	-2.780	0.691
D4000	2.636	-0.131	2.567	-0.221	2.539	-0.195	2.436	-0.190	1.489	0.051	1.459	0.039	1.488	0.030	1.569	0.024

T_{eff}	7250								10000						13000					
	1.5		2.5		3.5		4.5		2.5		3.5		4.5		2.5		3.5		4.5	
	I_{sol}	(δI)																		
CN1	-0.180	0.003	-0.193	0.002	-0.186	0.001	-0.169	0.001	-0.125	0.000	-0.227	0.000	-0.333	0.000	-0.075	0.000	-0.145	-0.001	-0.228	0.000
CN2	-0.116	0.003	-0.134	0.002	-0.132	0.002	-0.120	0.001	-0.071	0.000	-0.159	0.000	-0.267	0.000	-0.037	0.000	-0.092	0.000	-0.168	0.000
Ca4227	0.056	0.027	0.065	0.023	0.073	0.020	0.083	0.023	0.020	0.001	0.014	0.004	0.010	0.011	0.010	0.001	0.010	0.000	0.005	0.000
G4300	-1.536	0.191	-1.803	0.206	-1.797	0.213	-1.632	0.208	-1.233	0.037	-2.747	0.043	-4.093	0.040	-0.717	-0.006	-1.625	-0.007	-2.813	-0.003
Fe4383	-0.005	0.113	-0.583	0.059	-0.842	0.021	-0.847	-0.012	-0.185	0.022	-1.120	0.018	-3.370	0.016	0.059	0.011	-0.361	0.010	-1.449	0.005
Ca4455	-0.011	0.006	0.002	-0.005	0.025	-0.016	0.047	-0.018	-0.003	-0.011	-0.014	-0.013	-0.027	-0.018	0.169	-0.013	0.154	-0.013	0.138	-0.017
Fe4531	0.437	0.101	0.379	0.086	0.324	0.066	0.282	0.049	0.075	0.004	0.056	0.003	0.044	0.003	0.039	0.007	0.037	0.004	0.026	0.002
C ₂ 4668	-0.172	0.079	-0.122	0.060	-0.077	0.043	-0.034	0.034	0.019	-0.001	0.027	0.001	-0.033	0.004	0.113	0.002	0.104	-0.002	0.087	-0.002
H β	6.965	0.035	6.958	0.031	6.534	0.028	5.978	0.027	5.860	0.007	8.441	-0.001	9.371	-0.001	3.758	0.022	5.933	0.018	7.664	0.008
Fe5015	0.370	0.077	0.332	0.072	0.294	0.067	0.266	0.063	0.086	-0.035	0.068	-0.026	-0.009	-0.019	0.150	-0.033	0.102	-0.040	0.056	-0.037
Mg1	-0.001	0.000	-0.005	0.000	-0.007	0.000	-0.007	0.000	0.007	0.000	0.004	0.000	-0.008	0.000	0.007	0.000	0.007	0.000	0.003	0.000
Mg2	0.018	0.003	0.015	0.003	0.013	0.003	0.013	0.004	0.010	0.001	0.009	0.001	0.001	0.002	0.009	0.000	0.009	0.000	0.006	0.000
Mgb	0.441	0.089	0.431	0.092	0.423	0.100	0.460	0.147	0.082	0.023	0.107	0.044	0.141	0.062	0.044	-0.005	0.050	0.000	0.047	0.004
Fe5270	0.140	0.082	0.161	0.087	0.178	0.088	0.191	0.088	0.006	0.004	0.007	0.004	0.007	0.004	0.011	0.001	0.012	0.002	0.011	0.002
Fe5335	0.221	0.061	0.233	0.066	0.236	0.067	0.235	0.068	0.013	0.006	0.012	0.006	0.012	0.007	0.014	0.010	0.009	0.006	0.007	0.003
Fe5406	0.052	-0.018	0.084	-0.008	0.105	0.001	0.118	0.007	0.006	0.002	0.005	0.002	0.005	0.002	0.005	0.001	0.006	0.002	0.005	0.002
Fe5709	0.005	0.007	0.010	0.009	0.013	0.009	0.014	0.009	0.001	0.000	0.002	0.000	0.002	0.000	0.002	0.000	0.002	0.000	0.002	0.000
Fe5782	0.003	0.000	0.003	0.001	0.003	0.001	0.003	0.001	0.002	0.000	0.002	0.000	0.001	0.000	0.002	-0.001	0.002	-0.001	0.002	0.000
NaD	0.203	-0.005	0.206	-0.007	0.204	-0.008	0.208	-0.009	-0.006	-0.001	0.007	0.000	0.023	0.000	-0.061	-0.002	-0.044	-0.002	-0.032	-0.001
TiO1	0.002	0.000	0.002	0.000	0.001	0.000	0.001	0.000	0.003	0.000	0.003	0.000	0.003	0.000	0.003	0.001	0.003	0.000	0.003	0.000
TiO2	0.003	0.000	0.002	0.000	0.002	0.000	0.001	0.000	0.003	0.000	0.003	0.000	0.003	0.000	0.004	0.000	0.004	0.000	0.004	0.000
H δ A	8.707	-0.039	9.191	-0.008	8.795	0.005	7.988	0.023	6.382	0.000	10.840	-0.007	14.890	-0.012	4.039	0.013	7.264	0.022	10.780	0.015
H γ A	8.382	-0.105	8.985	-0.090	8.721	-0.089	7.970	-0.077	6.501	-0.023	11.030	-0.030	15.200	-0.030	4.057	0.024	7.276	0.025	10.900	0.016
H δ F	6.840	-0.015	6.816	0.002	6.399	0.011	5.819	0.022	5.404	-0.006	8.132	-0.010	9.622	-0.009	3.491	0.005	5.742	0.007	7.629	0.000
H γ F	6.864	0.005	6.908	0.004	6.534	0.000	5.967	0.001	5.577	0.001	8.274	-0.007	9.765	-0.008	3.621	0.023	5.845	0.020	7.742	0.010
D4000	1.235	0.013	1.293	0.012	1.312	0.011	1.311	0.012	1.079	0.001	1.198	0.001	1.378	0.002	1.017	0.000	1.083	0.000	1.186	0.001

Table A7. Spectra degraded to the Lick resolution: I_{sol} and $I_{\text{enh}} - I_{\text{sol}}$ for $[Z/Z_{\odot}] = -1.0$

T_{eff}	4000								5250							
	1.5		2.5		3.5		4.5		1.5		2.5		3.5		4.5	
$\log g$	I_{sol}	(δI)														
CN1	0.089	-0.029	0.071	-0.006	0.041	0.009	0.006	0.017	-0.057	-0.001	-0.059	0.000	-0.060	0.002	-0.063	0.007
CN2	0.164	-0.024	0.162	-0.005	0.146	0.009	0.108	0.017	-0.038	0.002	-0.044	0.003	-0.047	0.006	-0.051	0.014
Ca4227	1.588	1.771	2.708	1.534	4.224	1.299	4.968	1.107	0.220	0.205	0.138	0.296	0.177	0.411	0.473	0.560
G4300	8.022	-0.749	7.811	-1.072	7.276	-0.909	5.214	-0.422	6.567	-0.298	7.165	-0.386	7.436	-0.530	7.872	-0.901
Fe4383	7.025	-1.085	7.648	-1.589	8.145	-1.734	6.902	-1.454	2.438	-0.174	2.846	-0.379	3.420	-0.693	4.332	-1.167
Ca4455	1.554	0.001	1.637	-0.041	1.606	-0.021	1.290	-0.007	0.535	0.012	0.485	0.018	0.448	0.034	0.457	0.043
Fe4531	4.418	0.152	4.273	0.109	4.314	0.197	4.024	0.254	2.440	0.175	2.362	0.164	2.258	0.151	2.214	0.115
C24668	2.017	-0.218	1.141	0.184	0.559	0.768	0.093	1.004	0.637	-0.023	0.584	-0.051	0.528	-0.051	0.455	-0.008
H β	0.122	0.016	-0.177	0.031	-0.412	0.097	-0.507	0.105	1.857	0.160	1.584	0.153	1.351	0.144	1.184	0.115
Fe5015	4.545	-0.141	3.591	0.057	3.172	0.459	2.530	0.548	3.545	0.316	3.335	0.291	3.156	0.233	3.032	0.124
Mg1	0.192	0.042	0.283	0.039	0.367	0.052	0.396	0.077	0.009	0.000	0.009	0.000	0.008	0.003	0.009	0.013
Mg2	0.328	0.085	0.480	0.091	0.622	0.123	0.629	0.149	0.045	0.009	0.056	0.016	0.084	0.031	0.140	0.060
Mgb	3.513	1.364	5.151	1.465	6.175	1.679	5.304	1.629	0.325	0.327	0.799	0.574	1.816	0.970	3.485	1.560
Fe5270	3.181	-0.068	3.433	-0.205	3.710	-0.227	3.524	-0.162	1.354	0.193	1.398	0.168	1.551	0.116	1.851	0.048
Fe5335	3.079	-0.093	3.274	-0.288	3.471	-0.407	3.186	-0.426	1.315	0.098	1.402	0.085	1.543	0.044	1.809	-0.022
Fe5406	2.015	-0.120	2.258	-0.252	2.499	-0.303	2.335	-0.281	0.665	-0.008	0.725	-0.027	0.856	-0.078	1.099	-0.150
Fe5709	1.085	0.084	0.952	0.069	0.777	0.076	0.488	0.071	0.434	0.017	0.449	0.012	0.453	0.005	0.436	-0.003
Fe5782	0.733	-0.037	0.689	-0.095	0.551	-0.143	0.343	-0.147	0.110	0.020	0.120	0.019	0.124	0.017	0.120	0.014
NaD	2.289	-0.298	3.759	-0.601	5.984	-0.883	7.476	-0.993	0.384	-0.049	0.476	-0.076	0.730	-0.121	1.275	-0.178
TiO1	0.010	0.007	0.011	0.017	0.016	0.034	0.012	0.040	0.002	0.001	0.002	0.001	0.002	0.001	0.002	0.001
TiO2	0.037	0.006	0.036	0.022	0.043	0.049	0.033	0.060	0.008	0.000	0.007	0.000	0.006	0.000	0.005	0.000
H δ A	-6.301	1.919	-6.111	1.968	-5.889	1.747	-3.680	1.014	-0.279	0.275	-0.835	0.505	-1.718	0.821	-3.116	1.302
H γ A	-11.530	0.431	-12.670	1.272	-13.320	1.316	-10.760	0.904	-5.153	0.363	-6.153	0.520	-7.083	0.794	-8.627	1.446
H δ F	-3.226	0.253	-3.284	0.438	-3.251	0.508	-2.193	0.380	0.239	0.129	0.069	0.206	-0.252	0.323	-0.819	0.514
H γ F	-3.459	0.298	-3.955	0.562	-4.248	0.568	-3.435	0.392	-0.821	0.286	-1.477	0.373	-2.064	0.494	-2.879	0.774
D4000	2.935	-0.118	2.836	-0.238	2.884	-0.276	2.637	-0.197	1.652	0.055	1.621	0.021	1.667	-0.010	1.795	-0.048

T_{eff}	7250								10000						13000					
	1.5		2.5		3.5		4.5		2.5		3.5		4.5		2.5		3.5		4.5	
$\log g$	I_{sol}	(δI)																		
CN1	-0.174	0.002	-0.191	0.002	-0.185	0.002	-0.170	0.001	-0.124	0.002	-0.225	0.001	-0.333	0.003	-0.074	0.002	-0.143	0.002	-0.226	0.002
CN2	-0.109	0.002	-0.130	0.002	-0.129	0.002	-0.119	0.001	-0.069	0.002	-0.157	0.002	-0.267	0.003	-0.036	0.001	-0.091	0.002	-0.167	0.002
Ca4227	0.090	0.020	0.095	0.023	0.101	0.023	0.118	0.031	0.030	-0.004	0.028	0.000	0.036	0.007	0.026	-0.004	0.025	-0.004	0.018	-0.004
G4300	-1.295	0.268	-1.553	0.267	-1.514	0.250	-1.324	0.231	-1.163	0.101	-2.665	0.107	-4.058	0.107	-0.722	0.012	-1.613	0.025	-2.792	0.032
Fe4383	0.212	0.215	-0.434	0.150	-0.724	0.078	-0.772	-0.001	-0.096	0.038	-1.003	0.036	-3.254	0.056	0.103	0.006	-0.312	0.019	-1.401	0.036
Ca4455	0.076	0.000	0.064	0.001	0.062	-0.004	0.074	-0.015	-0.024	-0.007	-0.034	-0.012	-0.049	-0.019	0.164	-0.021	0.152	-0.024	0.134	-0.029
Fe4531	0.820	0.093	0.743	0.107	0.651	0.098	0.578	0.076	0.131	0.000	0.110	-0.002	0.100	-0.008	0.079	0.008	0.076	0.002	0.060	-0.003
C24668	-0.173	0.104	-0.144	0.087	-0.104	0.065	-0.040	0.045	-0.093	0.014	-0.050	0.018	-0.083	0.026	0.025	0.014	0.041	0.002	0.051	-0.001
H β	7.068	0.072	7.086	0.053	6.680	0.040	6.139	0.029	5.808	0.017	8.380	0.040	9.377	0.010	3.754	-0.056	5.902	-0.043	7.628	-0.035
Fe5015	0.946	0.045	0.913	0.048	0.851	0.042	0.793	0.034	0.118	-0.065	0.096	-0.053	0.020	-0.042	0.180	-0.056	0.123	-0.073	0.071	-0.075
Mg1	-0.002	0.000	-0.005	0.000	-0.008	-0.001	-0.008	-0.001	0.006	0.000	0.003	0.000	-0.009	0.001	0.007	0.000	0.007	0.000	0.003	0.000
Mg2	0.024	0.001	0.021	0.002	0.018	0.002	0.020	0.005	0.011	0.001	0.010	0.002	0.003	0.002	0.010	0.000	0.010	0.000	0.007	0.000
Mgb	0.424	0.105	0.405	0.122	0.409	0.159	0.512	0.266	0.091	0.059	0.151	0.078	0.219	0.077	0.034	-0.007	0.049	0.003	0.061	0.010
Fe5270	0.386	0.104	0.401	0.126	0.404	0.137	0.407	0.145	0.025	0.001	0.017	0.006	0.019	0.009	0.024	-0.001	0.025	0.002	0.021	0.004
Fe5335	0.439	0.055	0.469	0.072	0.480	0.086	0.486	0.101	0.029	0.015	0.030	0.013	0.036	0.013	0.028	0.024	0.019	0.015	0.014	0.009
Fe5406	0.131	-0.027	0.182	-0.030	0.222	-0.026	0.250	-0.017	0.018	0.003	0.014	0.003	0.014	0.002	0.015	0.000	0.017	0.003	0.014	0.004
Fe5709	0.020	0.012	0.037	0.014	0.048	0.013	0.053	0.010	0.000	0.001	0.001	0.001	0.002	0.001	0.000	0.001	0.001	0.000	0.001	0.000
Fe5782	0.008	0.003	0.007	0.004	0.007	0.005	0.007	0.005	0.007	-0.003	0.004	-0.001	0.003	0.000	0.006	-0.004	0.006	-0.004	0.004	-0.002
NaD	0.240	-0.004	0.235	-0.007	0.231	-0.010	0.241	-0.012	0.007	-0.003	0.026	-0.001	0.056	-0.003	-0.058	-0.004	-0.043	-0.003	-0.030	-0.001
TiO1	0.002	0.000	0.002	0.000	0.002	0.000	0.001	0.000	0.003	0.000	0.003	0.000	0.003	0.000	0.004	0.001	0.004	0.001	0.004	0.000
TiO2	0.004	0.000	0.003	0.000	0.002	0.000	0.002	0.000	0.004	0.000	0.003	0.000	0.003	0.000	0.004	0.000	0.004	0.000	0.004	0.000
H δ A	8.471	-0.005	9.119	0.005	8.749	0.021	7.986	0.060	6.301	-0.054	10.720	-0.034	14.840	-0.068	4.007	-0.104	7.212	-0.101	10.720	-0.093
H γ A	8.134	-0.144	8.847	-0.124	8.599	-0.101	7.888	-0.070	6.397	-0.095	10.890	-0.077	15.150	-0.114	4.048	-0.080	7.235	-0.089	10.840	-0.092
H δ F	6.664	0.038	6.718	0.041	6.328	0.049	5.782	0.065	5.327	-0.033	8.049	-0.008	9.594	-0.019	3.453	-0.078	5.686	-0.069	7.572	-0.056
H γ F	6.822	0.011	6.920	0.004	6.560	0.002	6.013	0.006	5.518	-0.021	8.207	-0.001	9.754	-0.023	3.618	-0.060	5.815	-0.053	7.704	-0.044
D4000	1.265	0.019	1.324	0.017	1.342	0.016	1.342	0.017	1.079	0.000	1.197	0.000	1.380	-0.001	1.016	0.000	1.082	-0.001	1.184	-0.002

Absorption line indices from high resolution spectra. I. New Response Functions

Table A8. Spectra degraded to the Lick resolution: I_{sol} and $I_{\text{enh}} - I_{\text{sol}}$ for $[Z/Z_{\odot}] = -0.5$

T_{eff}	4000				5250											
	1.5		2.5		3.5		4.5		1.5		2.5		3.5		4.5	
$\log g$	I_{sol}	(δI)														
CN1	0.133	-0.061	0.096	-0.038	0.043	-0.016	-0.015	0.002	-0.046	-0.016	-0.042	-0.018	-0.042	-0.015	-0.050	-0.007
CN2	0.219	-0.062	0.196	-0.042	0.160	-0.026	0.097	-0.001	-0.027	-0.013	-0.024	-0.014	-0.025	-0.011	-0.031	0.000
Ca4227	3.043	1.883	4.016	1.464	5.538	0.891	6.193	0.757	0.147	0.457	0.063	0.575	0.145	0.688	0.592	0.832
G4300	8.116	-0.524	7.797	-0.789	7.596	-0.809	5.725	0.230	7.432	-0.305	7.634	-0.368	7.659	-0.513	7.824	-0.869
Fe4383	8.648	-1.334	8.943	-1.926	9.779	-2.506	8.436	-1.769	3.393	-0.339	3.847	-0.560	4.441	-0.865	5.499	-1.420
Ca4455	1.982	-0.001	2.043	-0.043	2.104	-0.075	1.777	0.016	0.721	0.053	0.689	0.046	0.678	0.040	0.718	0.036
Fe4531	5.498	0.245	5.246	0.130	5.487	0.025	5.179	0.313	3.257	0.100	3.175	0.076	3.084	0.041	3.062	0.003
C24668	2.816	-0.258	1.734	0.803	1.257	2.095	0.799	2.812	1.593	-0.182	1.516	-0.264	1.317	-0.245	1.060	-0.124
H β	-0.001	0.073	-0.286	0.214	-0.505	0.469	-0.618	0.566	2.014	0.193	1.761	0.176	1.513	0.164	1.302	0.140
Fe5015	5.683	0.276	4.839	0.585	4.804	1.081	3.995	1.633	5.049	0.289	4.696	0.258	4.419	0.170	4.262	-0.007
Mg1	0.254	0.024	0.326	0.013	0.414	0.000	0.462	0.049	0.026	-0.003	0.026	-0.003	0.024	0.002	0.025	0.018
Mg2	0.428	0.088	0.564	0.083	0.724	0.068	0.748	0.136	0.069	0.010	0.084	0.019	0.122	0.039	0.200	0.075
Mgb	4.466	1.778	5.954	1.670	7.027	1.407	6.158	1.634	0.539	0.438	1.131	0.737	2.457	1.207	4.623	1.805
Fe5270	3.864	-0.193	3.986	-0.335	4.375	-0.463	4.278	-0.197	2.024	0.188	2.080	0.137	2.274	0.074	2.663	0.002
Fe5335	3.935	-0.229	4.025	-0.497	4.300	-0.811	3.952	-0.674	1.828	0.110	2.001	0.071	2.228	0.005	2.613	-0.093
Fe5406	2.608	-0.208	2.782	-0.344	3.106	-0.494	2.927	-0.325	0.977	-0.045	1.056	-0.060	1.219	-0.118	1.547	-0.219
Fe5709	1.439	0.092	1.265	0.069	1.090	0.067	0.754	0.137	0.744	0.039	0.745	0.024	0.738	0.009	0.711	-0.004
Fe5782	1.114	-0.084	1.010	-0.192	0.832	-0.322	0.557	-0.339	0.255	0.045	0.275	0.041	0.282	0.035	0.283	0.028
NaD	3.532	-0.479	5.149	-0.948	8.010	-1.760	9.862	-1.663	0.528	-0.065	0.663	-0.110	1.021	-0.174	1.785	-0.259
TiO1	0.018	0.021	0.025	0.044	0.043	0.077	0.043	0.100	0.002	0.001	0.003	0.001	0.003	0.001	0.003	0.001
TiO2	0.057	0.026	0.064	0.061	0.089	0.106	0.084	0.142	0.012	0.000	0.011	0.000	0.010	0.000	0.009	-0.001
H δ A	-8.662	2.520	-7.875	2.501	-7.731	2.428	-5.120	0.926	-1.283	0.566	-1.801	0.878	-2.666	1.268	-4.210	1.859
H γ A	-13.790	0.452	-14.360	1.343	-15.550	1.952	-12.960	0.386	-6.562	0.372	-7.170	0.510	-7.913	0.832	-9.410	1.607
H δ F	-4.454	0.431	-4.217	0.613	-4.183	0.778	-2.959	0.339	-0.124	0.124	-0.204	0.215	-0.466	0.360	-1.070	0.607
H γ F	-3.993	0.282	-4.241	0.486	-4.596	0.572	-3.871	0.060	-1.149	0.347	-1.591	0.385	-2.058	0.505	-2.784	0.802
D4000	3.357	-0.120	3.137	-0.253	3.203	-0.362	2.910	-0.212	1.897	0.069	1.826	0.028	1.863	-0.014	2.022	-0.077

T_{eff}	7250				10000			13000												
	1.5		2.5		3.5		4.5		2.5		3.5		4.5							
$\log g$	I_{sol}	(δI)																		
CN1	-0.168	0.001	-0.191	0.001	-0.185	0.001	-0.174	0.001	-0.122	0.003	-0.224	0.004	-0.332	0.006	-0.071	0.003	-0.140	0.003	-0.222	0.003
CN2	-0.102	0.001	-0.129	0.001	-0.128	0.001	-0.121	0.001	-0.067	0.003	-0.155	0.004	-0.265	0.006	-0.034	0.002	-0.087	0.002	-0.163	0.003
Ca4227	0.105	0.017	0.110	0.028	0.118	0.040	0.148	0.060	0.024	-0.001	0.031	0.006	0.054	0.005	0.036	-0.002	0.035	-0.003	0.029	-0.004
G4300	-0.966	0.314	-1.219	0.298	-1.146	0.274	-0.901	0.238	-1.073	0.157	-2.564	0.184	-3.980	0.190	-0.711	0.004	-1.576	0.032	-2.737	0.049
Fe4383	0.365	0.232	-0.321	0.190	-0.608	0.123	-0.652	0.005	0.014	0.078	-0.843	0.079	-3.078	0.123	0.159	0.021	-0.235	0.038	-1.296	0.059
Ca4455	0.184	0.002	0.164	-0.006	0.139	-0.008	0.122	-0.010	-0.043	-0.011	-0.055	-0.019	-0.071	-0.032	0.150	-0.011	0.141	-0.017	0.121	-0.026
Fe4531	1.289	0.111	1.228	0.150	1.111	0.171	0.995	0.167	0.208	0.014	0.181	0.008	0.171	-0.005	0.127	0.024	0.121	0.016	0.099	0.008
C24668	-0.049	0.089	-0.040	0.072	-0.045	0.062	-0.014	0.055	-0.274	0.014	-0.178	0.025	-0.163	0.045	-0.118	0.021	-0.083	-0.002	-0.036	-0.007
H β	7.192	0.112	7.239	0.096	6.858	0.081	6.332	0.069	5.838	-0.008	8.453	-0.022	9.447	-0.043	3.683	-0.066	5.825	-0.057	7.566	-0.057
Fe5015	1.890	0.087	1.832	0.108	1.701	0.108	1.573	0.100	0.182	-0.073	0.140	-0.062	0.062	-0.058	0.236	-0.052	0.156	-0.078	0.082	-0.095
Mg1	0.000	-0.001	-0.003	-0.002	-0.006	-0.002	-0.008	-0.002	0.006	-0.001	0.003	0.000	-0.009	0.001	0.008	-0.001	0.007	-0.001	0.003	0.000
Mg2	0.031	0.000	0.026	0.001	0.024	0.003	0.028	0.008	0.013	0.002	0.013	0.002	0.006	0.002	0.010	-0.001	0.010	0.000	0.007	0.001
Mgb	0.326	0.127	0.303	0.154	0.363	0.222	0.617	0.408	0.126	0.092	0.217	0.095	0.292	0.083	-0.010	-0.005	0.022	0.012	0.056	0.029
Fe5270	0.706	0.180	0.739	0.208	0.743	0.227	0.746	0.252	0.076	0.004	0.056	0.013	0.059	0.021	0.048	0.000	0.053	0.006	0.045	0.012
Fe5335	0.663	0.089	0.733	0.106	0.780	0.133	0.823	0.177	0.053	0.044	0.067	0.040	0.089	0.040	0.060	0.047	0.040	0.037	0.030	0.029
Fe5406	0.249	-0.002	0.301	-0.012	0.350	-0.020	0.398	-0.015	0.050	0.002	0.039	0.005	0.038	0.006	0.039	0.002	0.046	0.005	0.039	0.010
Fe5709	0.057	0.029	0.097	0.030	0.121	0.026	0.132	0.020	-0.004	0.002	-0.001	0.002	0.003	0.003	-0.004	0.002	-0.003	0.002	-0.001	0.001
Fe5782	0.024	0.007	0.025	0.010	0.025	0.012	0.025	0.013	0.017	-0.007	0.010	-0.004	0.006	-0.002	0.013	-0.011	0.015	-0.010	0.011	-0.007
NaD	0.273	-0.010	0.262	-0.017	0.259	-0.023	0.287	-0.029	0.041	-0.010	0.070	-0.007	0.109	-0.010	-0.042	-0.012	-0.031	-0.011	-0.020	-0.008
TiO1	0.003	0.000	0.003	0.000	0.002	0.000	0.002	0.000	0.004	0.001	0.004	0.001	0.003	0.000	0.005	0.001	0.005	0.001	0.005	0.001
TiO2	0.005	0.000	0.004	0.000	0.003	0.000	0.003	0.000	0.004	0.000	0.004	0.000	0.003	0.000	0.004	0.000	0.004	0.000	0.004	0.000
H δ A	8.153	0.015	9.056	0.046	8.718	0.047	8.049	0.089	6.187	-0.090	10.630	-0.111	14.780	-0.154	3.863	-0.126	7.049	-0.128	10.550	-0.125
H γ A	7.891	-0.205	8.721	-0.155	8.466	-0.117	7.762	-0.045	6.265	-0.156	10.790	-0.184	15.070	-0.233	3.942	-0.088	7.089	-0.114	10.680	-0.132
H δ F	6.433	0.074	6.596	0.083	6.240	0.082	5.749	0.098	5.246	-0.060	8.015	-0.061	9.580	-0.066	3.335	-0.091	5.563	-0.087	7.464	-0.081
H γ F	6.787	-0.004	6.948	0.003	6.600	0.007	6.062	0.025	5.471	-0.045	8.204	-0.060	9.765	-0.079	3.540	-0.062	5.724	-0.067	7.624	-0.068
D4000	1.308	0.034	1.370	0.032	1.384	0.029	1.388	0.029	1.081	0.000	1.199	-0.001	1.383	-0.004	1.014	-0.001	1.078	-0.002	1.179	-0.002

Absorption-line indices from high-resolution spectra.

I. New response functions

R. Tantalò¹, C. Chiosi¹, U. Munari², L. Piovan¹, & R. Sordo²

¹ *Department of Astronomy, University of Padova, Vicolo dell'Osservatorio 2, 35122 Padova, Italy*

² *INAF, Astronomical Observatory of Padova, Vicolo Osservatorio 5, 35122 Padova, Italy*

E-mail: chiosi@pd.astro.it; ulisse@pd.astro.it; piovan@pd.astro.it; sordo@pd.astro.it; tantalo@pd.astro.it

Submitted: May 2004; Revised: July 2004; November 2004

ABSTRACT

Basing on the huge library of 1-Å resolution spectra calculated by Munari et al. over a large range of $\log T_{\text{eff}}$, $\log g$, $[\text{Fe}/\text{H}]$ and both for solar and α -enhanced abundance ratios ($[X_{\text{el}}/\text{Fe}]$), we present theoretical absorption-line indices on the Lick system. First we derive the so-called response functions (\mathcal{RF} s) of Tripicco & Bell for a wide range of $\log T_{\text{eff}}$, $\log g$, $[\text{Fe}/\text{H}]$ and $[\alpha/\text{Fe}] = +0.4$. The \mathcal{RF} s are commonly used to correct indices with solar $[\alpha/\text{Fe}]$ ratios to indices with $[\alpha/\text{Fe}] > 0$. Not only the \mathcal{RF} s vary with the type of star but also with the metallicity. Secondly, with the aid of this and the fitting functions (\mathcal{FF} s) of Worthey et al., we derive the indices for single stellar populations and compare them with those obtained by previous authors, e.g. Tantalò & Chiosi. The new \mathcal{RF} s not only supersede the old ones by Tripicco & Bell, but also show that $H\beta$ increases with the degree of enhancement in agreement with the results by Tantalò & Chiosi. This finding lends support to the suggestion made by Tantalò & Chiosi that a significant part of the scatter in $H\beta$ shown by early-type galaxies of the local universe in the $H\beta$ versus $[\text{Mg}/\text{Fe}]$ plane (and similar) could be due to a spread in the mean enhancement factor from galaxy to galaxy and only occasionally to recent episodes of star formation. To explore this possibility we derive the age, metallicity and degree of enhancement for the galaxies of the Trager catalogue using the minimum-distance method, examine their position in suitable diagnostic planes and look for global correlations among the three parameters. Chief results of this analysis are (i) age and enhancement (together with metallicity) may concur to scatter the galaxies in the $H\beta$ versus $[\text{Mg}/\text{Fe}]$; (ii) at increasing age of the last episode of star formation, the mean metallicity decreases and the degree of enhancement increases as expected from current understanding of galactic chemical evolution and supernova contamination. Finally, we present preliminary indices on the same system directly measured on the theoretical 1-Å resolution spectra. The analysis is still preliminary because much narrower spacing in T_{eff} and $\log g$ than the one for the subset of the large library of Munari et al. we have adopted is indeed required. Work is in progress to include the desired spacing in the atmospheric parameters (T_{eff} , $\log g$ and $[\text{Fe}/\text{H}]$ or $[Z/Z_{\odot}]$).

Key words: Galaxies: spectroscopy – Galaxies: ages, metallicities, enhancement

1 INTRODUCTION

The Lick system of absorption-line indices developed over the years by Burstein et al. (1984), Faber et al. (1985), Worthey (1992), Worthey et al. (1992), Worthey et al. (1994) and Worthey (1994) was designed to infer the age and the metallicity of stellar systems, early-type galaxies in partic-

The Lick indices seem to have the potential of partially

resolving the age-metallicity degeneracy that is long known to affect the spectral energy distribution of stellar populations (Renzini & Buzzoni 1986).¹ Thanks to it, an extensive use of the Lick system of indices has been made by many authors (Bressan et al. 1996; Tantalò 1998; Tantalò et al. 1998; Trager et al. 2000a,b; Kuntschner 1998;

¹ An old metal-poor stellar population may happen to have the same spectral energy distribution of a young metal-rich one.

Kuntschner & Davies 1998; Jørgensen 1999; Kuntschner 2000; Poggianti et al. 2001; Kuntschner et al. 2001; Vazdekis et al. 2001; Davies et al. 2001; Maraston et al. 2003; Thomas et al. 2003a,b; Thomas & Maraston 2003; Tantalo & Chiosi 2004a). The main result of all those studies is that even in early-type galaxies some recent episodes of star formation ought to occur in order to explain the large scatter shown by the observational data for indices like $H\beta$ commonly thought to be sensitive to the turn-off stars and consequently to the age.

The problem is, however, further complicated by a third parameter, i.e. the abundance ratios $[\alpha/\text{Fe}]$ (where α stands for all chemical elements produced by α -captures on lighter nuclei). Absorption-line indices like Mg2 and $\langle\text{Fe}\rangle$ measured in the central regions of galaxies are known to vary passing from one galaxy to another (González 1993; Trager et al. 2000a,b). Looking at the correlation between Mg2 and $\langle\text{Fe}\rangle$ (or similar indices) for the galaxies in the above quoted samples, Mg2 increases faster than $\langle\text{Fe}\rangle$, which is interpreted as due to enhancement of α -elements in some galaxies. In addition to this, since the classical paper by Burstein et al. (1988), the index Mg2 is known to increase with the velocity dispersion (and hence mass and luminosity) of the galaxy. Standing on this body of data the conviction arose that the degree of enhancement in α -elements ought to increase passing from dwarf to massive early-type galaxies (Faber et al. 1992; Worthey et al. 1994; Matteucci 1994, 1997; Matteucci et al. 1998). These findings strongly bear on the theory of galaxy formation as super-solar $[\alpha/\text{Fe}]$ ratios require rather short star-formation time-scales (see for instance the discussion of this topic by Chiosi & Carraro (2002)) and the correlation with the velocity dispersion requires that the star formation time-scale should get longer at decreasing galaxy mass, in contrast with the standard supernova driven galactic wind model by Larson (1974), and instead supported by the N-Body-Tree-SPH models of early-type galaxies by Chiosi & Carraro (2002).

In presence of α -enhanced chemical compositions, ages and metallicities of early-type galaxies should be derived from indices in which α -enhancement is included. As long ago noticed by Worthey et al. (1992) and Weiss et al. (1995), indices for α -enhanced chemical mixtures of given total metallicity are expected to differ from those of the standard case. On one hand, this spurred new generations of stellar models, isochrones, SSPs with α -enhanced mixtures (Salasnich et al. 2000) and, on the other hand, led to many attempts of increasing complexity to simultaneously derive, from fitting the observational indices to their theoretical counterparts, the age, metallicity and degree of enhancement (Tantalo et al. 1998; Trager et al. 2000a,b; Maraston et al. 2003; Thomas et al. 2003a,b; Thomas & Maraston 2003; Tantalo & Chiosi 2004a). The formal solution for ages, metallicities and $[\alpha/\text{Fe}]$ ratios based on large samples of galaxies, e.g. the Trager (1997) list, once more yields a large range of ages, metallicities and abundance ratios, as amply discussed by Tantalo & Chiosi (2004a, TC04a).

Although the picture emerging from the above studies is a convincing one, there are still several points of weakness intrinsic even to the state-of-the-art theoretical indices that force us to reconsider the whole problem. Let us examine in some detail (i) the foundations of the Lick indices; (ii) the various steps that are required to derive theoretical in-

indices and their dependence on age, metallicity and degree of enhancement; (iii) the current method to estimate these parameters from the indices; (iv) and finally shortly comment on a few points of controversy among different groups.

- The information contained in the stellar spectra concerning the effective temperature (T_{eff}), gravity ($\log g$), and chemical composition (mainly the parameter $[\text{Fe}/\text{H}]$) has been coded in a system of indices measuring the strength of atomic and molecular lines (see Section 2). The Lick indices are defined and measured on a sample of stellar spectra with fixed mean resolution of 8.4\AA which in most cases is different from the resolution of theoretical spectra on which the indices are calculated. This simple fact will turn out to be a major reason of uncertainty.

- To overcome the above difficulty and to make possible the general use of the Lick indices, Worthey et al. (1994) introduced the concept of the so-called fitting functions (\mathcal{FF} s). The indices for a large sample of stars with known atmospheric parameters (T_{eff} , $\log g$ and $[\text{Fe}/\text{H}]$) are measured and then expressed as empirical polynomial fits as functions of these parameters. The major drawback with the \mathcal{FF} s is that they encompass a limited range of values in particular as far as $[\text{Fe}/\text{H}]$ is concerned. The sample of stars indeed was collected from the solar vicinity even if attempts to extend it to lower metallicities have been made (Idiart & de Freitas-Pacheco (1995), Cenarro et al. (2001, 2002)). Metallicities much higher than those in the solar vicinity are simply not included for obvious reasons. A new library is also available with unprecedented coverage of atmospheric parameters by Sánchez-Blázquez et al. (2003) and Sanchez-Blazquez et al. (in preparation).

- Despite it was long known that magnesium is perhaps enhanced with respect to iron ($[\text{Mg}/\text{Fe}]>0$) in giant elliptical galaxies (see e.g. Worthey et al. (1992) and above), the collection of stellar spectra and \mathcal{FF} s in turn did not allow for non-standard abundance ratios in the chemical composition. Only occasionally and for a few indices, e.g. Mg2 and NaD , \mathcal{FF} s including the effect of non-standard abundance ratios have been proposed, e.g. Borges et al. (1995).

- A milestone along the road was put by Tripicco & Bell (1995, TB95) who have modeled synthetic spectra of high-resolution (0.1\AA), degraded them to the mean 8.2\AA resolution of the Lick system, and derived from them the indices for three prototype stars, namely a cool-dwarf, a turn-off, and a cool-giant along a 5 Gyr isochrone matching the CMD of M67 (in other words for three different combinations of T_{eff} and $\log g$). Even more important here, they studied the response of the indices produced by changes in the abundance ratios of individual elements. In other words, thanks to their \mathcal{RF} s it was possible to evaluate the effect of abundance ratios different from solar.

- With the aid of the TB95 \mathcal{RF} s and suitable algorithms, the indices with solar abundance ratios have been transformed into those for non solar abundance ratios. The algorithms in use are not unique thus leading to uncertain results (see TC04a for more details).

- Passing now from individual stars to star clusters, reduced here to single stellar populations (SSPs), and galaxies (manifolds of SSPs), the derivation of theoretical indices (and spectra, magnitudes, and broad-band colours) is even more complicate because other ingredients intervene: (i) the

construction of realistic isochrones for SSPs including all evolutionary phases (even the unusual ones that are known to appear at very high metallicities, see Bressan et al. (1994) and TC04a); (ii) the initial mass function; (iii) and finally, in the case of galaxies, the past history of star formation and chemical enrichment weighing the contribution from stellar populations of different age and chemical compositions (see e.g. Bressan et al. 1994, for all details). It is worth commenting here that galaxy indices are almost always compared to SSP indices thus neglecting the mix of stellar populations and missing important contributions from some peculiar components. For instance an old SSP of very high metallicity and/ or a very old SSP of extremely low metal content, would possess strong $H\beta$ thus mimicking a young SSP of normal metallicity (see TC04a for more details). Integrated indices for model galaxies have been occasionally calculated and used (Tantalo 1998), but never systematically applied to this kind of analysis. This is a point that should be carefully investigated and kept in mind when comparing data with theory.

If for solar abundance ratios the dependence of the indices on age and metallicity is currently on a rather solid ground but for the effect of some unusual phases of stellar evolution, the same does not happen for non-solar abundance ratios because it is still highly controversial how some indices ($H\beta$, in particular) at given age and total metallicity would respond to changes in the abundance ratios. According to TC04a, SSPs of the same age and metallicity but different degrees of enhancement in α -elements may have significantly different $H\beta$: in brief keeping age and metallicity constant, $H\beta$ should increase at increasing degree of enhancement (see the discussion in Section 3.2 for more details). Basing on this, Tantalo & Chiosi (2004b) suggested an alternative, complementary interpretation of the large scatter in $H\beta$ shown by early-type galaxies of the local universe in two-indices diagnostic planes like $H\beta$ versus $[MgFe]$. Quickly summarizing their study: (i) most probably the majority of galaxies (those with $H\beta \leq 2$) are very old objects of the same age (say approximately 13 Gyr) but with a different degree of enhancement. (ii) Only for galaxies with $H\beta > 2$, the presence of secondary star forming activity ought to be invoked.

High-resolution synthetic spectra can greatly alleviate the above difficulties and shed light on these important issues, which is the aim of our study. The plan of the paper is as follows. Section 2 deals with the theory of absorption-line indices; Section 2.1 summarizes their definition for a single star; Section 2.2 derives the enhancement factor for a mixture in which the abundance of α -elements with respect to that of Fe is enhanced as compared to the solar mix; Section 2.3 recalls the dependence of the $\mathcal{F}\mathcal{F}$ s of the Lick system on the main stellar parameters, comments on the fact that they are based on solar-scaled chemical compositions and shortly describes the $\mathcal{F}\mathcal{F}$ s by Borges et al. (1995) in which for some indices the effect of enhancing α -elements is taken into account; finally Section 2.4 shortly reviews the method of the $\mathcal{R}\mathcal{F}$ s by TB95 and current algorithms that are adopted to transfer solar-scaled indices into the corresponding ones with α -enhancement. In Section 3 we present our new $\mathcal{R}\mathcal{F}$ s. We start presenting in Section 3.1 the library of synthetic spectra in use is. The covered T_{eff} and $\log g$ extend

nearly across the whole HR-diagram of real stars, the metallicity goes $[Z/Z_{\odot}] = -2.0$ to 0.5 for spectra with $[\alpha/Fe] = 0$ and up to -0.5 for spectra with $[\alpha/Fe] = +0.4$. Secondly, we calculate indices and $\mathcal{R}\mathcal{F}$. The analysis is made in two steps: (i) adopting the definition of the indices on the Lick system and the definition of $\mathcal{R}\mathcal{F}$ TB95 but using the stellar spectra at 1-Å resolution, we derive the indices for the calibrating stars (Section 3.2). They indices constitute the backbone of the new grid of TB95-like $\mathcal{R}\mathcal{F}$ s given in Section 3.3. Owing to the large body of data on the Lick system, it is worth providing indices and $\mathcal{R}\mathcal{F}$ s from spectra having the same resolution of the Lick system. They are presented in Section 3.4. The new $\mathcal{R}\mathcal{F}$ s (and indices) are now strictly equivalent to those of TB95. Together with the classical $\mathcal{F}\mathcal{F}$ s and they can be used to pass from solar to α -enhanced mixtures. These indices are immediately comparable to most of observational data in literature. To this end we need to calculate indices for SSPs. This the subject of Section 4. We start by shortly recalling the index definition for SSPs and the library of stellar spectra with medium resolution specifically used to this purpose (Section 4.1) and summarising the sources of stellar models and isochrones (Section 4.2). With the aid of the new $\mathcal{R}\mathcal{F}$ s we calculate absorption-line indices for SSPs at varying metallicity, degree of enhancement and age. The results are presented in Section 4.3 and compared to those by previous sources, e.g. TC04a, in Section 4.4. The increase of $H\beta$ with the degree of enhancement is fully confirmed, thus lending support to the conclusion reached by TC04a. In Section 5, the indices obtained with the new $\mathcal{R}\mathcal{F}$ s are compared with the data for globular clusters and galaxies of the Local Universe. Specifically, in Section 5.1 we compare the new indices with the observational data for Galactic globular clusters; in Section 5.3 we derive the age, metallicity and degree of enhancement for a sample of local early-type galaxies; in Section 5.4 we shortly discuss the suggestion made by Tantalo & Chiosi (2004b) that part of the scatter in $H\beta$ shown by early-type galaxies in the $H\beta$ versus $[MgFe]$ plane is due to different degree of enhancement in α -elements in addition to age dispersion; finally in Section 5.5, with the theoretical estimates for the age, metallicity and enhancement we look for general correlations among the three parameters. As a final exploratory step of this study, and for the first time in literature, in Section 6 we present indices derived directly from the theoretical 1-Å resolution spectra without passing through the $\mathcal{F}\mathcal{F}$ s and the $\mathcal{R}\mathcal{F}$ s. First we calculate the indices for the calibrating stars and compare them with the corresponding ones, roughly at the same atmospheric parameters for a selected sample of stars in STELIB (Section 6.1). Then we derive the indices for SSPs by means of the standard spectral synthesis technique by interpolating the high resolution spectra as function of T_{eff} and $\log g$ (at given metallicity and degree of enhancement). For the time being we prefer not to interpolate the spectra in metallicity and degree of enhancement and wait for a wider grid to become available. The new indices are given in Section. 6.2. Even if the current temperature-gravity grid is perhaps too coarse for this purpose, the results are acceptable. They will soon improve by adopting a library of spectra with much finer coverage of the temperature /gravity space. Finally, a summary of the results of this study and some concluding remarks are presented in Section 7.

2 THEORY OF ABSORPTION-LINE INDICES

2.1 Definition

The definition of an absorption-line index with pass-band Δ_λ is different according to whether it is measured in equivalent width (EW) or magnitude (mag). Those in EW are defined as

$$I_l = \Delta_\lambda \left(1 - \frac{F_l}{F_c} \right) \quad (1)$$

where F_l and F_c are the fluxes in the line and pseudo-continuum, respectively (see Fig. 6). The flux F_c is calculated by interpolating to the central wavelength of the absorption-line, the fluxes in the midpoints of the red and blue pseudo-continua bracketing the line (Worthey et al. 1994). The definition of indices expressed in mag is

$$I_l = -2.5 \log \left(\frac{F_l}{F_c} \right) \quad (2)$$

The pass-bands adopted for each index are listed in Table 1. As the Lick system of indices (Burstein et al. 1984; Faber et al. 1985; Worthey et al. 1994) stands on a spectra library with resolution of approximately 8.4\AA , whereas most of the spectral libraries in use have a different resolution, the straightforward application of equations (1) and (2) is not possible. To overcome this problem, the \mathcal{FF} s are introduced. They express the indices measured on the observed spectra of a large number of stars with known $\log g$, T_{eff} and chemical composition as functions of these parameters (Worthey et al. 1994).

We also add the index D4000 centered at the 4000\AA break. It is defined as the ratio of the average flux F_ν (in $\text{erg sec}^{-1}\text{cm}^{-2}\text{Hz}^{-1}$) in two bands at the long- and short-wavelength side of the discontinuity (Bruzual 1983), i.e.

$$\text{D4000} = \frac{\lambda_2^b - \lambda_1^b \int_{\lambda_1^b}^{\lambda_2^b} F_\nu d\lambda}{\lambda_2^s - \lambda_1^s \int_{\lambda_1^s}^{\lambda_2^s} F_\nu d\lambda}$$

The blue and red pass-bands are given in Table 1.

2.2 α -enhanced chemical compositions

The degree of enhancement in α -elements of a chemical mixture is measured by the so-called total enhancement parameter Γ , to distinguish it from the enhancement in individual species. Let us take a certain mixture of elements with total metallicity Z (sum of all elements heavier than He), denote with N_j the number density of the generic element j with mass abundance X_j ($N_j = \rho N_0 X_j / \mathcal{A}_j$, where ρ is the mass density, N_0 is the Avogadro number, and \mathcal{A}_j is the mass number) and define the quantity A_j

$$A_j = \log \left(\frac{N_j}{N_H} \right) + 12 \quad (3)$$

Ignoring elements from H to He, in this mixture $\sum_j X_j = Z$ by definition. The abundance by mass with respect to Fe is given by

$$\left[\frac{X_j}{X_{\text{Fe}}} \right] = \log \left(\frac{X_j}{X_{\text{Fe}}} \right) - \log \left(\frac{X_j}{X_{\text{Fe}}} \right)_\odot \quad (4)$$

or in terms of A_j

$$\left[\frac{X_j}{X_{\text{Fe}}} \right] = (A_{X_j} - A_{X_j}^\odot) - (A_{\text{Fe}} - A_{\text{Fe}}^\odot) \quad (5)$$

Keeping constant the number density of Fe, i.e. $(A_{\text{Fe}} - A_{\text{Fe}}^\odot) = 0$ and changing other elements (enhancement), we obtain

$$A_j^{\text{enh}} = \left[\frac{X_j}{X_{\text{Fe}}} \right] + A_j^\odot \quad (6)$$

Inserting the adopted $[X_j/X_{\text{Fe}}]$ and the solar values for A_j^\odot by Grevesse & Sauval (1998), respectively, from equation (3) we can calculate the new abundances by mass for any pattern of α -enhanced elements. In general, the sum of the X_j will be different from Z . The mass abundance must therefore be re-scaled to the true value X'_j given by

$$X'_j = \frac{X_j}{\sum X_j} \quad (7)$$

Finally the total enhancement factor Γ is

$$\Gamma = -\log \left(\frac{X'_{\text{Fe}}}{X_{\text{Fe}}^\odot} \right) \quad (8)$$

from which we immediately obtain the relationship between Γ and the new value of the Fe abundance in α -enhanced mixtures

$$\log \left(\frac{X_{\text{Fe}'}}{X_{\text{H}'}} \right) = -\Gamma + \log \left(\frac{X_{\text{Fe}}}{X_{\text{H}}} \right)_\odot + \log \left(\frac{X'}{X_{\text{H}}^\odot} \right) \quad (9)$$

The abundance ratios and total degree of enhancement for the case we are going to consider are listed in Table 2. The case with $\Gamma=0.25$ corresponds to the α -enhanced chemical compositions chosen by Munari et al. (2004) for their $1\text{-}\text{\AA}$ resolution spectra.

Finally, it is worth calling attention that at given total metallicity Z different patterns of $[X_j/X_{\text{Fe}}]$ may yield the same total enhancement factor Γ . This fact bears very much on the correction of indices for enhancement because each elemental species brings a different effect.

2.3 The Worthey et al. (1994) and Borges et al. (1995) fitting functions

The Lick \mathcal{FF} s refer to 25 absorption-line indices (Worthey 1992; Worthey et al. 1994; Worthey & Ottaviani 1997) and are based on a library of stellar spectra containing approximately 400 stars, observed at the Lick Observatory between 1972 and 1984, with an Image Dissector Scanner (IDS). In the following we adopt the Worthey (1992) \mathcal{FF} s, extended however to high temperature stars ($T_{\text{eff}} \approx 10000\text{K}$) as reported in Longhetti et al. (1998). Recently new \mathcal{FF} s are available also for the $\lambda 4000$ break by Gorgas et al. (1999) and Ca II triplet by Cenarro et al. (2001). All these \mathcal{FF} s

Table 1. 25 absorption-line indices on the Lick system: the pass-bands and the $\lambda 4000$ break.

Index	Type	Central Band		Blue Continuum		Red Continuum	
CN1	mag	4142.125	4177.125	4080.125	4117.625	4244.125	4284.125
CN2	mag	4142.125	4177.125	4083.875	4096.375	4244.125	4284.125
Ca4227	EW	4222.250	4234.750	4211.000	4219.750	4241.000	4251.000
G4300	EW	4281.375	4316.375	4266.375	4282.625	4318.875	4335.125
Fe4383	EW	4369.125	4420.375	4359.125	4370.375	4442.875	4455.375
Ca4455	EW	4452.125	4474.625	4445.875	4454.625	4477.125	4492.125
Fe4531	EW	4514.250	4559.250	4504.250	4514.250	4560.500	4579.250
C ₂ 4668	EW	4634.000	4720.250	4611.500	4630.250	4742.750	4756.500
H β	EW	4847.875	4876.625	4827.875	4847.875	4876.625	4891.625
Fe5015	EW	4977.750	5054.000	4946.500	4977.750	5054.000	5065.250
Mg1	mag	5069.125	5134.125	4895.125	4957.625	5301.125	5366.125
Mg2	mag	5154.125	5196.625	4895.125	4957.625	5301.125	5366.125
Mgb	EW	5160.125	5192.625	5142.625	5161.375	5191.375	5206.375
Fe5270	EW	5245.650	5285.650	5233.150	5248.150	5285.650	5318.150
Fe5335	EW	5312.125	5352.125	5304.625	5315.875	5353.375	5363.375
Fe5406	EW	5387.500	5415.000	5376.250	5387.500	5415.000	5425.000
Fe5709	EW	5696.625	5720.375	5672.875	5696.625	5722.875	5736.625
Fe5782	EW	5776.625	5796.625	5765.375	5775.375	5797.875	5811.625
NaD	EW	5876.875	5909.375	5860.625	5875.625	5922.125	5948.125
TiO1	mag	5936.625	5994.125	5816.625	5849.125	6038.625	6103.625
TiO2	mag	6189.625	6272.125	6066.625	6141.625	6372.625	6415.125
H δ A	EW	4083.500	4122.250	4041.600	4079.750	4128.500	4161.000
H γ A	EW	4319.750	4363.500	4283.500	4319.750	4367.250	4419.750
H δ F	EW	4091.000	4112.250	4057.250	4088.500	4114.750	4137.250
H γ F	EW	4331.250	4352.250	4283.500	4319.750	4354.750	4384.750
D4000				3750.000	3950.000	4050.000	4250.000

depend on stellar effective temperature, gravity and metallicity ([Fe/H]). They do not explicitly include the effect of α -enhancement.

Many studies have emphasized that absorption-line indices should also depend on the detailed pattern of chemical abundances (Barbuy 1994; Idiart & de Freitas-Pacheco 1995; Weiss et al. 1995; Borges et al. 1995), in particular when some elements are enhanced with respect to the solar value. Empirical \mathcal{FF} s for Mg2 and NaD in which the effect of enhancement is considered have been presented by Borges et al. (1995). For all other indices one has to use the Worthey (1992) \mathcal{FF} s, in which the effect of enhancement is missing, but for the re-scaling of [Fe/H] given by equation (9). A great deal of the effect of enhancing α -elements is simply lost.

2.4 The Tripicco & Bell (1995) response functions

A general method designed to include the effects of enhancement on all indices at once has been suggested by Tripicco & Bell (1995, TB95), who introduce the concept of \mathcal{RF} s. In brief from model atmospheres and spectra for three prototype stars, i.e. a cool-dwarf star (CD) with $T_{\text{eff}}=4575$ K and $\log g=4.6$, a turn-off (TO) star with $T_{\text{eff}}=6200$ K and $\log g=4.1$, and a cool-giant (CG) star with $T_{\text{eff}}=4255$ K and $\log g=1.9$, they calculate the reference indices I_0 for the solar abundance ratios. Separately doubling the abundance X_i of the C, N, O, Mg, Fe, Ca, Na, Si, Cr and Ti in steps of $\Delta[X_i/H]=0.3$ dex, they determine the variation $\Delta I = I_{\text{enh}} - I_0$ in units of the observational error σ_0 . The indices I_0 , the observational error σ_0 , and the normalized ΔI are given in Tables 4, 5 and 6 of TB95.

Table 2. Abundance ratios for the solar-scaled and α -enhanced mixtures adopted in this study. The solar scaled values are taken from Anders & Grevesse (1989) however as revised by Grevesse & Sauval (1998). The enhancement factor $[X_{\text{el}}/\text{Fe}]=+0.40$ is the same as in Castelli & Kurucz (2004).

Element	$\Gamma = 0$		$\Gamma = 0.25$	
	A_{el}	A_{el}	$[X_{\text{el}}/\text{Fe}]$	$[X_{\text{el}}/H]$
O	8.83	9.23	0.40	0.1490
Ne	8.08	8.08	0.00	-0.2510
Mg	7.58	7.98	0.40	0.1490
Si	7.55	7.95	0.40	0.1490
S	7.33	7.73	0.40	0.1490
Ca	6.36	6.76	0.40	0.1490
Ti	5.02	5.42	0.40	0.1490
Ni	6.25	6.25	0.00	-0.2510
C	8.52	8.52	0.00	-0.2510
N	7.92	7.92	0.00	-0.2510
Na	6.33	6.33	0.00	-0.2510
Cr	5.67	5.67	0.00	-0.2510
Fe	7.50	7.50	0.00	-0.2510

The definition of the generic \mathcal{RF} to be used for arbitrary variations $\Delta[X_i/H]$ is

$$R_{0.3}(X_i) = \frac{1}{I_0} \frac{\Delta I}{\Delta[X_i/H]} 0.3$$

The \mathcal{RF} s for cool-dwarfs, cool-giants and turn-off stars constitute the milestones of the calibration. They are used by Trager et al. (2000a), Thomas et al. (2003a) and TC04a to transfer indices with solar abundance ratios to those enhanced in α -elements by means of two different algorithms.

As they are not strictly equivalent, some clarification is worth here.

Without providing a formal justification, Trager et al. (2000a) propose that the fractional variation of an index to changes of the chemical parameters is the same as that for the reference index I_0 according to the relation

$$\frac{\Delta I}{I} = \frac{\Delta I_0}{I_0} = \left\{ \prod_i [1 + R_{0.3}(X_i)]^{\frac{[X_i/H]}{0.3}} \right\} - 1 \quad (10)$$

where $R_{0.3}(X_i)$ are the \mathcal{RF} s we have defined above. The explanation of relation (10) has been provided by TC04a to whom the reader should refer for details. The advantage with this formulation is that no particular constraint is required on the sign of I_0 , and the ΔI given by TB95 are straightforwardly used.

A different reasoning has been followed by Thomas et al. (2003a). In brief, they start from the observational hint that in galactic stars $\text{Mg}2 \propto \exp([\text{Mg}/\text{H}])$ (see Borges et al. 1995), assume that all indices depend exponentially on the abundance ratios and introduce the variable $\ln I \propto [X_i/H]$, expand $\ln I$ in the Taylor series and, by replacing the partial derivatives with respect to abundances by the finite incremental ratios of TB95, express the fractional variation of an index to changes in the abundance ratios as

$$\frac{\Delta I}{I} = \left\{ \prod_i \exp(R_{0.3}(X_i) \frac{[X_i/H]}{0.3}) \right\} - 1 \quad (11)$$

The reader is referred to Thomas et al. (2003a) for the formal derivation of relation (11). Although relations (10) and (11) may look similar, actually they do not because in the latter the partial derivatives in the Taylor expansion have been replaced by the finite incremental ratios. This topic has been thoroughly discussed by TC04a.

The following remarks are worth to be made here. First, as emphasized by Trager et al. (2000a) and Thomas et al. (2003a), equations (10) and (11) while securing that the indices tend to zero for small abundances they let them increase with the exponent $[X_i/H]/0.3$. For abundances higher than $[X_i/H]=+0.6$ dex, the exponent may become too large and consequently both types of correction may diverge. Secondly, the use of equations (10) and (11) requires that the sign of the index to be corrected is the same of the corresponding I_0 in TB95. In general this holds good. In principle, it may, however, happen that the signs do not coincide. Furthermore, some of the indices I_0 in TB95 are negative so that the $\ln I$ variable cannot be defined and the Taylor expansions can no longer be applied. To overcome this potential difficulty, Thomas et al. (2003a) apply a correcting procedure forcing the negative reference indices I_0 of TB95 to become positive. This occurs in particular for $\text{H}\beta$ of cool-dwarf stars (and other indices as well). The argument is that neglecting non-LTE effects TB95 underestimate the true values of $\text{H}\beta$ so that negative values found for temperatures lower than approximately 4500 K should be shifted to higher, positive values (see for instance Fig. 12 in TB95). We suspect that any change to the values tabulated by TB95 may be risky for a number of reasons: (i) The \mathcal{RF} s have been derived from a set of data that include a significant number of stars with negative values of $\text{H}\beta$; (ii) the incremental ratios by

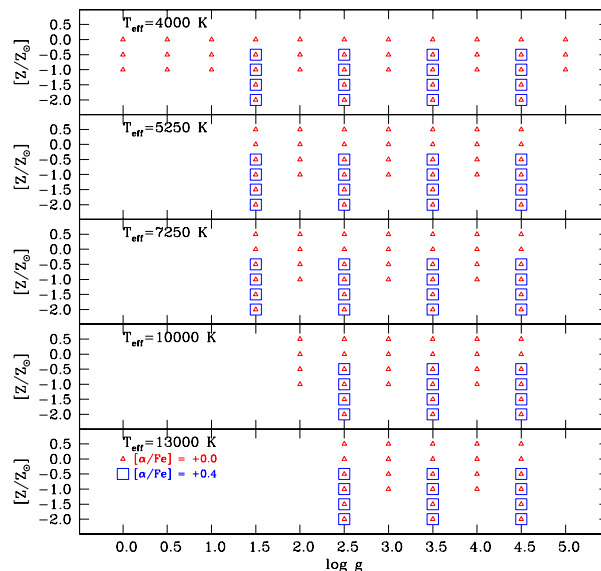


Figure 1. Coverage in the atmospheric parameters, and $[\alpha/\text{Fe}]$ of the 1-Å resolution spectra used in this study. The filled-triangles are for chemical compositions with solar abundance ratios $[\alpha/\text{Fe}]=0$ and $\Gamma=0$, whereas the open-squares are α -enhanced mixtures $[\alpha/\text{Fe}]=+0.4$ and $\Gamma=0.25$

TB95 have been calculated for particular stars (stellar spectra) with assigned T_{eff} , $\log g$ and I_0 . Changing the reference I_0 while leaving unchanged the incremental ratios (partial derivatives) may not be very safe. (iii) The replacement of the partial derivatives with the TB95 incremental ratios may be risky when dealing with exponential functions; (iv) the corrections found by Thomas et al. (2003a) for a number of indices are quite large; (v) finally, the use of $\ln I$ as dependent variable which requires that only positive values for I_0 are considered.

The application of equations (10) and (11) by TC04a has generated different and highly controversial results for some indices, $\text{H}\beta$ in particular, under unusual enhancements in some elements. In brief, TC04a presented grids of indices with α -enhanced abundance ratios. The indices were derived from the Salasnich et al. (2000) stellar models and isochrones with the abundance ratios by Ryan et al. (1991), and corrected by means of equation (10) of Trager et al. (2000a). The unusual abundance ratio for Ti ($[\text{Ti}/\text{Fe}]=0.63$) together with the interpolation among the fractional variations of the calibrating stars, yielded $\text{H}\beta$ strongly increasing with Γ . This immediately reflected on the ages assigned to galaxies by means of the minimum-distance method of Trager et al. (2000a,b) widely used by TC04a. The strong impact of Ti on $\text{H}\beta$ is due to the high \mathcal{RF} of this element for cool-dwarfs in the TB95 calibration. Decreasing the ratio $[\text{Ti}/\text{Fe}]$ to zero as in Trager et al. (2000a) or to 0.3 as in Thomas et al. (2003a), the results by TC04a were in close agreement with those by the other authors. It is worth recalling that the ratio $[\text{Ti}/\text{H}]$ entering equations (10) and (11), was 0 in Trager et al. (2000a), 0.023 in Thomas et al. (2003a) and nearly 0.2 in TC04a with obvious consequences. The effect was also confirmed by adopting the more recent determinations by Carney (1996) and Habgood (2001) of the $[\text{Ti}/\text{Fe}]$ in globular clusters that yield $\langle [\text{Ti}/\text{Fe}] \rangle \simeq 0.25 \div 0.30$, and by Gratton

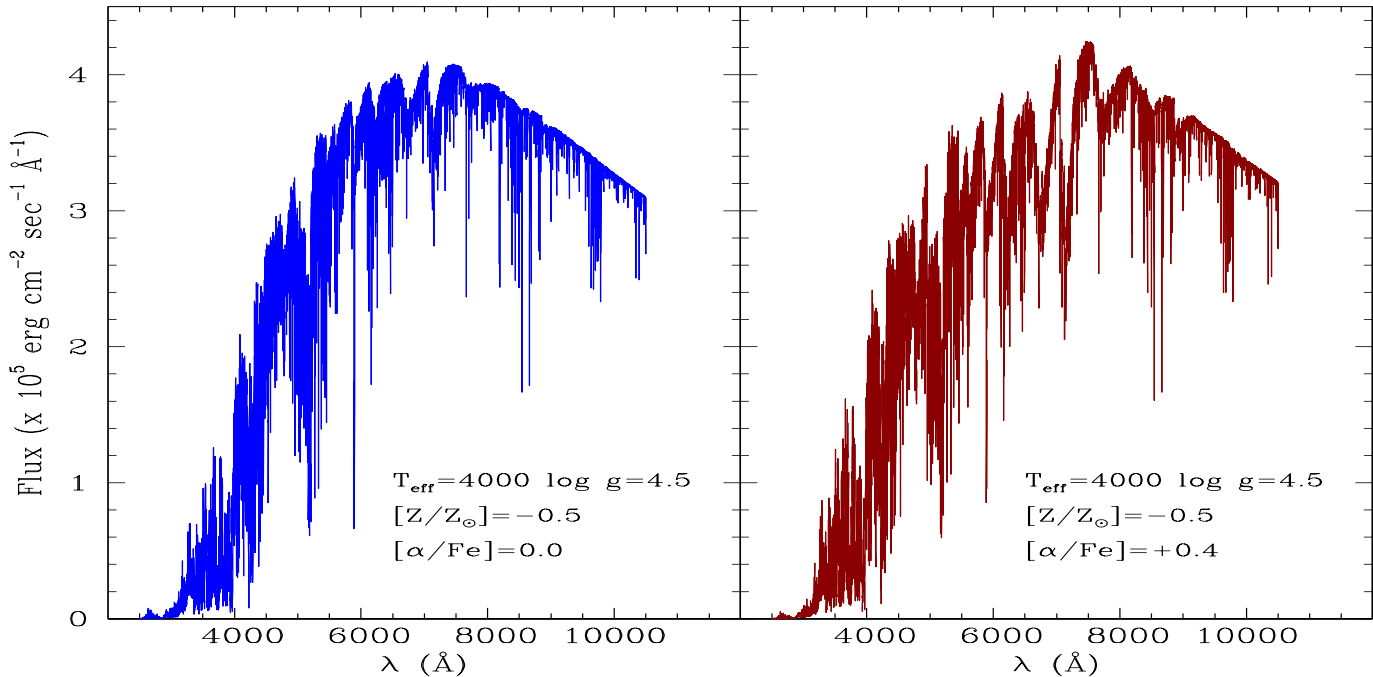


Figure 2. Left-hand panel: spectral energy distribution F_λ for the star with $T_{\text{eff}}=4000$ K, $\log g=4.5$, $[Z/Z_\odot]=-0.5$, $[\alpha/\text{Fe}]=0.0$ and $\Gamma=0$. The wavelength is in \AA . F_λ is in $\text{erg sec}^{-1}\text{cm}^{-2}\text{\AA}^{-1}$ and the resolution is 1\AA . Right-hand panel: the same but for $[\alpha/\text{Fe}]=+0.4$ and $\Gamma=0.25$

et al. (2003) for a sample of metal-poor stars with accurate parallaxes for which they yields $\langle[\text{Ti}/\text{Fe}]\rangle \simeq 0.20 \pm 0.05$ (TC04a). In any case the controversy about the correcting technique still remained. It can be reduced to the following statement: does $H\beta$ increase (significantly) with Γ or not? Or, even worse, does it decrease with it? According to Thomas et al. (2003a) there should be no difference in $H\beta$ at increasing Γ . The analysis below will clarify that this is not the case.

3 THE NEW RESPONSE FUNCTIONS

The above procedure for calculating indices and including α -enhancement will become obsolete when theoretical high-resolution spectra for different values of gravity, effective temperature, metallicity and degree of enhancement are available. In such a case, the indices can be straightforwardly calculated from the spectra with no need of \mathcal{FF} s and \mathcal{RF} s.

3.1 The high-resolution spectra

The spectra used in the present analysis are taken for a partial pre-release of the 2500–10500 \AA extensive synthetic spectral library computed by Munari et al. (2004). The spectral library is based on the new grid of ATLAS9 model atmospheres computed by Castelli & Kurucz (2004) for new opacity distribution functions that include, among other characteristics, the replacement of the solar abundances by Anders & Grevesse (1989) with those from Grevesse & Sauval (1998) and the TiO line-list by Kurucz (1993) with that of Schwenke (1998). The Munari et al. (2004) spectral library includes more than 200,000 spectra

at resolutions of 20,000 and 2000 (the latter matching the SLOAN spectra), as well as uniform dispersions of $1\text{\AA}/\text{pix}$ and $10\text{\AA}/\text{pix}$. In this work we have made use of the library version at $1\text{\AA}/\text{pix}$. The spectra cover the temperature range 3500–50000 K, gravity $0.0 \leq \log g \leq 5.0$, metallicities $-2.5 \leq [Z/Z_\odot] \leq +0.5$, micro-turbulence velocities 0,1,2,4 km/sec, enhancements $[\alpha/\text{Fe}]=0.0, +0.4$ and a dozen of different rotational velocities. When completed, the whole library will be used for a more complete analysis of the Lick indices and their applications. A strictly coordinated library of synthetic spectra is the one published by Zwitter et al. (2004) for the GAIA and RAVE wavelength range, amounting to 183,588 spectra covering a similar space of parameters.

The temperature, gravity and metallicity coverage of the stellar spectra in usage here is summarized in Fig. 1. Each panel is for a different effective temperature as indicated. The symbols show the combination of metallicity, expressed here in spectroscopic notation as $[Z/Z_\odot] = \log(Z/Z_\odot)$, and gravity ($\log g$) for which a spectrum has been calculated. The triangles are for $[\alpha/\text{Fe}]=0.0$ whereas the squares are for $[\alpha/\text{Fe}]=+0.4$. The parameters span the following ranges: two values of $[\alpha/\text{Fe}]$, i.e. $[\alpha/\text{Fe}]=0.0$ and $+0.4$; six values of $[Z/Z_\odot]$, i.e. $-2.0, -1.5, -1.0, -0.5, 0.0$ and 0.5 for $[\alpha/\text{Fe}]=0.0$, and only four values ($[Z/Z_\odot]=-2.0, -1.5, -1.0$ and -0.5) for $[\alpha/\text{Fe}]=+0.4$; five values of T_{eff} , i.e. 4000, 5250, 7250, 10000, and 13000 K; and finally eleven values of $\log g$ going from 0.0 to 5.0 in steps 0.5. The spectral grid is only a sub-set of the original model atmosphere grid, however fully adequate to the purposes of this study. The range of wavelength in each spectrum goes from 2500 \AA to 10500 \AA with resolution of 1\AA . The flux F_λ is in $\text{erg sec}^{-1}\text{cm}^{-2}\text{\AA}^{-1}$. In Fig. 2 we show for the sake of

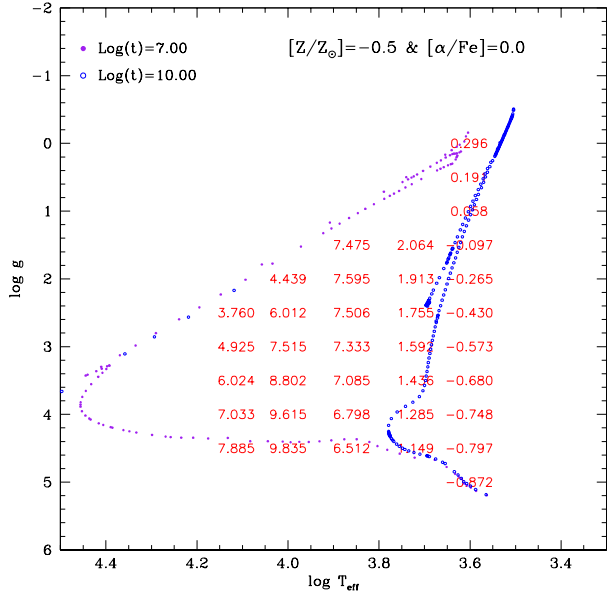


Figure 3. Variation of H β from 1- \AA resolution spectra across the HR-diagram in the $\log g$ versus $\log T_{\text{eff}}$ plane. Each value of H β corresponds to a star (theoretical spectrum) of given $\log g$, T_{eff} and $[Z/Z_{\odot}]$. The case under consideration is for $[Z/Z_{\odot}]=-0.5$ and $[\alpha/\text{Fe}]=0.0$. In the same diagrams we also plot two isochrones of the Padova Library with the same metallicity ($Z=0.008$) and ages of 0.01 and 10 Gyr.

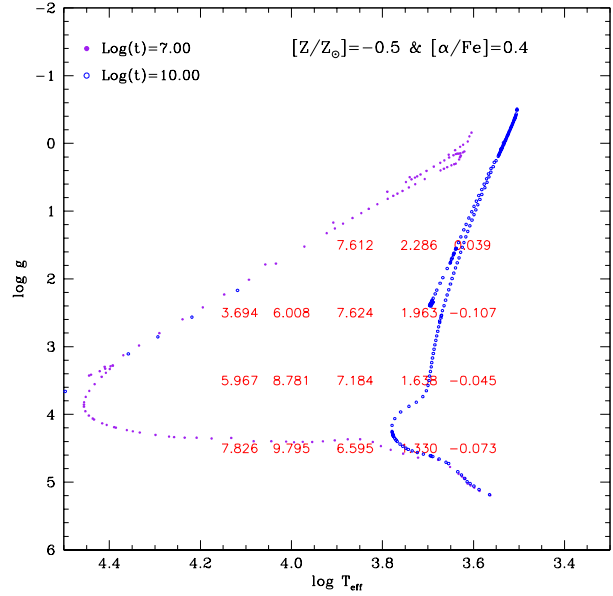


Figure 4. The same as in Fig. 3, but for $[\alpha/\text{Fe}]=+0.4$.

illustration the spectral energy distribution for the model with $T_{\text{eff}}=4000$ K, $\log g=4.5$, $[Z/Z_{\odot}]=-0.5$, micro-turbulence velocity $k=2$ km/sec, and $[\alpha/\text{Fe}]=0.0$ (left-hand panel) and $+0.4$ (right-hand panel). It fairly represents the case of a cool-dwarf star.

3.2 Indices from 1- \AA resolution spectra

With the aid of equations (1) and/or (2) and the pass-bands of Trager et al. (1998) listed in Table 1 we filter the energy distribution of each star in our grids and derive the indices. They are not strictly equivalent to the Lick system because the spectra in usage have 1- \AA resolution, whereas those on the Lick system have significantly smaller resolution (approximately 8.4 \AA) that also depends on the wavelength interval (see Worthey & Ottaviani 1997, for all details). This case will be considered in detail in Section 3.4.

The data for the whole sets of indices are not displayed but they are partly given in and partly recovered from Tables A1 through A4 to be described in Appendix A. We limit ourselves to show in Fig. 3 and 4 the variation of the index H β across the HR-diagram for the case with $[Z/Z_{\odot}]=-0.5$ and $[\alpha/\text{Fe}]=0.0$ and $+0.4$. In the same diagram we also plot two isochrones with the same metal content taken from the Padova Library (Girardi private communication): the ages are 0.01 Gyr and 10 Gyr. The grids of calibrating stars cover most of the HR-diagram in which real stars are found.

3.3 Response functions for 1- \AA resolution spectra

It is worth of interest here to present the analogue of the TB95 $\mathcal{R}\mathcal{F}$ s, the only major difference is that they cannot be

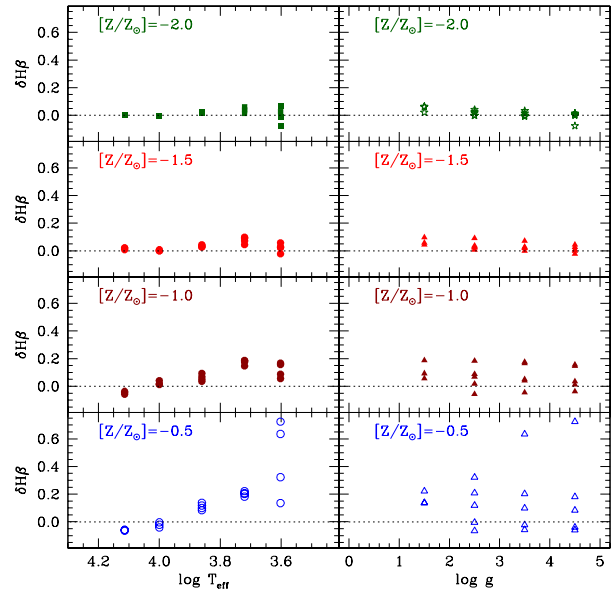


Figure 5. 1- \AA resolution spectra. Variations of the index H β passing from solar to α -enhanced chemical mixture. We plot the difference $(\delta I)_{T_{\text{eff}}, \log g, [Z/Z_{\odot}]}$ as a function of the atmospheric parameters as indicated. Left-hand panels: for each T_{eff} $\delta H\beta$ increases with $\log g$. Right-hand panels: for each $\log g$ $\delta H\beta$ decreases with T_{eff} .

evaluated for separate increases in the abundance of individual species $[\alpha_i/\text{Fe}]$ but only for all elements enhanced with respect to the solar value lumped together. Now the dependence of the $\mathcal{R}\mathcal{F}$ s on temperature, gravity, metallicity, and enhancement can be evaluated in detail. This was not the

case with TB95 calibration which stood on three stars with solar metallicity. We start calculating the differences

$$(\delta I)_{T_{\text{eff}}, \log g, [Z/Z_{\odot}]} = I_{\text{enh}} - I_{\text{sol}} \quad (12)$$

taken at fixed T_{eff} , $\log g$ and metallicity ($[Z/Z_{\odot}]$) and varying $[\alpha/\text{Fe}]$ from 0.0 to +0.4, whose corresponding indices are indicated as I_{sol} and I_{enh} , respectively. The difference for the whole sets of values are given in Tables A1-A4 for $[Z/Z_{\odot}] = -2.0, -1.5, -1.0$ and -0.5 , respectively.

In the four panels of Fig. 5 we show the case of $\text{H}\beta$. Each panel displays the variation of $\text{H}\beta$ at changing T_{eff} (left-hand panels) and /or $\log g$ (right-hand panels). We note that, for any metallicity and passing from $[\alpha/\text{Fe}] = 0.0$ to +0.4: (i) at given T_{eff} $\delta\text{H}\beta$ increases at increasing $\log g$; (ii) at given $\log g$ $\delta\text{H}\beta$ increases at decreasing T_{eff} . For most cases $\delta\text{H}\beta$ is positive, i.e. the index $\text{H}\beta$ increases at increasing $[\alpha/\text{Fe}]$ or, in other words, $\text{H}\beta$ for α -enhanced mixtures is greater than the solar case, keeping all other parameters constant. The increase is always significant, say approximately $0.1 \div 0.2$, but it can amount to nearly 0.8 for stars of low T_{eff} and high gravity, roughly in the intervals covered by cool-dwarf and old turn-off stars, which are the most interesting in view of the forthcoming applications.

Why such an increase with α ? The answer lies in relative variation of F_l and F_c . In the case of $\text{H}\beta$ (our prototype index) we derive the variation (δI) passing from solar to α -enhanced mixtures. Upon differentiating the index with respect to F_l and F_c ($\frac{\partial I}{\partial F_l} = -\frac{1}{F_c} \Delta \lambda$ and $\frac{\partial I}{\partial F_c} = \frac{F_l}{F_c^2} \Delta \lambda$) we obtain

$$(\delta I) = \Delta \lambda \left(\frac{F_l}{F_c} \right)_{\text{sol}} [\Delta \ln F_c - \Delta \ln F_l] \quad (13)$$

where $\Delta \ln F_l$ and $\Delta \ln F_c$ are the differences in the line and continuum fluxes passing from enhanced to solar. Plugging the values of F_l and F_c as appropriate, it turns out that the index increases with α . What happens is best illustrated in Fig. 6 which, limited to the case of a typical cool-dwarf with $T_{\text{eff}} = 4000$, $\log g = 4.5$ and $[Z/Z_{\odot}] = -0.5$ ($Z = 0.008$), shows how the index $\text{H}\beta$ is built up and how it varies passing from $[\alpha/\text{Fe}] = 0.0$ to $[\alpha/\text{Fe}] = +0.4$. First in the bottom panel we display the ratio $F_{\lambda, \text{enh}}/F_{\lambda, \odot}$ and the pass-bands defining the index $\text{H}\beta$. The absorption in the α -enhanced spectrum is significantly larger than in the solar-scaled one. The effect is larger in the blue pseudo-continuum and central band than in the red pseudo-continuum. This means that α -enhanced mixtures distort the spectrum in such a way that simple predictions cannot be made. This is due to the contribution of hundreds of molecular and atomic lines falling into the spectral regions over which the index is defined. Secondly, in the upper panel we show the spectral energy distribution of the solar-scaled (solid line) and α -enhanced (dotted line) spectrum and once more the pass-bands for $\text{H}\beta$. The open-circles and the big empty star show the mean fluxes in the three pass-bands and the interpolation of the pseudo-continuum to derive F_c in the case of solar-scaled spectrum. The filled-triangles and the empty pentagon are the same but for the α -enhanced mixture. The increase of $\text{H}\beta$ passing from solar to α -enhanced abundance ratios is straightforward.

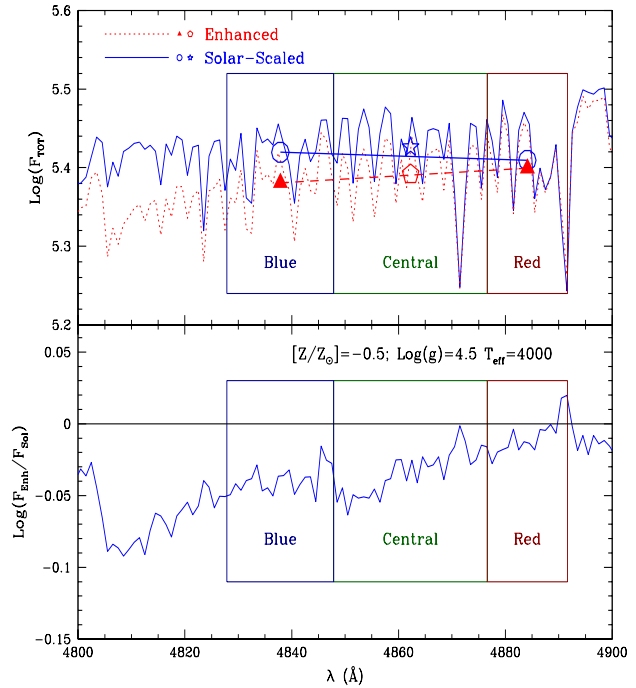


Figure 6. 1-Å resolution spectra. Building-up of the index $\text{H}\beta$ in the cool-dwarf with $T_{\text{eff}} = 4000$, $\log g = 4.5$ and $[Z/Z_{\odot}] = -0.5$ both for the solar scaled and enhanced pattern of abundance ratios with $[\alpha/\text{Fe}] = +0.4$. The bottom panel shows the ratio $F_{\lambda, \text{enh}}/F_{\lambda, \odot}$. The absorption in the α -enhanced spectrum is significantly larger than the solar-scaled one. The effect is larger in the blue wing of the pseudo-continuum and central band than in the red pseudo-continuum. Upper panel the spectral energy distribution of the solar-scaled (solid line) and α -enhanced (dotted line) spectrum and the passbands defining the index $\text{H}\beta$. The open-circles and star show the mean fluxes in the three pass-band and the interpolation of the pseudo-continuum to derive F_c in the case of solar scaled spectrum. The filled-triangles and pentagon are the same but for the α -enhanced mixture. The increase of $\text{H}\beta$ passing from solar to α -enhanced abundance ratios is straightforward.

With the differences (δI) , the equivalent of the TB95 $\mathcal{R}\mathcal{F}$ s [i.e. $R_{0.3}(X_i)$ s] is

$$R_{0.4}(\alpha) = \frac{1}{I_{\text{sol}}} \frac{I_{\text{enh}} - I_{\text{sol}}}{\Delta[\alpha/\text{Fe}]} 0.4 \quad (14)$$

where the symbol α reminds the reader that only variation for all elements enhanced at a time are available (the products in equations (10) and (11) would extend over one term only). Work is in progress to exactly repeat the analysis made by TB95, i.e. to provide partial $\mathcal{R}\mathcal{F}$ s by separately enhancing individual elements at a time. This would improve upon the $\mathcal{R}\mathcal{F}$ s and yet maintain alive the $\mathcal{F}\mathcal{F}$ s until high-resolution spectra will become a general tool.

Having done that, for the sake of a preliminary investigation of the whole subject, we linearly extrapolate the results obtained for $[Z/Z_{\odot}] = -2.0, -1.5, -1.0$, and -0.5 to higher values of the metallicity, i.e. $[Z/Z_{\odot}] = 0$ and 0.5 . The extrapolation is safe, because $(\delta I) = I_{\text{enh}} - I_{\text{sol}}$ smoothly change with the metallicity at given T_{eff} and $\log g$. Limited to the case of $\text{H}\beta$, this is shown in Fig. 7. The dependence is almost linear and nearly insensitive to gravity for $T_{\text{eff}} = 5250, 7250,$

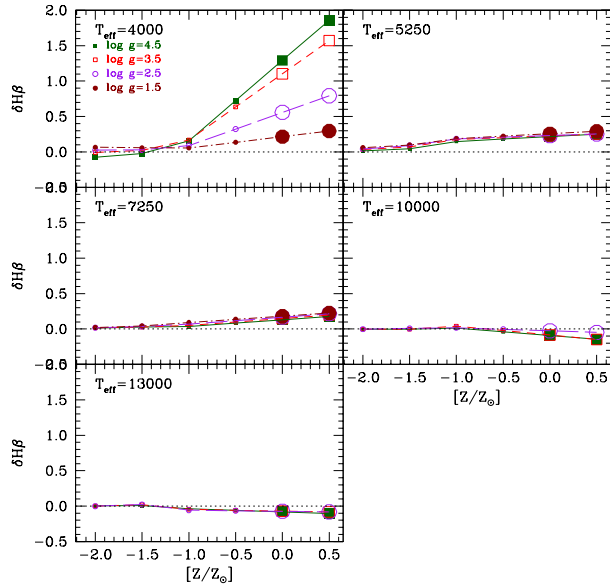


Figure 7. 1-Å resolution spectra. The variation $\delta H\beta$ as a function of the metallicity $[Z/Z_{\odot}]$ at fixed T_{eff} and $\log g$ as indicated. In each panel the big symbols display the value of $\delta H\beta$ linearly extrapolated to the metallicity $[Z/Z_{\odot}] = 0$ and 0.5.

Table 3. Varying FWHM as a function of the wavelength in the Lick system taken from Worthey & Ottaviani (1997).

Wavelength (in Å)	FWHM (in Å)
4000	11.5
4400	9.2
4900	8.4
5000	8.4
6000	9.8

10000 and 13000 K. The case of $T_{\text{eff}} = 4000$ deserves little attention, because $\delta H\beta$ tends to increase with $[Z/Z_{\odot}]$ and gravity. Adopting the simple linear extrapolation on $[Z/Z_{\odot}]$, we probably underestimate $\delta H\beta$ for solar and higher metallicities.

3.4 Indices and response functions at the Lick resolution

The 1-Å resolution spectra have been degraded to the resolution of the Lick system following Worthey & Ottaviani (1997). We have interpolated the FWHM given in Table 3 as a function of the wavelength. The new spectral energy distribution of each star in the calibrating grid have been filtered to derive the indices and the whole procedure described in Section 3.3 has been repeated. The data are given in Tables A5–A8 of Appendix A. These are the analogue of Tables A1 through A4. For the sake of comparison we show in Fig. 8 the differences $(\delta I)_{T_{\text{eff}}, \log g, [Z/Z_{\odot}]} = I_{\text{enh}} - I_{\text{sol}}$. In general, the new $(\delta I)_{T_{\text{eff}}, \log g, [Z/Z_{\odot}]}$ share the same trends as in the previous case, been however only slightly smaller. The most noticeable change is for H β , whose largest (δI) amounts to 0.6 instead of 0.8 for the case of a cool-dwarf ($T_{\text{eff}} = 4000$, $\log g = 4.5$) and $[Z/Z_{\odot}] = 0.008$. Also in this case

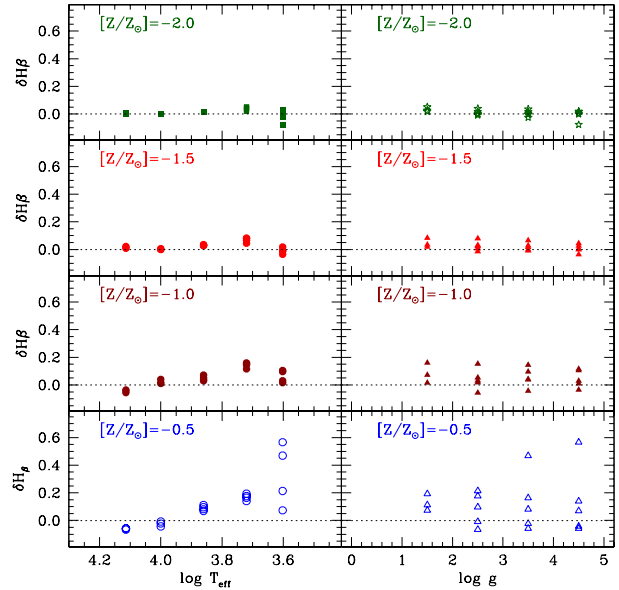


Figure 8. The same as in Fig. 5 but for spectra degraded to the resolution of the Lick system. The details are given in Section 3.4. In the various panels we show the variations of the index H β passing from solar to α -enhanced chemical mixture. We plot the difference $(\delta I)_{T_{\text{eff}}, \log g, [Z/Z_{\odot}]}$ as a function of the atmospheric parameters as indicated. Left-hand panels: for each T_{eff} $\delta H\beta$ increases with $\log g$. Right-hand panels: for each $\log g$ $\delta H\beta$ decreases with T_{eff} .

we linearly extrapolate the data to higher values of the metallicity for the sake of preliminary investigation. Indices and (δI) fully consistent with the Lick system will be used in the discussion below.

4 SSP INDICES FROM \mathcal{FF}_S AND NEW \mathcal{RF}_S

Owing to the large body of data and synthetic indices on the Lick system, it might be worth of interest to derive indices still based on the \mathcal{FF}_S but in which the old \mathcal{RF}_S are replaced by the new ones. This means that indices for $[\alpha/\text{Fe}] = 0.0$ are calculated as amply described in TC04a, whereas those for $[\alpha/\text{Fe}] > 0.0$ are obtained according to the following equation

$$I_{i,\text{enh}} = I_{i,\text{sol}} + \delta \mathcal{I}_i \quad (15)$$

where $I_{i,\text{sol}}$ is the solar-scaled index of the generic star in the SSP and $I_{i,\text{enh}}$ the is same but corrected for enhancement by $\delta \mathcal{I}_i$. This is derived by linearly interpolating both in $\log g$ and T_{eff} the new \mathcal{RF}_S (listed in Tables A5–A8)².

² It is worth recalling that an equivalent procedure would be to use equation (10) combined with (14) instead of equation (15).

4.1 Definition of SSP indices

The integrated indices of SSPs can be derived in the following way. We start from the flux in the absorption-line of the generic star of the SSP, $F_{l,i}$ ³

$$F_{l,i} = F_{c,i} \left(1 - \frac{I_{l,i}}{\Delta_\lambda} \right) \quad (16)$$

where $I_{l,i}$ is the index derived from the \mathcal{FF} s using the T_{eff} , $\log g$ and chemical composition of the star, and, in the case of α -enhancement, also corrected according to equation (15). $F_{c,i}$ is the pseudo-continuum flux and $F_{l,i}$ is the flux in the pass-band. The flux $F_{c,i}$ is calculated by interpolating to the central wavelength of the absorption-line, the fluxes in the midpoints of the red and blue pseudo-continua bracketing the line (Worthey et al. 1994).

To calculate the flux $F_{c,i}$ of a generic star one needs the theoretical spectrum of the same star. To be able to compare our results based on the \mathcal{RF} s with old ones by (Trager et al. (2000a); Thomas et al. (2003a) and TC04a) based on low-resolution spectra, we have to make use of stellar spectra with similar resolution. Therefore we leave aside the library of high-resolution spectra of Munari et al. (2004) and adopt the low-resolution one amalgamated by Girardi et al. (2002) and adopted by TC04a. As the backbone of this library are the Kurucz ATLAS9 model atmospheres and stellar spectra, there is partial consistency between the spectra adopted to evaluate the pseudo-continuum and the 1-Å resolution spectra adopted to derive the new \mathcal{RF} s.

Known the fluxes $F_{l,i}$ and $F_{c,i}$ for a single star, we weigh its contribution to the integrated value on the relative number of stars of the same type. Therefore the integrated index is given by

$$I_l^{\text{SSP}} = \Delta_\lambda \left(1 - \frac{\sum_i F_{l,i} N_i}{\sum_i F_{c,i} N_i} \right) \quad (17)$$

where N_i is the number of stars in the bin.⁴

When computing actual SSPs, single stars are identified to the isochrone elemental bins defined in such a way that all relevant quantities, i.e. luminosity, T_{eff} , $\log g$ and mass vary by small amounts. In particular, the number of stars in an isochrone bin is given by

$$N_i = \int_{m_a}^{m_b} \phi(m) dm \quad (18)$$

where m_a and m_b are the minimum and maximum star mass in the bin and $\phi(m)$ is the mass function in number. These are the equations adopted to calculate the indices of SSPs.

Finally, in view of the discussion below it is worth reminding the reader the definition of two indices that are

³ The relation for indices measured in magnitudes is

$$F_{l,i} = F_{c,i} 10^{-0.4I_{l,i}}$$

⁴ The same expression for indices measured in magnitudes becomes

$$I_l^{\text{SSP}} = -2.5 \log \left(\frac{\sum_i F_{l,i} N_i}{\sum_i F_{c,i} N_i} \right)$$

Table 4. Chemical composition and [Fe/H] as a function of Γ for the SSPs in use.

Z	Y	X	$\Gamma = 0.0$ [Fe/H]	$\Gamma = 0.25$ [Fe/H]
0.008	0.248	0.7440	-0.3972	-0.6472
0.019	0.273	0.7080	0.0000	-0.2501
0.040	0.320	0.6400	0.3672	0.1172
0.070	0.338	0.5430	0.6824	0.4324

commonly used but which do not belong to the original Lick system. They are $\langle \text{Fe} \rangle$ and $[\text{MgFe}]$

$$\langle \text{Fe} \rangle = 0.5 \times (Fe5270 + Fe5335)$$

$$[\text{MgFe}] = \sqrt{\text{Mgb} \times (0.5 \times Fe5270 + 0.5 \times Fe5335)}$$

4.2 Stellar models and isochrones

For the purposes of this study, we adopt the Padova Library of stellar models and companion isochrones according to the release by Girardi et al. (2000). This set of stellar models /isochrones differs from the classical one by Bertelli et al. (1994) for the efficiency of convective overshooting and the prescription for the mass-loss rate along the asymptotic red giant branch (AGB) phase. The stellar models extend from the zero-age mean sequence (ZAMS) up to either the start of the thermally pulsing AGB phase (TP-AGB) or carbon ignition. No details on the stellar models are given here; they can be found in Girardi et al. (2000) and Girardi et al. (2002). Suffice it to mention that: (i) in low-mass stars passing from the tip of red giant branch (T-RGB) to the horizontal branch (HB) or clump, mass-loss by stellar winds is included according to the Reimers (1975) rate with $\eta=0.45$; (ii) the whole TP-AGB phase is included in the isochrones with ages older than 0.1 Gyr according to the algorithm of Girardi & Bertelli (1998) and the mass-loss rate of Vassiliadis & Wood (1993); (iii) four chemical compositions are considered as listed in Table 4.

4.3 Results for SSP indices on the Lick resolution

Going into a detailed description of the dependence of the absorption-line indices for SSPs on age, chemical composition and Γ , is beyond the scope of this study.⁵ Suffice it to show in Fig. 9 the temporal evolution of eight important indices, i.e. Mgb, Mg2, H β , $\langle \text{Fe} \rangle$, H γ F, H δ F, [MgFe] and C₂4668, for the following combinations of metallicity and Γ , namely Z=0.008 (solid lines) and Z=0.070 (broken lines), $\Gamma=0$ (heavy lines) and $\Gamma = 0.25$ (light lines). The age goes from 0.01 to 18 Gyr. These results are very similar to those found by TC04a adopting the same library of stellar spectra, the Worthey et al. (1994) \mathcal{FF} s, the old \mathcal{RF} s of TB95 and the algorithm of Trager et al. (2000a). Finally, we note that the most controversial result in the studies by Tantaló &

⁵ The complete grids of absorption-line indices can be found on the web site <http://dipastro.pd.astro.it/galadriel>.

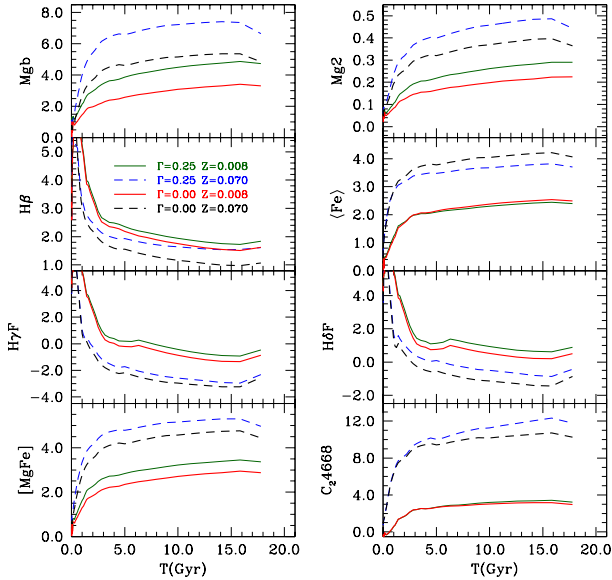


Figure 9. Indices on the Lick resolution calculated with the old $\mathcal{F}\mathcal{F}$ s and the new $\mathcal{R}\mathcal{F}$ s. The panels show the temporal variation of six different indices.

Chiosi (2004a,b), i.e. the increase of H β with Γ , is recovered by the present analysis.

4.4 Passing from old to new $\mathcal{R}\mathcal{F}$ s

To quantify the effect of the new $\mathcal{R}\mathcal{F}$ s with respect to the old ones by TB95, we compare here indices calculated with same pattern of abundances for the α -enhanced mixtures, using the classical $\mathcal{F}\mathcal{F}$ s of Worthey et al. (1994) but different $\mathcal{R}\mathcal{F}$ s and associated correcting algorithm. We shortly indicate with $I_{N\mathcal{R}\mathcal{F}}$ the indices calculated with the present $\mathcal{R}\mathcal{F}$ and equation (15) and with $I_{O\mathcal{R}\mathcal{F}}$ those calculated with the TB95 $\mathcal{R}\mathcal{F}$ and equation (10). The latter set of indices has been calculated assuming the same Γ and abundance ratios $[X_{\text{el}}/\text{Fe}]$ listed in Table 2. They are equivalent to those of Tantalo & Chiosi (2004a,b).

To exactly single out what is the behaviour of the two types of $\mathcal{R}\mathcal{F}$ s is a cumbersome affair due to the different stellar spectra and coverage of the T_{eff} and $\log g$ space. Most likely the main reason is the different quality of the spectra for the calibrating stars adopted by TB95 and Munari et al. (2004). Owing to the many improvements in the physics of stellar atmospheres introduced by Munari et al. (2004) and Castelli & Kurucz (2004), the more recent compilations for the solar abundances and many other details that are shortly summarized in Section 3.1, the new $\mathcal{R}\mathcal{F}$ s likely supersede the old ones. Looking at the indices in some detail, for the sake of brevity, we compare four indices, namely H β , Mg b, (Fe) and Mg 2, for the metallicities $Z=0.008$, 0.019 and 0.070 and $\Gamma=0.25$. This choice for the metallicity will allow us to check cases for which the $\mathcal{R}\mathcal{F}$ s have been extrapolated. The correlations between $I_{O\mathcal{R}\mathcal{F}}$ and $I_{N\mathcal{R}\mathcal{F}}$ are shown in Fig. 10. In each panel three groups of models are displayed whose metallicity increases going from bottom-left to top-right, whereas the age increases as indicated.

For Mg b there is no significant difference between the two groups. $\langle \text{Fe} \rangle_{N\mathcal{R}\mathcal{F}}$ is systematically larger than $\langle \text{Fe} \rangle_{O\mathcal{R}\mathcal{F}}$

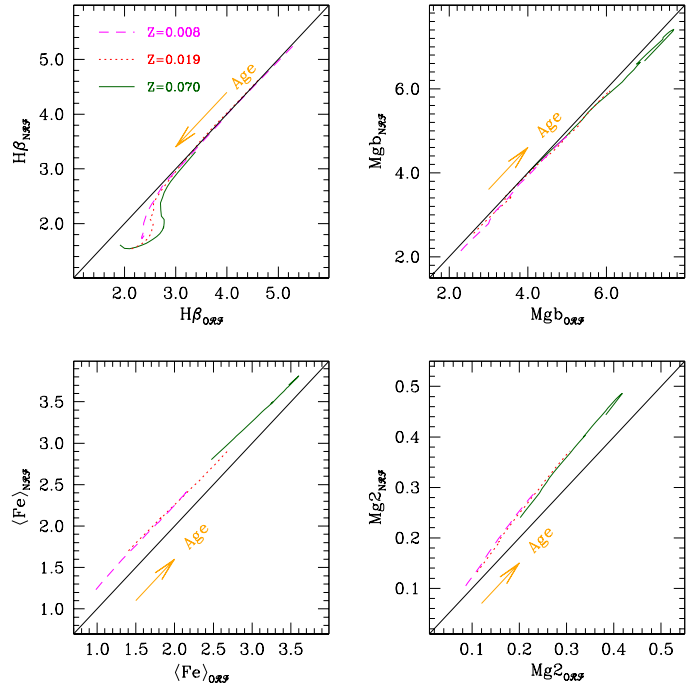


Figure 10. Indices on the Lick resolution: comparison between H β (top-left panel), Mg b (top-right panel), (Fe) (bottom-left panel) and Mg 2 (bottom-right panel) calculated with the $\mathcal{F}\mathcal{F}$ s of Worthey et al. (1994) but different $\mathcal{R}\mathcal{F}$ s and algorithms. They are shortly indicated as $I_{O\mathcal{R}\mathcal{F}}$ and $I_{N\mathcal{R}\mathcal{F}}$, respectively. $I_{O\mathcal{R}\mathcal{F}}$ means old $\mathcal{R}\mathcal{F}$ s by TB95 and equation (10), whereas $I_{N\mathcal{R}\mathcal{F}}$ means new $\mathcal{R}\mathcal{F}$ s and equation (15). The comparison is limited to the case with $\Gamma=0.25$ and three different metallicity as indicated.

by 0.2 \AA independently of metallicity and age; Mg 2 $_{N\mathcal{R}\mathcal{F}}$ becomes larger than Mg 2 $_{O\mathcal{R}\mathcal{F}}$ at decreasing age by as much as approximately 20 per cent. We suspect that for both indices the offset is due to differences in the stellar spectra that are difficult to pin down. Finally, in the case of H β there is coincidence independently of the metallicity for young ages, whereas for ages older and younger than 2 to 13 Gyr, respectively, H $\beta_{O\mathcal{R}\mathcal{F}}$ is larger than H $\beta_{N\mathcal{R}\mathcal{F}}$ and the difference increasing with metallicity. At older ages the two groups once again coincide. In the age range of the largest deviation occurs, the maximum difference amounts to approximately 30 per cent. We suspect that the reason for this difference is the correcting algorithm in usage when applied to elements for the $\mathcal{R}\mathcal{F}$ is strong. Recalling that the indices $I_{O\mathcal{R}\mathcal{F}}$ are calculated with $[\text{Ti}/\text{Fe}]=0.40$, one of the elements with the strongest $\mathcal{R}\mathcal{F}$ in TB95, the excess of H $\beta_{O\mathcal{R}\mathcal{F}}$ over H $\beta_{N\mathcal{R}\mathcal{F}}$ is most probably due to the correcting algorithm of equation (10) which tends to diverge whenever $[\alpha/\text{Fe}]$ or $[X_i/\text{H}]/0.3$ and $R_{0.3}(X_i)$ are high (see equation 10). In the case H $\beta_{N\mathcal{R}\mathcal{F}}$ the correction with respect to solar is smaller (even though sizable) because of the linearity of the algorithm in usage. For more details on this subject the reader is referred to the discussion by Tantalo & Chiosi (2004a).

In general, there seems to be overall agreement between the two groups of indices. What we learn from this comparison is that

- i) The new $\mathcal{R}\mathcal{F}$ s take into account effects that would otherwise be missed, in particular their dependence on the metallicity.

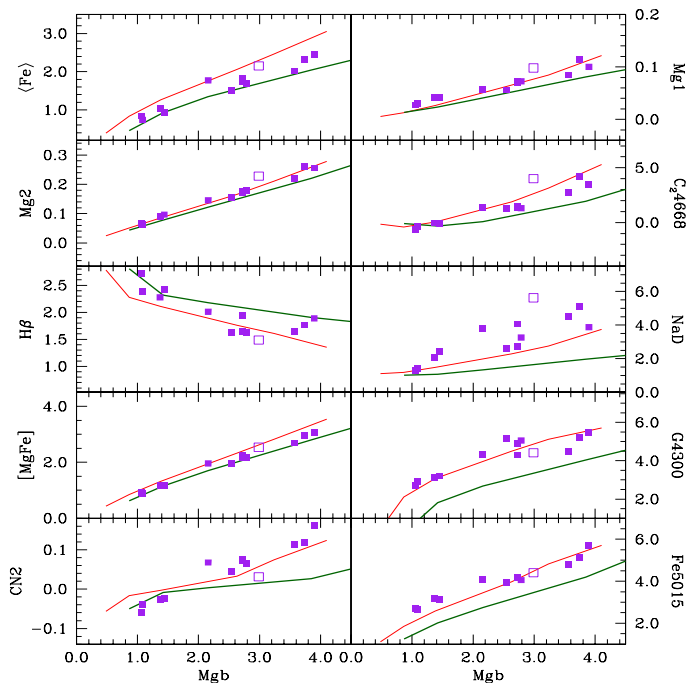


Figure 11. The Mg b index versus ten different indices on the Lick resolution calculated with metallicities typical of globular clusters. The thin-solid lines are the models with solar-scaled pattern of abundances, whereas the thick-solid are the models with $\Gamma=0.25$ and/or $[\alpha/\text{Fe}]=+0.4$. Along each line are shown the indices of SSPs with the same age, 12 Gyr and different metallicity from $[Z/Z_{\odot}]=-2$ ($Z\sim 0.0001$) to 0.0 ($Z\sim 0.019$). These models are calculated with the classical $\mathcal{F}\mathcal{F}$ s and the new $\mathcal{R}\mathcal{F}$ s. The filled-squares are the globular cluster data, the open-square is the galactic bulge from Puzia et al. (2002).

ii) The new $\mathcal{R}\mathcal{F}$ s for some indices and some stars, e.g. $H\beta$ for cool-dwarfs, have the opposite dependence on $[\alpha/\text{Fe}]$ as compared to that predicted by TB95. The result stems from the modern physical input of the new spectra.

No better comparison can be made at the present time, because we would need stellar spectra with abundances of elemental species increased one-by-one to derive the strict analogue of the $\mathcal{R}\mathcal{F}$ s by TB95. All this is still out of reach for obvious reasons. Work is progress to this aim.

5 COMPARISON WITH OBSERVATIONS: GLOBULAR CLUSTERS & GALAXIES

5.1 Galactic globular clusters

Prior to any other consideration, it is worth checking whether the present indices can reproduce the data for the galactic globular clusters and bulge of Puzia et al. (2002). To this end we have taken the isochrones of the Padova Library with chemical composition typical of the galactic globular clusters (Girardi et al. 2000), and derived the indices using the classical $\mathcal{F}\mathcal{F}$ s and the new $\mathcal{R}\mathcal{F}$ s. The results are shown in Fig. 11 for a number of indices. Along each line, are shown the indices of SSPs with same age but different metallicity from $[Z/Z_{\odot}]=-2.0$ ($Z\sim 0.0001$) to $[Z/Z_{\odot}]=0.0$ ($Z\sim 0.019$). The thin-solid lines are the models with solar-scaled pattern of abundances, whereas the thick-solid are the

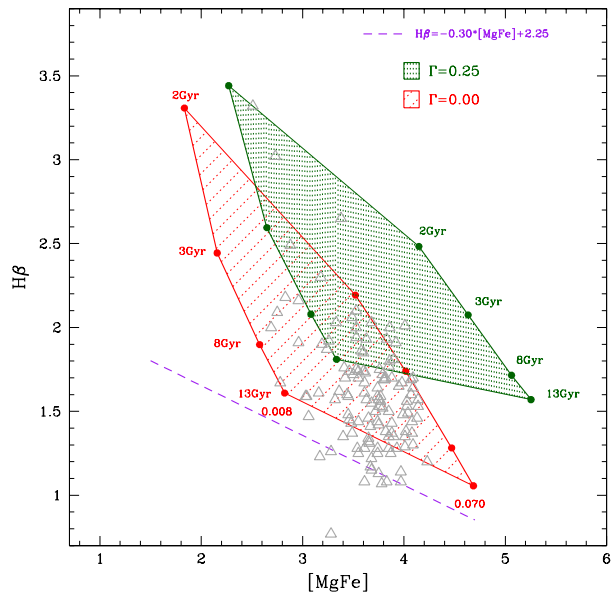


Figure 12. $H\beta$ versus $[\text{Mg}/\text{Fe}]$ plane on the Lick resolution. Comparison between theory and observational data for galaxies in the local universe. The theoretical indices are calculated with the old $\mathcal{F}\mathcal{F}$ s and the new $\mathcal{F}\mathcal{F}$ s. Each hatched area is comprised between two SSP of different metallicity ($Z=0.008$ left-side and $Z=0.070$ right-side). Along each SSP the age increases from 2 (top) to 13 Gyr (bottom) and two more values of the age are marked (3 and 8 Gyr). Two lines of constant age are displayed, i.e. 2 and 13 Gyr. Each area is for a different Γ as indicated. The data are the normal galaxies (open-triangles) of Trager (1997) corrected for emission. The dashed line is meant to provide a lower limit to $H\beta$ below which observational uncertainties may be so strong to render the comparison with theory meaningless (see the text for more details).

models with $\Gamma=0.25$ and/or $[\alpha/\text{Fe}]=+0.4$. Despite the fact that these indices were not particularly designed to match the globular clusters, the overall agreement is satisfactory. The new indices are of the same quality as those in TC04a and Thomas et al. (2003a). In general, the agreement is better for the solar-scaled mixture even though values of Γ in the range from 0.0 to 0.3 cannot be excluded. The index NaD depart from the observational value both in Thomas et al. (2003a), TC04a, and here.

5.2 Early-type galaxies: the observational sample to analyse

The two-indices diagnostic planes are often used to infer the age, metallicity and degree of enhancement, see TC04a for a thorough discussion of the subject. The most popular one is the $H\beta$ versus $[\text{Mg}/\text{Fe}]$ plane shown in Fig. 12 which displays the whole range of values that are expected for the indices in question at varying metallicity (heavy-solid lines), age (dots as labelled) and Γ (hatched areas as indicated). Each hatched area is enclosed between the two SSPs with the lowest and highest metallicity in our sample, i.e. $Z=0.008$ (left-hand) and $Z=0.070$ (right-hand) and two lines of constant age (13 Gyr bottom and 2 Gyr top). Along each SSP four values of the age are marked, so that other lines of constant age can be drawn. The hatched areas are for $\Gamma=0$ and

$\Gamma=0.25$ as indicated. The indices with $\Gamma=0.25$, for the highest metallicity have been obtained using (δI) extrapolated to higher values of $[Z/Z_{\odot}]$ (see Section 3.3). As our indices are strictly on the Lick resolution, they can be compared with the observational data for nearby galaxies based on spectra with similar resolution. In the following we make use of the data for early-type galaxies by Trager (1997) corrected for emission. The González (1993) list is part of this sample. The comparison with the theoretical indices is shown in the $H\beta$ versus $[MgFe]$ plane of Fig. 12.

Considering that the age of the Universe provided by WMAP is 13.7 ± 0.2 Gyr (Spergel et al. 2003), there is a significant number of galaxies falling below the 13 Gyr age-line even for the solar-scaled compositions (no enhancement in α -elements) (see also models by Vazdekis (1999) and Thomas et al. (2003a)). Moving to older ages is not viable and in any case would not remove the discrepancy because the age lines do not shift downward by the required amount. There are several reasons for observational $H\beta$ being too low compared to the theoretical expectation. First obvious observational uncertainties, secondly incompleteness of stellar models and isochrones, thirdly insufficient contamination by emission in particular for $H\beta$ (it worth recalling that the data under consideration have already been corrected for emission). Observational errors are estimated to amount to $\Delta H\beta \pm 0.22$ and $\Delta[MgFe] \pm 0.17$. Accuracy and completeness of stellar models have been examined in detail by TC04a to whom the reader should refer. The stellar models/isochrones in use are fairly accurate for our purposes. Emission not included in our theoretical indices is by far more uncertain to quantify (see Trager 1997; Trager et al. 2000a, for more details). To reconcile things the correction already applied by Trager (1997), the mean value of which amounts to about 0.1\AA , should be increased to about 0.2\AA . However, instead of arbitrarily changing the data, in order to somehow take all this into account, we prefer to drop from the sample all galaxies whose $H\beta$ falls below a suitable limit. This is represented by dashed line shown in Fig. 12, which runs parallel to the 13 Gyr age-line of the solar case ($\Gamma=0$), however shifted by -0.2\AA . It is implicitly assumed that owing the observational uncertainty the data for remaining galaxies are not in conflict with the theoretical expectation. In view of the discussion below it is worth mentioning that the limit we have assumed is not severe because only a dozens of galaxies of the Trager list are discarded.

5.3 Age, metallicity and α -enhancement in early type galaxies

In this section we highlight the effect of the new $\mathcal{R}\mathcal{F}$ s as compared to the old ones on the determination of the age, metallicity and enhancement factor of the stellar content of EGs. We adopt the minimum-distance method originally proposed by Trager et al. (2000a). In brief, suppose that a galaxy is characterized by a set of observationally measured indices $I_{i,obs}$, from which we want to infer the age, the metallicity (Z) and the degree of enhancement (Γ). On the theoretical side, suppose we have the corresponding indices tabulated as a function of the same quantities in form of discrete grids of values $I_{i,th}(t_j, Z_k, \Gamma_l)$ where j , k , and l vary from 1 to a certain value as appropriate. In the space of the indices I_i we define the distance between the obser-

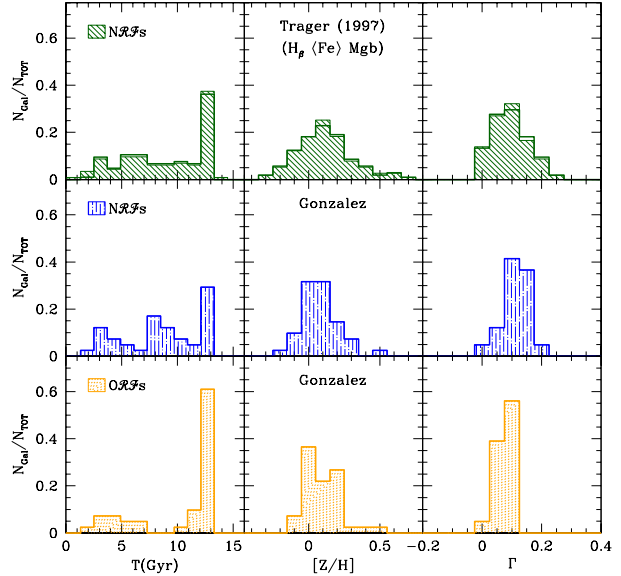


Figure 13. Distribution histograms of the age T (in Gyr), metallicity ($[Z/H]$) and enhancement factor Γ (from left to right) for the galaxies of the González (1993) and Trager (1997) catalogues. The results are obtained applying the minimum-distance method to the index-triplet $H\beta$, Mgb and $\langle Fe \rangle$. All models have the same pattern of chemical abundances, but make use of different $\mathcal{R}\mathcal{F}$ s as indicated. The top panel is for the Trager (1997), the mid panel is for the González (1993) sub-set, both adopt the new $\mathcal{R}\mathcal{F}$ s. Finally, the bottom panel is once again for the González (1993) list but adopt the old $\mathcal{R}\mathcal{F}$ s.

vational set $I_{i,obs}$ and a generic point of the correspondent space $I_{i,th}$:

$$D = \left[\sum_i (I_{i,th} - I_{i,obs})^2 \right]^{0.5} \quad (19)$$

By varying $I_{i,th}$ over the whole grid space we find the particular triplet j, k, l for which D is minimal. This means to fix the age, metallicity (Z) and Γ . To this aim, we generate the large grids of SSP indices spanning the following ranges of age, metallicity and Γ : $0 \leq T \leq 14$ Gyr, $0.008 \leq Z \leq 0.070$ in steps of $\Delta[Z/H]=0.022$ and $0 \leq \Gamma \leq 0.25$ in steps of $\Delta\Gamma = 0.005$. The upper limit for the age takes into account the recent estimate for the age of the Universe provided by WMAP, 13.7 ± 0.2 Gyr (Spergel et al. 2003).⁶ The analysis is made using the indices $H\beta$, $\langle Fe \rangle$ and Mgb , on which much work has been done in the past so that the comparison is possible. The observational indices are taken from the catalogs of González (1993) and Trager (1997). The analysis is made in two steps: first all galaxies are considered, secondly only those falling above the dashed line drawn in Fig. 12. The results are shown in Fig. 13. The top and middle panels display the distributions for the Trager and González lists obtained using the new $\mathcal{R}\mathcal{F}$ s: approximately 30 to 40 per cent of the galaxies are old objects in the age range 12-13 Gyr (remind that the maximum allowed age in the

⁶ It is worth recalling that at given Z and Γ , all enhanced elements are increased by the same factor ($[\alpha/Fe]=0.4$) and the iron abundance $[Fe/H]$ is accordingly scaled.

grids is 14 Gyr), the remaining show ages (i.e. traces of recent stellar activity) all over the age range from 2 to 12 Gyr. The situation is similar for case of the old $\mathcal{R}\mathcal{F}$ s applied to the González list (bottom panel), the only difference being that old galaxies are more numerous, approximately 70 per cent of the total. This case can be compared with similar results obtained by TC04a (see their Figs. 4 and 14).

The age distributions obtained with the new $\mathcal{R}\mathcal{F}$ s are fully consistent with those from the old ones despite the completely different technique to pass from solar-scaled indices to α -enhanced ones. Furthermore, without repeating here the thorough analysis made by TC04a, it is also evident how the age is sensitive to the specific pattern of abundance adopted to the total metallicity Z and total enhancement factor Γ . Enhancing some elements instead of others does not lead to the same results owing to their effect on specific indices (e.g. $H\beta$). It is not a mere coincidence that both here and in TC04a, in which $[\text{Ti}/\text{Fe}]=0.4$ and even higher has been used (other elements in common are enhanced by the same factor) solutions favouring old ages are found. The correcting technique, i.e. equation (10) or equation (15), plays a secondary role. Although we cannot prove it with detailed model calculations, because $\mathcal{R}\mathcal{F}$ s for separate changes in the enhancement are not available for the new high-resolution spectra, the hint arises that if we had assumed $[\text{Ti}/\text{Fe}]=0$ (as in Trager et al. 2000a) or $[\text{Ti}/\text{Fe}]<0.3$ (as in Thomas et al. 2003a,b; Thomas & Maraston 2003; Tantaló & Chiosi 2004a) the age distribution would be skewed toward younger ages. There is nothing special with Ti, other elements like Mg would likely yield the same effect provided they have strong $\mathcal{R}\mathcal{F}$ s at changing their enhancement factor.

Finally, we clean the samples of those galaxies with unusually low $H\beta$ (i.e. falling below the line in Fig. 12) and re-derive the age, metallicity and Γ . The distributions are shown by the bold lines drawn in the three panels of Fig. 13. As the limit is not a severe one, the net effects are small. Nevertheless, this source of uncertainty cannot be neglected because including galaxies with unusually low $H\beta$ s would certainly affect the age, metallicity and Γ distributions. It would force the assignment of formally old ages (often at the edge of the age-grid) to objects that probably are not that old. The effects on the metallicity and Γ are less crucial even if they are there.

5.4 The $H\beta$ versus $[\text{Mg}/\text{Fe}]$ plane: age or enhancement or both?

The large scatter in $H\beta$ shown by galaxies in the diagnostic plane of Fig. 12 is commonly attributed to a large scatter in the age caused by secondary episodes of star formation (see Tantaló & Chiosi 2004b, for a thorough discussion of this topic). However, it is also evident that galaxies with the same metallicity and age may have significantly different $H\beta$ and $[\text{Mg}/\text{Fe}]$ because of enhancement effects. The effect of Γ on $H\beta$ in particular, is far from being negligible as claimed in previous studies. Other values of Γ cannot be investigated at the present time since we simply lack the calibration (extrapolation to higher values of Γ is not safe). However, even with the present results, we may predict that among old objects of the same age there could be a natural scatter in the diagnostic planes caused by galaxy to galaxy variation in

the mean degree of enhancement due to the particular star formation history (Tantaló & Chiosi 2004b).

To cast light on this issue and the role played by the three parameters on the observational scatter in the $H\beta$ versus $[\text{Mg}/\text{Fe}]$ plane the following analysis is made. We start selecting from the sample of galaxies shown in Fig. 12 a sub-set suited to our purposes: first we drop all galaxies with very large $H\beta$ (larger than 2.5) as they are very likely affected by ongoing or recent star formation; secondly we drop all galaxies whose $H\beta$ is below the dashed line shown in Fig. 12. The remaining galaxies should represent a fair sub-sample in which the effects of the three parameters are evenly balanced. We need now to specify what we mean by normal- and strong- $H\beta$. As the range spanned by $H\beta$ for variations in Z , Γ and age (we assume 1/3 of the Hubble time, i.e. 4 Gyr) is of the order of 0.3\AA , we add this quantity to the mean value for a solar scaled old galaxy and take $H\beta=1.6$ as the transition from typical to high values.

Using the ages, metallicities and Γ found with the minimum-distance method for this sub-sample of galaxies, in Fig. 14 we correlate the age with Γ using different symbols for galaxies with low- and high- $H\beta$. Galaxies with $H\beta\leq 1.6$ (empty circles) are preferentially old (13 Gyr) and spanning a large range of Γ ; in this group, however, there are also a few younger objects with $\Gamma\leq 1$. Galaxies with $H\beta>1.6$ tend to be younger (more recent episodes of star formation) and less enhanced in α -elements, and to span a narrower range of Γ than in the previous group. However also in this case there are objects of both old age and high Γ . The age and Γ distributions for the two groups are shown in the top and right-hand panels of Fig. 14.

Finally, taking the linear best fit of the data regardless of $H\beta$ (long-dashed line) the general trend emerges: at increasing age the degree of enhancement increases as shown by the long dashed line in the central panel of Fig. 14.

To conclude, the possibility that old galaxies of the same age scatter in the diagnostic plane because of the enhancement is proved.

5.5 Is there a global age-metallicity-enhancement relationship?

We may also take into account the third parameter, i.e. the metallicity, and search for global correlations.

Grouping galaxies according to the value of Γ and/or metallicity and looking at the age distributions shown in the top and bottom panel of Fig. 15 we note that: (i) approximately 70 per cent of the galaxies with $\Gamma>0.10$ (dashed histogram) are associated to ages of 12-13 Gyr, whereas approximately 70 per cent of the galaxies with $\Gamma\leq 0.10$ are distributed from 2 to 10 Gyr (dotted histogram); (ii) about 80 per cent of galaxies with $[\text{Z}/\text{H}]\leq 0$ are 12-13 Gyr old, whereas 70 per cent of galaxies $[\text{Z}/\text{H}]>0$ have ages in the range 2-7 Gyr.

An attempt to describe the global correlation among age, metallicity and degree of enhancement is shown in Fig. 16 where we draw the 3D-linear fit of the three parameters. The situation can be summarized as follows: at increasing age, the mean metallicity decreases whereas Γ increases. The opposite at decreasing age. In more detail, old galaxies with no subsequent episodes of star formation have metallicities in the range $-0.4<[\text{Z}/\text{H}]<0.2$ and enhancement

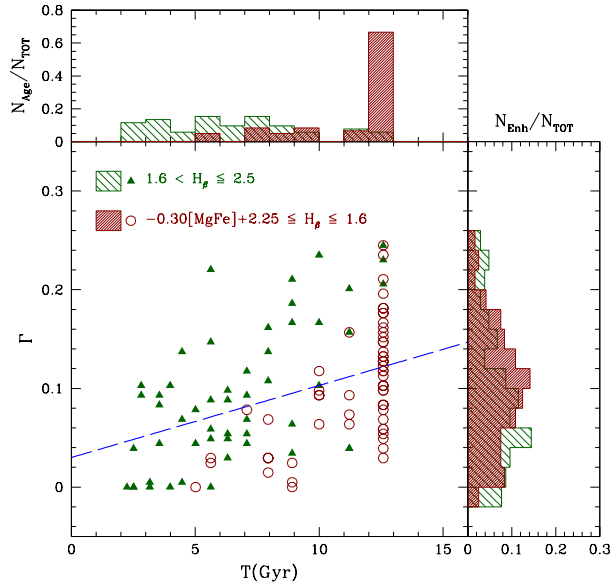


Figure 14. Γ versus T (in Gyr) plane. The data correspond to the sub-sample of the Trager (1997) catalogues selected to have $-0.30[\text{MgFe}] + 2.25 \leq H\beta \leq 2.5$ (see Fig. 12 and text for more details). Open circles are for $-0.30[\text{MgFe}] + 2.25 \leq H\beta \leq 1.6$ and filled triangles for $1.6 < H\beta \leq 2.5$. Dotted and dashed lines represent the linear best fit of the galaxies with higher and lower $H\beta$, respectively. Long-dashed line show the same but for the whole sample. Top panel gives the age distribution for both sub-sample as indicated, whereas the right-hand gives the Γ distribution.

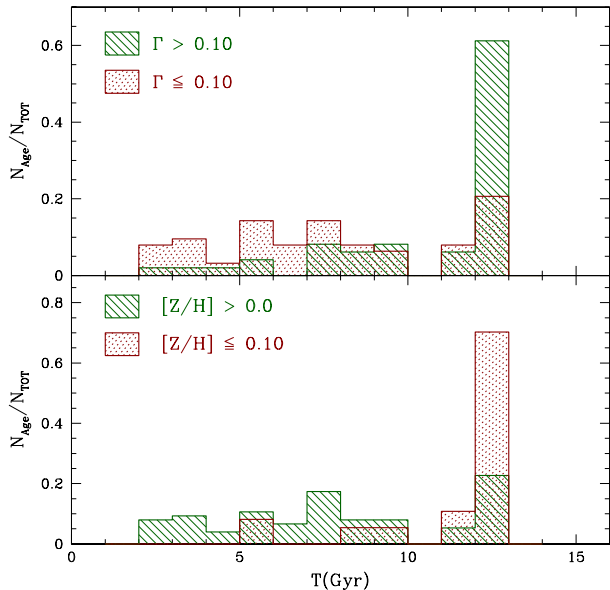


Figure 15. Age distribution for the sub-sample of galaxies with $-0.30[\text{MgFe}] + 2.25 \leq H\beta \leq 2.5$ (see Fig. 12 and text for more details). Top panel for $\Gamma > 0.10$ (dashed histogram) and $\Gamma \leq 0.10$ (dotted histogram). Bottom panel for $[\text{Z}/\text{H}] > 0$ (dashed histogram) and $[\text{Z}/\text{H}] \leq 0$ (dotted histogram).

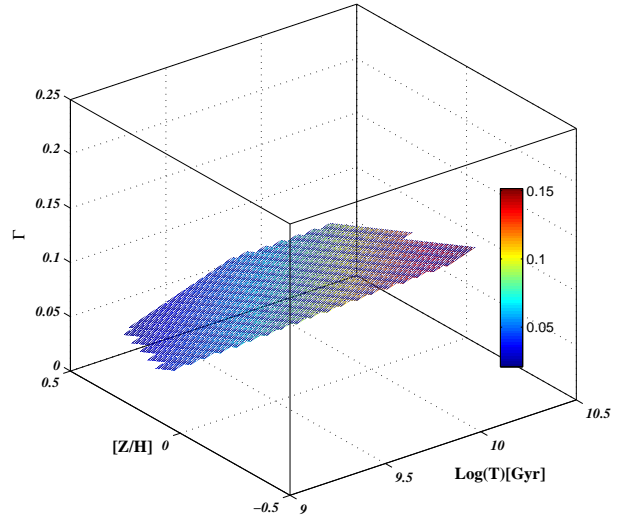


Figure 16. 3D-linear fit of the parameter space age (on logarithmic scale), metallicity $[\text{Z}/\text{H}]$ and Γ obtained with the minimum-distance method for the galaxies of Trager (1997). See the text for more details

factors in the interval $0 < \Gamma < 0.25$; galaxies with more recent episodes of star formation (younger ages) span the ranges $0 < [\text{Z}/\text{H}] < 0.6$ and $0 < \Gamma < 0.1$. This means that in the course of time, stars are made out of gas that has been highly reprocessed thus forcing high metallicities and low enhancement. All this in agreement with current understanding of chemical enrichment in galaxies and the effects by Type II and Type Ia supernova explosions.

6 SSPs INDICES DIRECTLY MEASURED ON 1-Å RESOLUTION SPECTRA

In so far the key result of this study are the new $\mathcal{R}\mathcal{F}$ s derived for a wider range of the atmospheric parameters and metallicities with respect to TB95. Even if this is a significant step forward, indices of the Lick system (or another system in general) can be directly obtained from high-resolution spectra without passing through the $\mathcal{F}\mathcal{F}$ s and $\mathcal{R}\mathcal{F}$ s, but simply filtering the spectral energy distribution of a star and/or SSP and/or galaxy. The only requirement to keep in mind is that the theoretical and observational spectra on which indices are measured, must have the same resolution. In this section we present for the first time indices on the Lick system directly measured on synthetic 1-Å resolution spectra.

First we derive the theoretical indices for single stars of assigned atmospheric parameters, and compare them those for the stars in STELIB by Le Borgne et al. (2003) containing spectra at ~ 3 -Å resolution. Owing to the small difference in resolution between STELIB and Munari et al. (2004) spectra, we may reasonably surmise that the empirical indices of STELIB do not significantly differ from those obtained from the 1-Å resolution spectra. Secondly, we analyse the behaviour of the new high-resolution indices in the same fashion as done in Section 4.3.

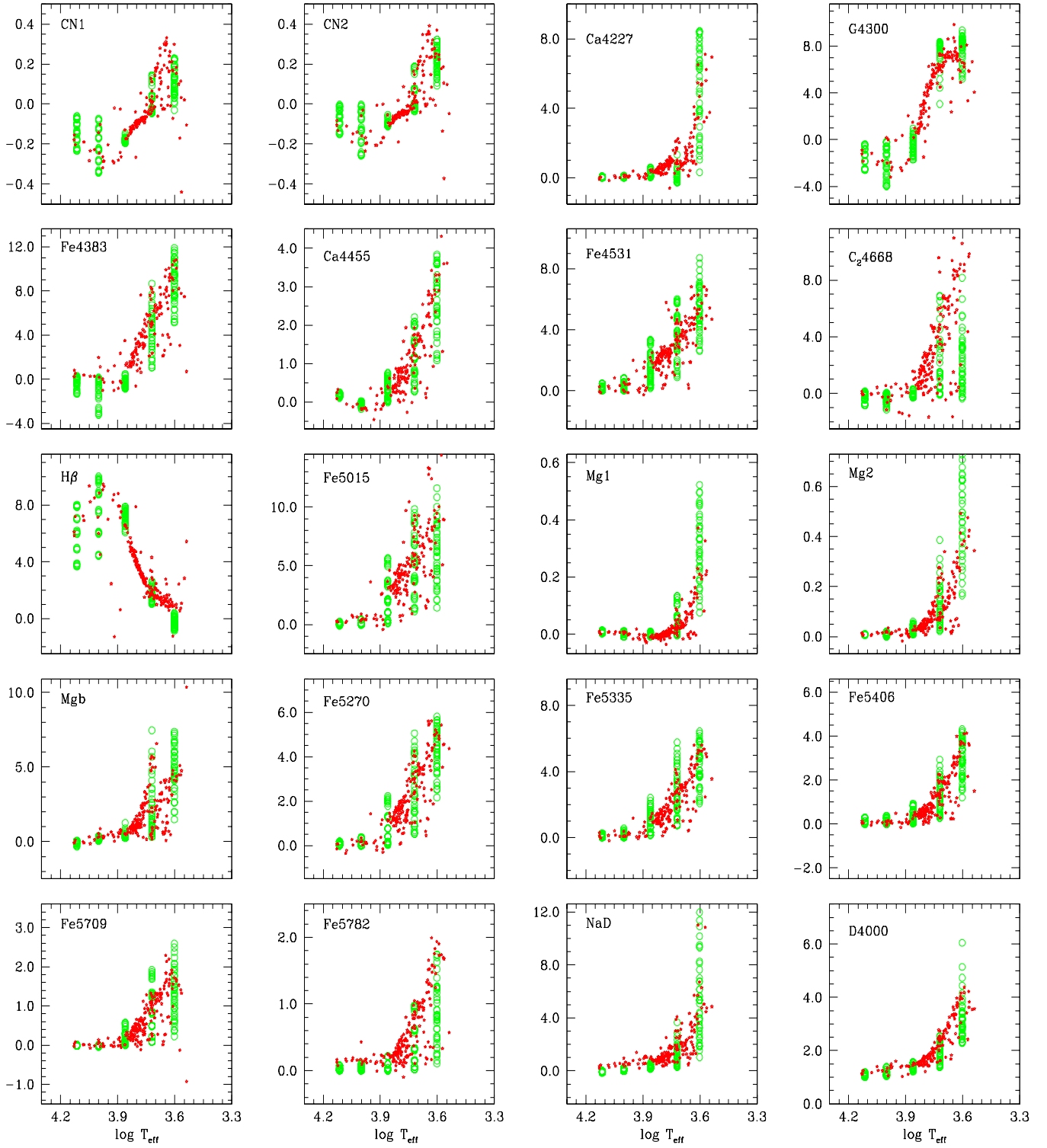


Figure 17. Comparison of 19 indices of the Lick system plus D4000 measured on a selected sample of stars of STELIB, for which the atmospheric parameters are known and the spectrum is complete, with the indices derived from theoretical 1-Å resolution spectra of the whole T_{eff} , $\log g$ and $[\text{Fe}/\text{H}]$ grid adopted in this work. The small dots are the STELIB objects whereas the open-circles are the theoretical spectra. The comparison is made as a function of T_{eff} .

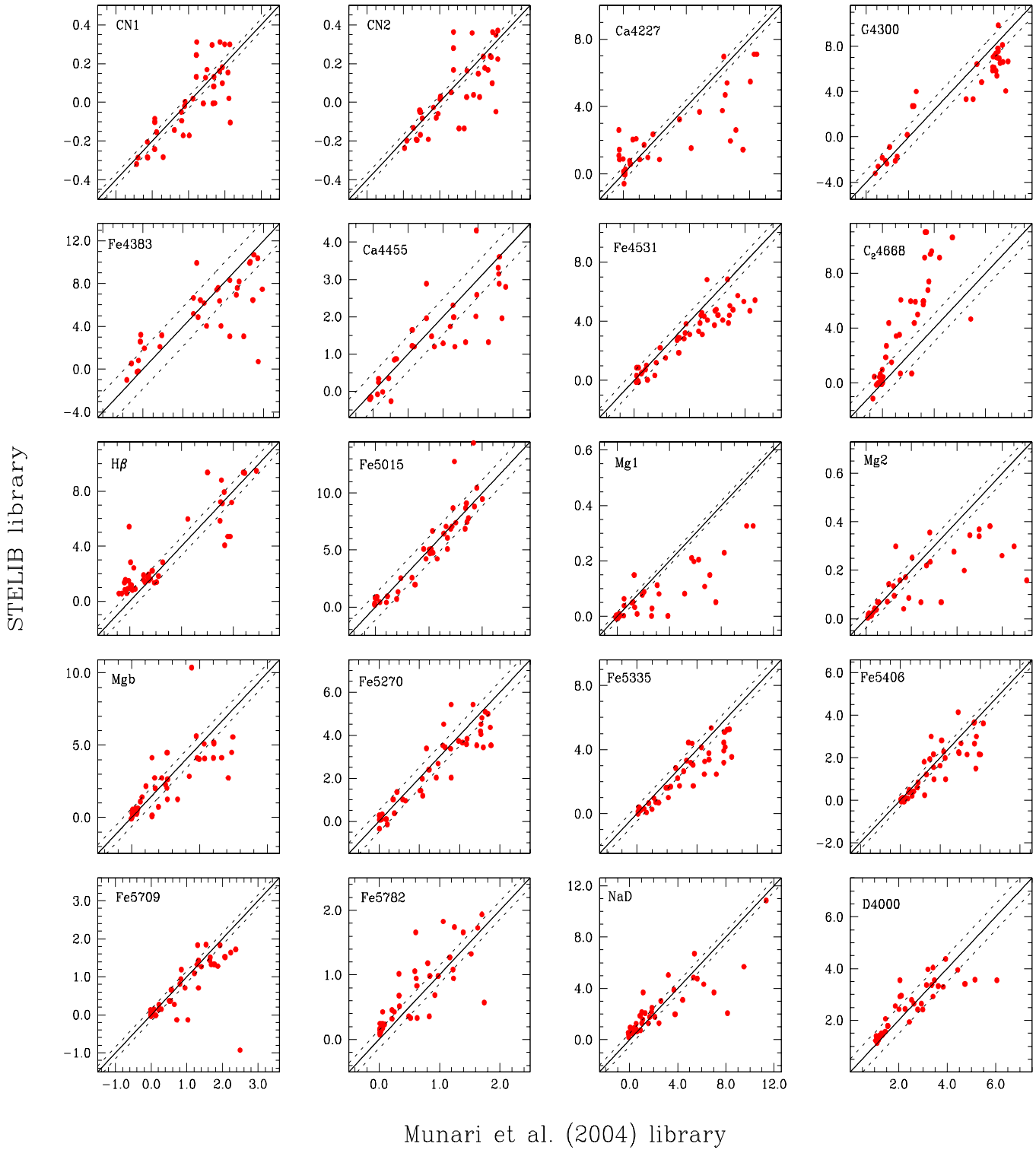


Figure 18. Index-index comparison between the value measured from the theoretical spectra of the Munari et al. (2004) library and the one derived from stars of STELIB selected to have the closest matches of the T_{eff} , $\log g$ and $[\text{Fe}/\text{H}]$ of our library. The transverse solid and dotted lines show the loci of equality and ± 20 per cent uncertainty.

6.1 Indices for single stars and comparison with STELIB

The first step to undertake is to derive indices for a template of stars and compare them with the theoretical counterparts

obtained from our library of 1-Å resolution spectra. To this end we sort out from STELIB (Le Borgne et al. 2003) all stars with known T_{eff} , $\log g$, metallicity and, more relevant here, complete spectra. Approximately 141 stars meet the four requirements. Each star of our library is then associ-

ated to a star of the STELIB sub sample by means of the minimum distance method in the space T_{eff} , $\log g$ and $[\text{Fe}/\text{H}]$ (or $[\text{Z}/\text{Z}_{\odot}]$). Only theoretical spectra of the solar partition case ($\Gamma=0$) are considered. The empirical and theoretical spectra of the selected sample are finally filtered with the Lick system and their indices are derived.

In Fig. 17 we show for each index the correspondence between the empirical (small-dots) and the theoretical spectra (open-circles) as a function of $\log T_{\text{eff}}$. Considering the underlying scatter in $\log g$ and $[\text{Fe}/\text{H}]$ and the coarse grid of T_{eff} for the theoretical spectra, the agreement is fairly good.

Fig. 18 compares index-by-index the results obtained from STELIB (y axis) and our library of theoretical spectra (x axis) for the reference stars. In each panel the dotted diagonal lines define the strip of 20 per cent uncertainty with respect to equality. The scatter can be accounted for by (i) the coarse association of the three parameters ($\log T_{\text{eff}}$, $\log g$ and $[\text{Fe}/\text{H}]$), the slightly different resolution of the STELIB (3\AA) and our spectra (1\AA), and (iii) perhaps real difference in the chemical parameters passing from data to theory.

6.2 Indices for SSPs

In this section we derive the Lick indices for SSPs. As extrapolating spectra out of the parameter range for which they have been calculated may be risky, the analysis is limited to the metallicities in the range $Z=0.0004$ to $Z=0.008$, i.e. $[\text{Z}/\text{Z}_{\odot}]=-2.0$ to -0.5 and $\Gamma=0$ to $\Gamma=0.25$.

To derive the spectral energy distribution of a SSP we apply the standard population synthesis technique (see Bressan et al. 1994, for all details). In brief, along each elemental bin of an isochrone (characterized by $\log T_{\text{eff}}$, $\log g$ and the relative number of stars dN) we associate the spectrum derived from linearly interpolating the 1-\AA resolution spectral grid. Then we sum up all elemental contributions along the isochrone weighed on the relative number of stars and luminosity of the bin. The SSP spectrum is filtered with the passbands for each index according to its definition to derive $F_{l,i}$ and $F_{c,i}$ for each elemental bin and finally equation (15) is applied to obtain the total index.

The results are shown in Fig. 19, which displays the temporal evolution of the indices $\text{H}\beta$, $\text{H}\gamma\text{F}$, $\text{H}\delta\text{F}$, (Fe) , Mgb , $\text{Mg}2$, $[\text{Mg}/\text{Fe}]$ and C_24668 , and in Fig. 20, that is the analogue of Fig. 12 limited to the sub-solar metallicities ($Z \leq 0.008$). First of all it is evident that the new indices share the same trends of the old ones thus lending internal consistency to the whole problem. Secondly, the effects of enhancement are in agreement with the expectation for the metallicities in use. Thirdly despite the limited and coarse coverage of the spectral library in the temperature-gravity space the results seem to be adequate. However, no comparison with the observational data can be made because they should be obtained with the same resolution as the theoretical indices.

However, there are systematic differences. Looking at metallicity $Z=0.008$ in common between the SSPs displayed in Fig. 12 and those of Fig. 20 we note:

(i) for the solar-scaled mixture ($\Gamma=0$) at the age of 2 Gyr $\Delta\text{H}\beta=0.0$ and $\Delta[\text{Mg}/\text{Fe}]=0.45$ passing from the indices with the old $\mathcal{F}\mathcal{F}$ s and the new $\mathcal{R}\mathcal{F}$ s to those straight from the spectra, at the age of 13 Gyr the same differences amount to $\Delta\text{H}\beta=0.20$ and $\Delta[\text{Mg}/\text{Fe}]=0.15$;

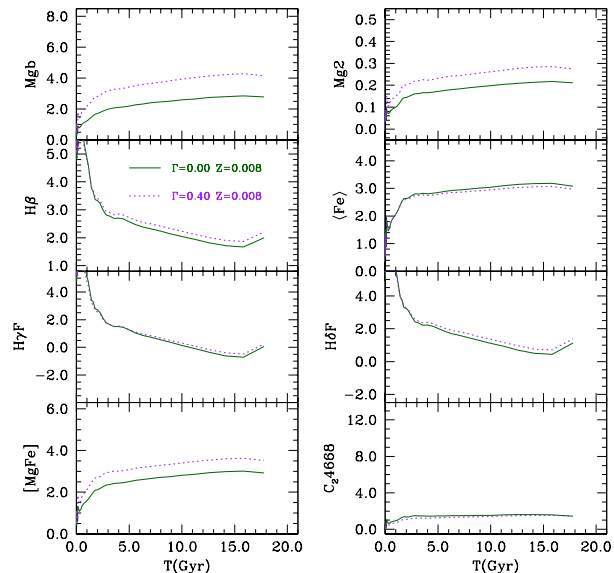


Figure 19. Indices straight from 1-\AA resolution spectra: the temporal variation of indices. No use of $\mathcal{F}\mathcal{F}$ s and $\mathcal{R}\mathcal{F}$ s is made. The metallicity is $Z=0.008$. The thin lines are for $\Gamma=0$, whereas the thick lines are for $\Gamma=0.25$.

(ii) for α -enhanced mixture ($\Gamma=0.25$) at age of 2 Gyr $\Delta\text{H}\beta = -0.05$ and $\Delta[\text{Mg}/\text{Fe}]=0.45$, whereas at the age of 13 Gyr the same differences amount to $\Delta\text{H}\beta=0.10$ and $\Delta[\text{Mg}/\text{Fe}]=0.20$. Whether these differences are real or due to the coarse grids in T_{eff} and $\log g$ cannot be assessed at the present time. Work is in progress to calculate indices with a finer spacing in temperature and gravity and a range of different resolutions.

7 DISCUSSION AND CONCLUSIONS

We have generated synthetic absorption-line indices on the Lick system based on the recent library of 1-\AA resolution spectra calculated by Munari et al. (2004) over a large range of atmospheric parameters ($\log T_{\text{eff}}$, $\log g$ and $[\text{Fe}/\text{H}]$) and both for solar and α -enhanced abundance ratios in the chemical composition. The study is made in two steps:

(i) First we derive a modern version of the so-called $\mathcal{R}\mathcal{F}$ s of TB95. Contrary to the previous situation in which the $\mathcal{R}\mathcal{F}$ s were known only for three stars of given T_{eff} and $\log g$, now the $\mathcal{R}\mathcal{F}$ s are given for large range ranges of T_{eff} , $\log g$ and $[\text{Fe}/\text{H}]$ (or $[\text{Z}/\text{Z}_{\odot}]$). Not only the $\mathcal{R}\mathcal{F}$ s vary with the type of star but also with the metallicity.⁷ The effect of metallicity is important and cannot be neglected.

(ii) With the aid of the new $\mathcal{R}\mathcal{F}$ s and the $\mathcal{F}\mathcal{F}$ s of Worthey et al. (1994) indices for SSPs are calculated and compared with the old ones by TC04a. But for the differences caused by the new $\mathcal{R}\mathcal{F}$ s, the agreement is good thus confirming that the method adopted by TC04a to correct for the effect of α -enhancement albeit hampered by the coarse grid of calibrating stars in TB95 was correct. These results

⁷ The new $\mathcal{R}\mathcal{F}$ s are given as large 3D-matrices made available on the web page <http://dipastro.pd.astro.it/galadriel>.

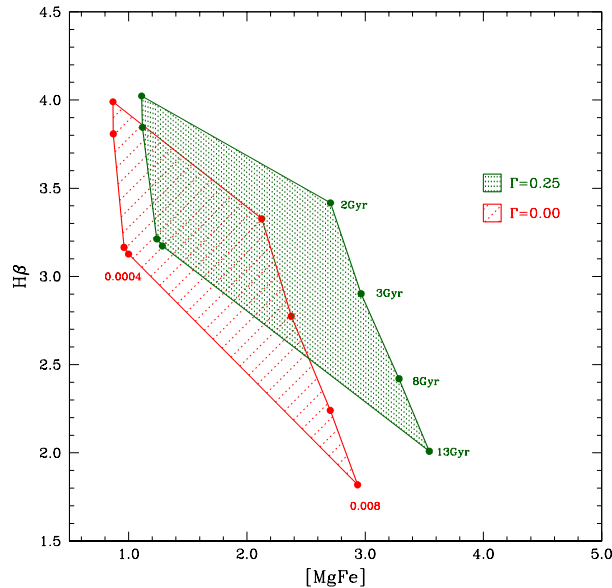


Figure 20. Indices straight from 1-Å resolution spectra: the $H\beta$ versus $[Mg/Fe]$ plane. No use of $\mathcal{F}\mathcal{F}$ s and $\mathcal{R}\mathcal{F}$ s is made. The metallicity goes from $Z=0.0004$ to $Z=0.008$ ($[Z/Z_{\odot}]=-2.0$ to $[Z/Z_{\odot}]=-0.5$). This is the analogue of Fig. 12 however limited to sub-solar metallicities. The effect of the α -enhancement on $H\beta$ is once more confirmed and in addition to this the dependence on the metallicity is highlighted. The correction $\delta H\beta = H\beta_{enh} - H\beta_{sol}$ increases with the metallicity. The various symbols are the same as in Fig. 12. In this case no comparison with observational data can be made because the theoretical indices are from spectra with 1-Å resolution and no data are yet available at the same resolution.

clearly demonstrate that not only all indices depend on the enhancement but also that $H\beta$ increases with it as already anticipated by TC04a and contrary to what claimed by Thomas et al. (2003a,b).

(iii) The above results lend strong support to the suggestion made by Tantalo & Chiosi (2004b) that a significant part of the scatter along the $H\beta$ axis shown by galaxies in the $H\beta$ versus $[Mg/Fe]$ plane (and similar) could be due to a spread in the mean enhancement factor from galaxy to galaxy and only occasionally to recent episodes of star formation. We carefully investigate this possibility. First we derive ages, metallicities and enhancement factor for the galaxies in the Trager sample. Secondly we analyze the position of galaxies with low- and high- $H\beta$ in various diagnostic planes. Finally using the theoretical estimates of the three parameters for general correlations and find that at increasing age of the last episode of star formation, the mean metallicity decreases and the mean enhancement increases in agreement with current understanding of supernova explosions on galactic chemical enrichment.

(iv) In the last part of this study, we present preliminary synthetic indices on the Lick system directly measured on theoretical 1-Å resolution spectra. The analysis is considered to be preliminary because much narrower spacing in T_{eff} and $\log g$ than the one for the subset of the Munari et al. (2004) library to our disposal is indeed required. Work is in progress to include the desired spacing in T_{eff}

and $\log g$. Nevertheless the results obtained in so far are satisfactory because the overall dependence on the main parameters of the problem, i.e. chemical composition, degree of enhancement and age are recovered. Finally, we plan to provide in a forthcoming paper (Tantalo & Chiosi in preparation) libraries of theoretical indices based on spectra with same resolution of the observational ones so that comparison with the wealthy of data coming from modern spectro-photometric surveys, e.g. SLOAN, is possible.

As a conclusion, given that the absorption-line indices proved to be useful tools to infer the age, metallicity and degree of enhancement of composite stellar populations, there is no reason to abandon them. However the present day availability of large libraries of theoretical and empirical spectra at high resolution together with fast numerical techniques make obsolete the use of the $\mathcal{F}\mathcal{F}$ s and $\mathcal{R}\mathcal{F}$ s, which have always been sources of uncertainty. Nevertheless, recalling that all indices of the Lick system stand on the ratio F_l/F_c , which is equivalent to a narrow band colour, it would be better to define all of them in the classical way, i.e. on a magnitude scale. The present day definition part in pseudo equivalent width and part in magnitude is often cause of misunderstanding.

Qu'à la fin de l'envoi je touche!

Cyrano de Bergerac

Edmond Rostand (1868 – 1918)

ACKNOWLEDGEMENTS

This study has been financed by the Italian Ministry of Education, University, and Research (MIUR), and the University of Padua under the special contract ‘Formation and evolution of elliptical galaxies: the age problem’.

REFERENCES

- Anders E., Grevesse N., 1989, *Geochim. Cosmochim. Acta*, 53, 197
- Barbuy B., 1994, *ApJ*, 430, 218
- Bertelli G., Bressan A., Chiosi C., Fagotto F., Nasi E., 1994, *A&AS*, 106, 275
- Borges C. A., Idiart T. P., de Freitas-Pacheco J. A., Thevein F., 1995, *AJ*, 110, 2408
- Bressan A., Chiosi C., Fagotto F., 1994, *ApJS*, 94, 63
- Bressan A., Chiosi C., Tantalo R., 1996, *A&A*, 311, 425
- Bruzual G., 1983, *ApJ*, 273, 205
- Burstein D., Bertola F., Buson L. M., Faber S. M., Lauer T. R., 1988, *ApJ*, 328, 440
- Burstein D., Faber S. M., Gaskell C. M., Krumm N., 1984, *ApJ*, 287, 586
- Carney B., 1996, *PASP*, 108, 900
- Castelli F., Kurucz R. L., 2004, in Piskunov N. E., Weiss W. W., Gray D. F., eds, *Modelling of Stellar Atmospheres* IAU Symposium. p. 189

- Cenarro A. J., Cardiel N., Gorgas J., Peletier R. F., Vazdekis A., Prada F., 2001, *MNRAS*, 326, 959
- Cenarro A. J., Gorgas J., Cardiel N., Vazdekis A., Peletier R. F., 2002, *MNRAS*, 329, 863
- Chiosi C., Carraro G., 2002, *MNRAS*, 335, 335
- Davies R. L., Kuntschner H., Emsellem E., Bacon R., Bureau M., Carollo C. M., Copin Y., Miller B. W., Monnet G., Peletier R. F., Verolme E. K., de Zeeuw P. T., 2001, *ApJL*, 548, L33
- Faber S. M., Friel E. D., Burstein D., Gaskell C. M., 1985, *ApJS*, 57, 711
- Faber S. M., Worthey G., González J. J., 1992, in Barbuy B., Renzini A., eds, *The Stellar Population of Galaxies* IAU Symp. 149. Kluwer Academic Publishers: Dordrecht, p. 255
- Girardi L., Bertelli G., 1998, *MNRAS*, 300, 533
- Girardi L., Bertelli G., Bressan A., Chiosi C., Groenewegen M., Marigo P., Salasnich B., Weiss A., 2002, *A&A*, 391, 195
- Girardi L., Bressan A., Bertelli G., Chiosi C., 2000, *A&AS*, 141, 371
- González J. J., 1993, PhD thesis, University of California, Santa Cruz
- Gorgas J., Cardiel N., Pedraz S., González J. J., 1999, *A&AS*, 139, 29
- Gratton R., Carretta E., Claudi R., Lucatello S., Barbieri M., 2003, *A&A*, 404, 187
- Grevesse N., Sauval A. J., 1998, *Space Sci. Rev.*, 85, 161
- Habgood M.-J., 2001, PhD thesis, Univ. of North Carolina at Chapel Hill
- Idiart T. P., de Freitas-Pacheco J. A., 1995, *AJ*, 109, 2218
- Jørgensen I., 1999, *MNRAS*, 306, 607
- Kuntschner H., 1998, PhD thesis, Univ. of Durham
- Kuntschner H., 2000, *MNRAS*, 315, 184
- Kuntschner H., Davies R. L., 1998, *MNRAS*, 295, L29
- Kuntschner H., Lucey J. R., Smith R. J., Hudson M. J., Davies R. L., 2001, *MNRAS*, 323, 615
- Kurucz R. L., 1993, in *Diatomic Molecular Data for Opacity Calculations* CD-ROM No. 15
- Larson R. B., 1974, *MNRAS*, 142, 501
- Le Borgne J.-F., Bruzual G., Pelló R., Lançon A., Rocca-Volmerange B., Sanahuja B., Schaerer D., Soubiran C., Vilchez-Gómez R., 2003, 402, 433
- Longhetti M., Bressan A., Chiosi C., Rampazzo R., 2000, *A&A*, 353, 917
- Longhetti M., Rampazzo R., Bressan A., Chiosi C., 1998, *A&AS*, 130, 251
- Maraston C., Greggio L., Renzini A., S.Ortolani Saglia R., Puzia T., Kissler-Patig M., 2003, *A&A*, 400, 823
- Matteucci F., 1994, *A&A*, 154, 279
- Matteucci F., 1997, *Fundam. Cosmic Phys.*, 17, 283
- Matteucci F., Ponzzone R., Gibson B. K., 1998, *A&A*, 335, 855
- Munari U., Sordo R., Castelli F., Zwitter T., 2004, *A&A*, to be submitted
- Poggianti B., Bridges T., Mobasher B., Carter D., Doi M., Iye M., Kashikawa N., Komiyama Y., Okamura S., Sekiguchi M., Shimasaku K., Yagi M., Yasuda N., 2001, *ApJ*, 562, 689
- Puzia T., Saglia R., Kissler-Patig M., Maraston C., Greggio L., Renzini A., Ortolani S., 2002, *A&A*, 395, 45
- Reimers D., 1975, *Mem. Soc. R. Sci. Liege*, ser. 6, 8, 369
- Renzini A., Buzzoni A., 1986, in Chiosi C., Renzini A., eds, *Spectral Evolution of Galaxies* Dordrecht: Reidel, p. 213
- Ryan S., Norris J., Bessell M., 1991, *AJ*, 102, 303
- Salasnich B., Girardi L., Weiss A., Chiosi C., 2000, *A&A*, 361, 1023
- Sánchez-Blázquez P., Peletier R., Vazdekis A., Gorgas J., Cardiel N., Selam S., Falcón J., 2003, in Avila-Reese V., Firmani C., Frenk C., Allen C., eds, *Revista Mexicana de Astronomia y Astrofisica Conference Series* Vol. 17. p. 192
- Schwenke D. W., 1998, *Faraday Discussion*, 109, 321
- Spergel D. N., Verde L., Peres H. V., et al. 2003, *ApJS*, 148, 175
- Tantalo R., 1998, PhD thesis, Univ. of Padova
- Tantalo R., Chiosi C., 2004a, *MNRAS*, 353, 917
- Tantalo R., Chiosi C., 2004b, *MNRAS*, 353, 405
- Tantalo R., Chiosi C., Bressan A., 1998, *A&A*, 333, 419
- Thomas D., Maraston C., 2003, *A&A*, 401, 429
- Thomas D., Maraston C., Bender R., 2003a, *MNRAS*, 339, 897
- Thomas D., Maraston C., Bender R., 2003b, *MNRAS*, 343, 279
- Trager S., 1997, PhD thesis, Univ. of California, Santa Cruz
- Trager S. C., Faber S. M., Worthey G., González J. J., 2000a, *AJ*, 119, 1645
- Trager S. C., Faber S. M., Worthey G., González J. J., 2000b, *AJ*, 120, 165
- Trager S. C., Worthey G., Faber S. M., Burstein D., González J. J., 1998, *ApJS*, 116, 1
- Tripicco M. J., Bell R. A., 1995, *AJ*, 110, 3035
- Vassiliadis D. A., Wood P. R., 1993, *ApJ*, 413, 641
- Vazdekis A., 1999, *ApJ*, 513, 224
- Vazdekis A., Kuntschner H., Davies R. L., Arimoto N., Nakamura O., Peletier R. F., 2001, *apj*, 551, 127
- Weiss A., Peletier R. F., Matteucci F., 1995, *A&A*, 296, 73
- Worthey G., 1992, PhD thesis, Univ. of California
- Worthey G., 1994, *ApJS*, 95, 107
- Worthey G., Faber S. M., González J. J., 1992, *ApJ*, 398, 69
- Worthey G., Faber S. M., González J. J., Burstein D., 1994, *ApJS*, 94, 687
- Worthey G., Ottaviani D., 1997, *ApJS*, 111, 377
- Zwitter T., Castelli F., Munari U., 2004, *A&A*, 417, 1055

APPENDIX A:

Tables A1–A4 list the new $\mathcal{R}\mathcal{F}$ s calculated with the 1-Å resolution spectra from Munari et al. (2004) as function of T_{eff} and $\log g$ and for four different metallicities: $[Z/Z_{\odot}] = -2.0, -1.5, -1.0, -0.5$. For each index we give the value I_{sol} for the solar abundance ratios and the difference $(\delta I) = I_{\text{enh}} - I_{\text{sol}}$ between the α -enhanced and the solar case. The corresponding $\mathcal{R}\mathcal{F}$ s can immediately be derived from relation (14). Tables A5–A8 are the same but for the high-resolution spectra degraded to the Lick resolution.